

1
2
3
4
5
6
7

8 **Causal evidence for a domain-specific role of left superior frontal sulcus in 9 human perceptual decision making**

10
11
12
13
14 Miguel Barreto García,^{1,2†} Marcus Grueschow,^{1†} Marius Moisa,¹ Rafael Polania,³ Christian C. Ruff¹
15
16 [†] These authors contributed equally to this paper.

17
18
19
20 **Affiliations:**
21 ¹ Zurich Center for Neuroeconomics (ZNE), Department of Economics, University of Zurich, Zurich,
22 Switzerland.
23 ² Department of Neuroscience, Washington University in St. Louis, Missouri, United States.
24 ³ Decision Neuroscience Lab, Department of Health Sciences and Technology, ETH Zurich, Zurich,
25 Switzerland.

26 **ABSTRACT**

27 Humans and animals can flexibly choose their actions based on different information, ranging from
28 objective states of the environment (e.g., apples are bigger than cherries) to subjective preferences
29 (e.g., cherries are tastier than apples). Whether the brain instantiates these different choices by
30 recruiting either specialised or shared neural circuitry remains debated. Specifically, domain-general
31 accounts of prefrontal cortex (PFC) function propose that prefrontal areas flexibly process either
32 perceptual or value-based evidence depending on what is required for the present choice, whereas
33 domain-specific theories posit that PFC sub-areas, such as the left superior frontal sulcus (SFS),
34 selectively integrate evidence relevant for perceptual decisions. Here we comprehensively test the
35 functional role of the left SFS for choices based on perceptual and value-based evidence, by
36 combining fMRI with a behavioural paradigm, computational modelling, and transcranial magnetic
37 stimulation. Confirming predictions by a sequential sampling model, we show that TMS-induced
38 excitability reduction of the left SFS selectively changes the processing of decision-relevant perceptual
39 information and associated neural processes. In contrast, value-based decision making and
40 associated neural processes remain unaffected. This specificity of SFS function is evident at all levels
41 of analysis (behavioural, computational, and neural, including functional connectivity), demonstrating
42 that the left SFS causally contributes to evidence integration for perceptual but not value-based
43 decisions.

44

45

46

47

48

49

50

51

52

53

54

55

56

57

58 INTRODUCTION

59 Humans and animals alike perform a mélange of goal-directed decisions that require the accumulation
60 of different types of information. If the goal, for example, is to accurately determine whether an apple
61 is bigger than a cherry (perceptual choice), the decision-maker accumulates size information of each
62 fruit; or, the decision-maker may draw out information from personal taste profiles if the goal is to
63 determine whether consuming a cherry over an apple maximises their subjective preferences (value-
64 based choice). Previous studies have shown that different brain circuitries are recruited to accumulate
65 evidence that would instantiate such distinct goal-directed decisions (Summerfield and Tsetsos, 2012;
66 Polanía et al., 2014, 2015; Grueschow et al., 2015); thus, it remains debated to what degree certain
67 decision-making processes share neural circuitry or whether these processes operate under
68 specialised systems. However, prior studies were largely correlational (Heekeren et al. 2004, 2008;
69 Polanía et al., 2014; Grueschow et al., 2015), and most causal studies were only limited to one type
70 of choice (Philiastides et al., 2011; Rahnev et al., 2016) and performed in animals (Ding and Gold,
71 2012b; Erlich et al., 2015; Hanks et al., 2015). Animal studies provide critical causal insights, yet direct
72 translation to humans can be limited by species-specific anatomy and potential non-homologies (e.g.,
73 human SFS versus frontal orienting fields in rodents). Therefore, establishing causal contributions in
74 the human brain remains essential.

75 In the absence of a comparison choice task, it is impossible to ascertain whether neural circuitry is
76 domain-specific to a particular process, or domain-general that it may be involved across many types
77 of choices. Very few studies (Polanía et al., 2014, 2015; Grueschow et al., 2015) have carefully
78 matched perceptual and value-based decisions in terms of evidence strength, stimulus display, and
79 response modality, and compare them through the lens of a common sequential-sampling framework
80 of evidence accumulation (Dutilh and Rieskamp, 2016; Gold and Shadlen, 2007; Krajbich, 2019),
81 which has long been applied to both perceptual (Ratcliff and Mckoon, 1988) as well as value-based
82 (Busemeyer and Townsend, 1993; Usher and McClelland 2001) decisions. Such studies were able to
83 identify common and specialised circuitries and mechanisms associated to perceptual or value-based
84 decisions or both (Polanía et al., 2014; Grueschow et al., 2015).

85 But unless causality is established, it is even more difficult to attribute the circuitry's role in evidence
86 accumulation for one or several choice domains, or whether its involvement is peripheral and merely
87 functionally supporting a larger system. Given task complexity, such studies of observing causal neural
88 effects in healthy human populations using non-invasive brain stimulation are incredibly sparse. One
89 previous study has, at least, shown that causally de-synchronising frontoparietal connectivity
90 specifically increased choice variability during value-based choice, but had no effect on perceptual
91 decisions (Polanía et al., 2015); thus, establishing the causal role of the frontoparietal network during
92 value-based choice. But while indeed causal, the study was limited, relative to the standards of
93 evidence in animal studies (Erlich et al., 2015; Hanks et al., 2015; Piet et al., 2017), since its results,
94 as in many causal stimulation studies in humans (Philiastides et al., 2011; Rahnev et al., 2016),
95 showed behavioural, but no neural effects. Furthermore, we only have evidence of a single
96 dissociation that shows a causal stimulation effect specific to value-based, and not perceptual choice.
97 What candidate region would show a causal effect that is specific to perceptual, not value-based
98 decisions in a way that would demonstrate a double dissociation?

99 Seminal human imaging studies have repeatedly implicated the superior frontal sulcus (SFS), a
100 posterior portion of the dorsolateral prefrontal cortex (dlPFC), during perceptual decision-making
101 (Heekeren et al., 2004, 2008; Mulder et al., 2014). While these studies have shown correlational
102 evidence, it remains challenging to establish whether the SFS is directly involved in evidence
103 accumulation or whether its observed activity reflects upstream or downstream support processes
104 (e.g., attention or working-memory maintenance) rather than the accumulation computation per se. In
105 this context, it is conceivable to imagine that the SFS would only play a role in a broader network that
106 is not specific to the evidence accumulation process. Moreover, causal evidence from human studies

107 is difficult to obtain because most prior causal studies were only limited to one type of choice or
108 performed in animals, and it is unclear if findings can be translated from animal models to human
109 decision-making. However, disruption of human left SFS with non-invasive stimulation has been
110 shown to impact behavioural performance and response speed in a dynamic face-house classification
111 task, in a manner consistent with a reduction of evidence accumulation during decision-making.
112 However, the domain-specificity of SFS contribution is unclear. Some studies have shown that dlPFC
113 activity may reflect value-based evidence integration (Basten et al., 2010; Sokol-Hessner et al., 2012),
114 suggesting the domain-generality of prefrontal function (Owen, 1997; Petrides, 2005). However, it is
115 hard to directly compare the implicated neural processes to those that underlie perceptual decision-
116 making processes, due to major differences in the stimuli and experimental approaches classically
117 used in each domain (Gold and Shadlen, 2007; Heekeren et al., 2004), and that direct and principled
118 comparisons with other decision-making domains, in general, are largely missing.

119 Here, we test the domain-specificity of the left SFS, and address the crucial double-dissociation gap
120 in the literature by applying continuous theta-burst transcranial magnetic stimulation (cTBS) followed
121 by functional magnetic resonance imaging (fMRI) while human participants alternated between
122 matched perceptual and value-based choices (Polanía et al., 2014, 2015). We modelled the observed
123 behavioural changes with the DDM, allowing us to causally associate the stimulated SFS region to
124 specific underlying latent subprocesses of the unfolding decision (Mulder et al., 2014; Polanía et al.,
125 2015) as well as BOLD activation. Thus, this common evidence accumulation framework provides us
126 with clear testable hypotheses regarding possible effect patterns across behavioural, computational,
127 and neural levels.

128

129 RESULTS

130 **The experiment.** We recorded functional magnetic resonance imaging (fMRI) data from hungry,
131 healthy participants ($n = 20$) performing perceptual- and value-based choice-tasks in alternation
132 (**Methods** and **Fig. 1b**). For perceptual decisions, participants chose the larger food item, while for
133 value-based decisions, participants chose the food item that they would preferably receive and
134 consume by the end of the experiment. The stimuli and motor responses were identical for both tasks,
135 as in previous experiments (Polanía et al., 2014, 2015). Choice pairings were predetermined based
136 on participant's individual subjective perceptual- and value-based ratings of the food items, obtained
137 just prior to the scanning session. Perceptual evidence was defined as the size difference (SD)
138 between the food items, whereas value evidence was defined as the difference in value ratings (VD)
139 between the choice alternatives (see **Methods** and **Fig. 1b**). A choice was classified as correct when
140 it was consistent with the previously acquired ratings regarding size and preference respectively, i.e.,
141 when the larger-rated item was chosen for perceptual decisions or the higher-valued item was chosen
142 for value-based decisions (Polanía et al., 2014, 2015). Our sample size is well within acceptable range,
143 similar to that of previous TMS studies (Philiastides et al., 2011; Rahnev et al., 2016; Jackson et al.,
144 2021; van der Plas et al., 2021; Murd et al., 2021).

145 Our experiment was divided into pre- and post-stimulation blocks. After participants had performed
146 four pre-stimulation session-blocks inside the scanner, they received continuous theta burst
147 stimulation (cTBS) (Huang et al., 2005; Di Lazzaro et al., 2005, 2008) over the left SFS (MNI
148 coordinates, $x = -24, y = 24, z = 36$; Heekeren et al., 2004; Philiastides et al., 2011; Grueschow et
149 al., 2018). Following this intervention, participants completed four post-stimulation fMRI blocks. By
150 comparing the effects of stimulation on both types of behaviour and brain activity between post- and
151 pre-stimulation blocks, we identify the role of SFS for either type of decision making. In particular, we
152 examined whether the SFS is indeed selectively involved in perceptual decisions as previously
153 suggested (Heekeren et al., 2004, 2006; Rahnev et al., 2016; Philiastides et al., 2011).

154 Our initial fMRI analyses were conducted at two levels. The first analysis aimed to broadly identify
155 brain areas recruited for each choice task and those common to both. In this analysis, we assessed
156 the average BOLD activity at the task level (perceptual versus value-based), irrespective of
157 evidence accumulation. The second analysis focused on areas representing evidence
158 accumulation specific to each type of choice. Here, we assessed how BOLD activity is modulated
159 by trial-by-trial evidence strength. For this analysis, we used evidence strength from each choice
160 task (perceptual or value-based) as a parametric modulator and regressed trial-by-trial evidence
161 strength with BOLD (see **Methods**).

162 **Study hypotheses.** Previous studies have identified the causal mechanistic role of the SFS in
163 evidence accumulation during perceptual decision-making (Heekeren et al., 2004, 2006; Rahnev et
164 al., 2016), and its effect on stimulation may arise from one of either two channels. That is, one study
165 reported that SFS disruption during a speeded perceptual categorisation task reduced accuracy and
166 increased response times (Philiastides et al., 2011) and found associated decreases in drift rate, the
167 DDM parameter describing the efficiency of sensory evidence integration. In contrast, another human
168 brain stimulation study suggested that behavioural changes due to SFS disruption during a perceptual
169 two-alternative-forced-choice (2AFC) task reflect decreased in the decision threshold, characterised
170 by faster response speed but decreased choice precision. Simulations with the same DDM modelling
171 framework (Rahnev et al., 2016) suggested that the decision threshold parameter could account for
172 individual behavioural changes. Simultaneously acquired fMRI data suggested that SFS does not code
173 the rate of integration but rather the necessary amount of evidence to be accumulated for the
174 perceptual choice at hand (Rahnev et al., 2016).

175 To this end, we hypothesise that if SFS neurons indeed selectively accumulate perceptual evidence,
176 we should find that their inhibition by cTBS leads to decreases in choice precision and increases in
177 reaction times, a behavioural pattern that corresponds to a decrease in the DDM drift-rate parameter,
178 and to concurrent increases in BOLD signals (caused by prolonged neural evidence accumulation;
179 **Fig. 2a-c**). Critically, a different pattern can be expected when SFS neurons are involved in setting the
180 criterion, i.e., determining the amount of evidence that needs to be accumulated for a perceptual
181 choice to be taken. In this case, SFS inhibition should result in decreases in both choice precision and
182 reaction times, a decrease in the DDM boundary parameter (Rahnev et al., 2016), and a reduction in
183 associated neural activity due to the lower amount of evidence accumulated during the shorter
184 response time (**Fig. 2d-f**). Here we directly test these two contrasting scenarios, by characterising the
185 behavioural, neural, and neuro-computational consequences of cTBS to the left superior frontal sulcus
186 (SFS). Crucially, we also investigate for both possible outcomes whether the functional contribution of
187 the SFS during decision making is indeed specific for perceptual choices, by comparing the results
188 between the two matched types of choices.

189 **Behaviour: validity of task-relevant pre-requisites.** Before scrutinising the role of the left SFS for
190 either type of choice, we first behaviourally and neurally confirmed the validity of our task paradigm.
191 To establish a fair comparison between perceptual (PDM) and value-based decision-making (VDM),
192 we must necessarily show that we can distinctly identify the brain regions associated for each type of
193 choice, and that behaviour is systematically a function of their respective evidence measures. Initial
194 visual inspection shows that choice accuracy/consistency systematically increases (**Fig. 2a**) and RTs
195 become faster (**Fig. 2b**) the larger the evidence difference, and this holds across tasks and stimulation
196 conditions. All behavioural and fMRI analyses were performed on valid trials only (see Methods for
197 inclusion criteria). Behavioural regressions confirmed that our task design allowed for a clear
198 computational separation of both choice types: during perceptual decisions, participants relied
199 exclusively on perceptual evidence, as reflected in both increased choice accuracy (main effect SD,
200 $\beta = 0.560, p < 0.001$ and VD, $\beta = 0.023, p = 0.178$; **Fig. 1b**) and faster reaction times (RTs) with larger
201 perceptual evidence, but not value-based evidence (main effect SD, $\beta = -0.057, p < 0.001$ and VD,
202 $\beta = 0.002, p = 0.281$; **Fig. 1c**). Conversely, participants relied only on value evidence during VDM, as
203 evident from both choice consistency (main effect VD, $\beta = 0.249, p < 0.001$ and SD, $\beta = 0.005, p =$

204 0.826; **Fig. 1b)** and RTs (main effect VD, $\beta = -0.016, p = 0.011$ and SD, $\beta = -0.003, p = 0.419$; **Fig.**
205 **1c)** irrespective of the items' size difference. Thus, our results replicate previous findings obtained with
206 a similar paradigm (Polanía et al., 2014, 2015; Grueschow et al., 2015) showing that participants can
207 use exclusively task-relevant evidence to make choices, and they confirm the suitability of our
208 paradigm for directly comparing perceptual and value-based decisions with matched stimuli and motor
209 responses. Across sessions, RTs tended to shorten in both tasks. In line with the HDDM results—
210 selective boundary reductions for PDM and selective nDT shortening for VDM—we interpret the VDM
211 RT speed-ups as reflecting more efficient non-decision (sensorimotor) components rather than
212 changes in evidence accumulation. To illustrate baseline trends, we provide session-wise RT
213 trajectories in the Supplement (see **Supplementary Fig. 11** for RT-by-session). For completeness,
214 group-mean accuracies by task are provided descriptively in **Fig. 3a**; inferential tests focus on
215 evidence-specific effects and TMS-induced changes within task.

216 **fMRI: VDM and PDM distinctly recruit brain processes, while recruiting similar visual and motor**
217 **processes.** In line with the behavioural results that participants depended on different evidence for
218 the two types of choices, initial fMRI analysis revealed that neural activations strongly differed
219 between choice types, despite the fact that participants saw the same images and gave the same
220 motor responses.

221 We performed two levels of fMRI analyses. The first analysis examined average BOLD activity at
222 the task level, contrasting perceptual versus value-based decisions, irrespective of whether the
223 differences were driven by evidence accumulation or other cognitive processes. This initial analysis
224 aimed to broadly identify brain areas recruited for each choice task and those common to both.
225 First, we found visual and motor areas were jointly activated for both types of choices ($p < 0.05$,
226 FWE-corrected with cluster forming thresholds at $T(19) > 2.9$; **Supplementary Fig. 1a** and
227 **Supplementary Table 1**). Second, PDM led to stronger recruitment of the posterior parietal cortex
228 whereas VDM led to stronger activations of the medial prefrontal cortex and posterior cingulate
229 cortex (**Supplementary Fig. 1b** and **Supplementary Table 2**), all in line with previous findings
230 (Grueschow et al., 2015).

231 Notably, the left SFS does not yet appear in this contrast analysis. This is because this initial
232 analysis did not include the parametric modulator for evidence accumulation. At this stage, we were
233 evaluating whether the brain can flexibly recruit distinct brain regions based on task design,
234 irrespective of whether these differences arise from variations in evidence accumulation or other
235 cognitive processes. The second analysis assessed how BOLD activity is modulated by trial-by-
236 trial evidence strength. Here, we identified a parametric modulator for evidence accumulation and
237 regressed it on BOLD activity using a general linear model. This analysis revealed that the left SFS
238 shows significant activation specifically when perceptual evidence is parametrically modulated.
239 BOLD activity in the left SFS is detectable only when perceptual evidence is considered⁶. In fact,
240 previous studies have similarly shown that the SFS only appears once a variable that measures
241 the degree of evidence accumulation is included in the analysis⁶. Thus, these choice-type-specific
242 brain activations, in response to identical visual input and motor output, ascertain that participants
243 recruit task-specific brain regions depending on the choice domain.

244 **Behaviour: theta-burst stimulation reduces choice accuracy for perceptual decisions only.** Our
245 results support the hypothesis that the SFS has a specific role for perceptual decision-making, on
246 several experimental levels. Using a differences-in-differences (DID) logistic regression (**Methods**),
247 we found that SFS-ctBS led to a significant decrease from pre- to post-ctBS blocks in accuracy for
248 PDM (main stimulation effect, $\beta = -0.465 \pm 0.342, p = 0.008$; **Fig. 3a** and **Supplementary Fig. 2a**),
249 while VDM choice consistency remained unaffected by SFS stimulation ($\beta = -0.042 \pm 0.205, p =$
250 0.691 ; **Fig. 3a** and **Supplementary Fig. 2a**). These differences were significant in direct comparison
251 (stimulation \times task interaction, $\beta = -0.094 \pm 0.087, p = 0.034$; **Fig. 3a**; **Supplementary Fig. 2c** and

252 **Supplementary Table 2)** fatigue or habituation effects after checking that the average accuracies in
253 PDM were actually recovering in the second post-stimulation session while there was no change in
254 choice consistency at all during VDM (**Supplementary Fig. 2a**). Interestingly, our DID linear
255 regression (**Methods**) revealed that SFS-cTBS had comparable effects on reaction times in both
256 tasks: faster RTs were observed after SFS-cTBS for both PDM (main stimulation effect, $\beta = -0.116 \pm$
257 $0.067, p = 0.003$; **Fig. 3b** and **Supplementary Fig. 2b**) and VDM (main stimulation effect, $\beta =$
258 $-0.125 \pm 0.063, p = 0.001$; **Fig. 3b** and **Supplementary Fig. 2b**), with no significant difference
259 between these two effects (stimulation \times task interaction, $\beta = 0.009 \pm 0.069, p = 0.795$; **Fig. 3b**;
260 **Supplementary Fig. 2c** and **Supplementary Table 2**). Overall, the specific changes in choice
261 accuracy indeed reflect cTBS disruption in left SFS in perceptual decisions. At the same time, the
262 common changes in RTs from the first to the second half of the experiment may not necessarily reflect
263 TMS-related changes in SFS function but rather general training effects common to both tasks
264 (Mawase et al., 2018), but this possibility can only be examined in more detail with computational
265 modelling.

266 **Modelling: SFS-TMS reduces decision boundary only for perceptual decisions.** To examine in
267 detail which specific latent decision process was affected by SFS-cTBS, we fit the hierarchical drift
268 diffusion model (HDDM) simultaneously to the accuracy and RT data of our participants. This
269 canonical model of choices allowed us to identify and disentangle the effect of stimulation on various
270 latent variables representing distinct components of the choice mechanism (Ratcliff and Smith, 2004;
271 Ratcliff and McKoon, 2008; Polania et al., 2015; **Supplementary Fig. 3** and see **Methods**).

272 To investigate the underlying processes through which the cTBS stimulation induced the observed
273 behavioural changes, we fitted a hierarchical Bayesian drift-diffusion model (HDDM; see **Methods**)
274 simultaneously to the accuracy and RT data of our participants (**Fig. 3b-d**). Critically, we used the
275 DDM parameters to identify and disentangle the effect of stimulation on choice accuracy from that on
276 RTs (Ratcliff and Smith, 2004; Ratcliff and McKoon, 2008; Polania et al., 2015; **Supplementary Fig.**
277 **3** and see **Methods**). A specific focus of this analysis was on whether SFS-cTBS would change the
278 way participants set the choice criterion (decision threshold; Rahnev et al., 2016; Bogacz et al., 2010;
279 Domenech and Dreher, 2010; Herz et al., 2016) or the efficiency with which choice-relevant evidence
280 is accumulated (drift-rate, Philiastides et al., 2011; Basten et al., 2010) (see **Methods** for more details
281 and **Fig. 1b,e**). We found that theta-burst stimulation selectively reduced the decision boundary in
282 perceptual decision making (PDM) (see **Methods**; $p_{mcmc} = 0.003$; **Fig. 3c** and **Supplementary Fig.**
283 **5a**), while leaving the decision-relevant parameters, including the drift rate, unchanged ($p_{mcmc} = 0.822$
284 for drift rate; **Fig. 3d** and **Supplementary Fig. 5b,c**). For VDM, by contrast, no effect of cTBS was
285 observed for either of the two decision-relevant parameters ($p_{mcmc} = 0.115$ for boundary and $p_{mcmc} =$
286 0.758 for drift rate; **Fig. 3c,d** and **Supplementary Fig. 5a,b,c**), supporting the specificity of the SFS
287 involvement in perceptual decisions. Full posterior summaries are provided in **Supplementary Tables**
288 **8–11**, and model adequacy is confirmed by posterior-predictive checks of accuracies and RT
289 distributions (**Supplementary Figs. 11–17**). However, we found that non-decision time (nDT) was
290 selectively reduced in VDM. Overall, our findings indicate that the left SFS is causally involved in
291 modulating the decision threshold. This conclusion was further corroborated by direct comparison of
292 these effects, which showed that SFS-cTBS had a significantly stronger impact on the boundary
293 parameter for PDM compared to VDM (stimulation \times task interaction for the decision threshold,
294 $p_{mcmc} = 0.045$; **Supplementary Fig. 5a**; there were no such differences for drift-rate; $p_{mcmc} = 0.685$;
295 **Supplementary Fig. 5b**).

296 **Modelling: faster RTs during value-based decisions is related to non-decision-related**
297 **sensorimotor processes.** To address the underlying latent process driving RT effects in both
298 choices, we examined other DDM parameters and measurements. The DDM assumes that RTs can
299 be disentangled into a non-decision-related (nDT) component as well as decision times (DT). The nDT
300 is a DDM parameter that indexes constant latencies associated with sensory and motor preparation

301 processes that are invariant across trials with different choice evidence (Verdonck and Tuerlinckx,
302 2016; Starns and Ma, 2018); in other words, this parameter forms no part of the evidence accumulation
303 process (Feltgen and Daunizeau, 2020; White et al., 2018) and may therefore reflect task learning
304 processes from movement repetition (Mawase et al., 2018). In contrast, decision times is the
305 component of RT where evidence accumulation actually takes place, and we can measure and derive
306 DT using the evidence-dependent DDM parameters (see **Methods** for more details).

307 Our results showed that the faster RTs observed for value-based decisions after the stimulation indeed
308 did not reflect evidence-dependent choice processes, but rather a change in non-decision-related
309 sensorimotor processes (nDT) (see **Methods**; **Supplementary Fig. 3**): this parameter was decreased
310 after stimulation for VDM ($p_{MCMC} = 0.062$) but not PDM ($p_{mcmc} = 0.707$) (**Supplementary Fig. 4b** and
311 **5c**), with a significant difference between these effects ($p_{mcmc} = 0.041$; **Supplementary Fig. 5c**). In
312 contrast, estimated decision times was smaller after stimulation during PDM ($p_{mcmc} = 0.003$;
313 **Supplementary Fig. 6a**, left), but not VDM ($p_{mcmc} = 0.100$; **Supplementary Fig. 6a**, right). Taken
314 together, these results suggest that the simultaneous change in RT reveal completely different
315 computational processes, whereby faster RTs during value-based choice is simply a by-product of
316 task-related learning that may perhaps be unrelated to stimulation, while faster RTs during perceptual
317 choice is actually related to decision-relevant, evidence-dependent latent choice processes. However,
318 completely ascertaining whether such effect from stimulation is due to SFS inhibition, we need clear
319 causal evidence of changes from neural processing. The pattern of non-decision time and decision-
320 time changes is consistent with the posterior-predictive fits shown in **Supplementary Figs. 11–17**,
321 with numerical posterior summaries in **Supplementary Tables 8–11**.

322 **fMRI: SFS activation changes for perceptual choices in line with model predictions.** To
323 investigate whether our behavioural and computational results directly relate to task-specific disruption
324 of neural activity in left SFS, we investigated BOLD response changes in this brain area after
325 stimulation. We exploited the fact that our fitted DDM and its latent parameters make clear predictions
326 about how BOLD responses in this area should change if the stimulation affects the neural
327 computations involved in setting the boundary for the necessary amount of evidence accumulation.
328 Importantly, these predictions translate to clear parametric regressors that we can use for trialwise
329 analysis of fMRI data (Basten et al., 2010; Domenech et al., 2017; Liu and Pleskac, 2011). More
330 specifically, we expected that the BOLD signal level is proportional to the DDM's accumulated
331 evidence (aE), defined as the area below the modelled evidence accumulation curve up until the
332 accumulator reaches the decision boundary (Liu and Pleskac, 2011; Domenech et al., 2017; Basten
333 et al., 2010). Using subject-wise DDM latent parameters, the average area below the decision
334 boundary for each evidence level can be computed as a function of each participant's decision
335 boundary divided by the mean drift rate (see **Fig. 1c** and **1f** and **Methods** for more details). Using the
336 more detailed trialwise measures, however, the same area can be computed as a function of each
337 trial's RTs divided by the evidence level, since according to the DDM, the duration of response times
338 is directly proportional to the decision boundary, and the evidence level is directly proportional to the
339 slope of the drift rate (Ratcliff and Rouder, 1998; Ratcliff and McKoon, 2008; see **Methods** for more
340 details). Exploiting these two known facts from the DDM thus allows us to extend our test of the
341 stimulation effect from individual-specific latent parameters to trialwise regressors and behavioural
342 measures. Higher SFS BOLD signals are associated with higher aE and vice versa (Basten et al.,
343 2010; Liu and Pleskac, 2011; Filimon et al., 2013; Tosoni et al., 2008), implying that a TMS intervention
344 lowering the decision boundary should lower aE and therefore BOLD signals. Crucially, these latent
345 changes predicted by the DDM should also be reflected in the subject-level simulations of accumulated
346 evidence constructed from the DDM parameters.

347 Thus, we first tested whether our neural hypotheses would already be evident in the simulated trial-
348 wise aE regressors. We used individual parameters identified by fitting our computational framework
349 to simulate expected neural activity on a trial-wise basis across participants. To this end, we derived
350 the predicted aE from the model parameters for each participant. A comparison across cTBS and task

351 conditions confirmed the predicted cTBS-related decrease in accumulated perceptual evidence for
352 PDM ($p_{mcmc} = 0.003$; **Fig. 4a** and **Supplementary Fig. 6b**), the corresponding null effect for VDM
353 ($p_{mcmc} = 0.100$; **Fig. 4b** and **Supplementary Fig. 6b**), and a significant difference for this effect
354 between both choice types (one-sided $p_{mcmc} = 0.048$; **Supplementary Fig. 6b**).

355 In the next step, we used the trial-by-trial accumulated evidence as a regressor in the statistical
356 analysis of the BOLD signals, allowing us to test whether the left SFS shows the predicted changes in
357 neural response to varying levels of perceptual evidence. First, we tested whether our predictor of
358 neural accumulated evidence was represented in BOLD signals of similar task-specific areas as
359 reported previously for PDM in SFS (Heekeren et al., 2004, 2006) and for VDM in vmPFC (De Martino
360 et al., 2013; Grueschow et al., 2015). This was confirmed by the data: During PDM, trialwise *aE*
361 correlated with BOLD activity in the left SFS (peak at $= -21$, $= 26$, $= 37$; $SV < 0.05$; **Supplementary**
362 **Fig. 7b** and **Supplementary Table 3**) whereas, critically, no significant BOLD activity in the left SFS
363 was observed during VDM. During VDM, *aE* related to BOLD activity in the ventromedial prefrontal
364 cortex (vmPFC) (peak at $= 3$, $= 38$, $= -17$; $SV < 0.05$; Supplementary Fig. 7e) and the nucleus
365 accumbens (peak at $x = 9$, $y = 11$, $z = -11$; < 0.05 , FWE-corrected with cluster-forming thresholds at
366 $T(19) > 2.9$; Supplementary Fig. 7e). For both types of choices, domain-general representations of *aE*
367 were also evident (see **Supplementary Fig. 7** and **Supplementary Table 3**).

368 We then tested whether cTBS specifically reduced the neural representation of accumulated
369 perceptual evidence in the left SFS for PDM, as predicted by the behavioural and modeling results. In
370 line with these predictions, comparison of the post – pre trial-*aE* regressor showed a lower BOLD
371 response in left SFS to the trialwise perceptual evidence during PDM ($SV < 0.05$; **Fig. 4c**, green patch).
372 This effect was significantly stronger than the corresponding effect on evidence representations in this
373 area during VDM ($SV < 0.05$; **Fig. 4c**, blue patch). No effect was found for VDM alone. This indicates
374 that the TMS effect is specific to the SFS during perceptual decisions, not value-based ones, as
375 supported by the BOLD activity analysis. The reduction in BOLD activity in the left SFS during PDM
376 after TMS is consistent with the DDM prediction of a reduction in the accumulated evidence due to a
377 lower decision boundary. Convergent evidence for the specificity of this effect was provided by an
378 alternative hypothesis-guided region-of-interest (ROI) analysis of the regression weights extracted
379 from an *a priori* ROI-mask of the SFS (see **Methods**). This showed lower post-stimulation beta values
380 for the trial-*aE* regressor during PDM (main stimulation effect, $\beta = -0.153 \pm 0.054$, $p = 0.004$; **Fig. 4a**)
381 but not VDM (main stimulation effect, $\beta = 0.078 \pm 0.053$, $p = 0.140$; **Fig. 4b**) and a significant
382 difference in these effects (stimulation \times task interaction, $\beta = -0.232 \pm 0.075$, $p = 0.002$; **Fig. 4a,b**).
383 Thus, the fMRI results show that cTBS of the left SFS indeed affects neural processing in this brain
384 structure selectively during perceptual choices, in a way that is consistent with a lowering of the
385 boundary and less accumulated evidence as predicted by the fitted DDM model. This remarkable
386 convergence between the behavioural, modelling, and fMRI results suggests that the left SFS is
387 indeed causally involved in setting decision criteria for choices based on perceptual evidence, but not
388 based on subjective values.

389 **fMRI and modelling: neural-HDDM shows that perceptual-choice accuracy and boundary**
390 **setting reflect trial-by-trial changes in SFS activity.** If perceptual-decision performance depends
391 specifically on activity in the left SFS, then trial-wise choice accuracy should relate to trial-wise BOLD
392 activity in the SFS during perceptual decisions, over and above the mean effects of evidence level. To
393 test this, we regressed choice accuracy/consistency on trial-by-trial BOLD activity extracted from the
394 left SFS ROI, choice type, and TMS, while controlling for the evidence provided by the stimulus pairs
395 on each trial (see **Methods** for details). In line with our prediction, we observed that the relation
396 between perceptual-choice accuracy and trial-by-trial SFS activity was significantly decreased by
397 TMS (SFS \times stimulation interaction, $\beta = -0.196 \pm 0.128$, $p = 0.003$; **Fig. 4d**), independently of the
398 corresponding effects for choice evidence (SD main effect, $\beta = 0.524 \pm 0.082$, $p < 0.001$, VD main
399 effect, $\beta = 0.197 \pm 0.012$, $p = 0.001$, SFS \times SD interaction, $\beta = -0.041 \pm 0.046$, $p = 0.365$, SFS \times

400 VD interaction, $\beta = 0.055 \pm 0.041, p = 0.183$). This effect was clearly specific for PDM, since no such
401 effects were observed for VDM (SFS \times stimulation interaction $\beta = 0.099 \pm 0.242, p = 0.422$; SFS \times
402 stimulation \times task interaction, $\beta = -0.072 \pm 0.051, p = 0.005$; **Fig. 4d**) and for RTs during both types
403 of choices (SFS \times stimulation interaction, perceptual: $\beta = -0.031 \pm 0.053, p = 0.367$; **Fig. 4d**;
404 accuracy: SFS \times stimulation interaction, $\beta = -0.012 \pm 0.050, p = 0.650$; **Fig 4d**).

405 We further investigated whether the relation between trialwise SFS activity and choice outcome indeed
406 reflected an SFS role for perceptual boundary setting, as suggested by the DDM results presented
407 above. To confirm this neurally, we set up several DDMs with trialwise SFS activity as an additional
408 modulator for DDM parameters (on top of choice evidence; see **Methods** and Herz et al., 2016, 2017;
409 Turner et al., 2015). More specifically, we tested several neural-DDMs in which trialwise SFS activity
410 either modulated the decision threshold only (**Model 1**; **Supplementary Fig. 8a**), the drift rate only
411 (**Model 2**; **Supplementary Fig. 8b**), or both parameters separately (**Model 3**; **Supplementary Fig.**
412 **8c**) or jointly (**Model 4**; **Supplementary Fig. 8d**). We compared these neural HDDMs to our baseline
413 HDDM without neural inputs (see **Methods** for more details and **Supplementary Fig. 3**), allowing us
414 to test across all conditions and choice types whether model evidence was enhanced when adding a
415 potential trial-by-trial influences of SFS activity to the experimental inputs. Thus, the reported model
416 evidence criterion (DIC) provides an additional formal test of whether the cTBS-influenced SFS activity
417 relates selectively to the decrease of the decision boundary for perceptual choices only. Consistent
418 with this prediction, Model 1 where SFS activity modulated the decision threshold only, outperformed
419 all other models and model evidence showed improvements versus the baseline model (relative DIC =
420 -28.65 ; **Fig. 4b**). These results provide direct evidence that neural computations in the left SFS
421 support criterion setting for perceptual evidence accumulation.

422 **fMRI and connectivity: TMS affects SFS functional connectivity during perceptual choices.**
423 Overall, our results clearly indicate that cTBS to the left SFS disrupts selectively a neural process
424 related to setting the criterion for perceptual evidence accumulation. At this point, we consider the
425 possibility that cTBS may conceivably change the functional communication of the SFS with other
426 brain areas involved in initial processing of the perceptual information necessary to make a choice.
427 We explored this possibility by investigating whether cTBS affected functional coupling of the SFS. A
428 psychophysiological interaction (PPI) analysis seeded in left SFS and modulated by aE indeed
429 revealed stronger coupling with occipital cortex (OCC) after cTBS (peak at $x = -28, y = -85, z = -2$;
430 $p < 0.01$ FWE-cluster-forming thresholds at $T(19) > 2.9$; **Fig. 5a**). Interestingly, the activity peak in
431 visual cortex showing evidence-dependent coupling with SFS, overlaps with the spatiotopic neural
432 representation of the stimulus items in the visual field during decision making. We identified this
433 overlap using a conjunction analysis of the PPI result and a contrast regressing BOLD signal on trial-
434 by-trial stimulus onsets of both choice types (at familywise-error-corrected thresholds). Moreover, we
435 used the latter contrast to define fully independent regions-of-interest (ROIs) in occipital cortex
436 processing the visual stimuli independent of task type and performed an ROI analysis on the individual
437 SFS-OCC-PPI betas extracted for each participant. This confirmed that evidence-related functional
438 coupling is increased by stimulation during PDM (main stimulation effect, $\beta = 0.330 \pm 0.284, p =$
439 0.022) but not VDM (main stimulation effect, $\beta = -0.186 \pm 0.247, p = 0.139$; **Fig. 5b**; stimulation \times task
440 interaction, $\beta = 0.517 \pm 0.44, p = 0.021$; **Fig. 5a**). Thus, our exploratory analysis shows that cTBS to
441 the left SFS leads to stronger functional coupling with occipital areas involved in processing the visual
442 stimuli, perhaps consistent with increased downstream demand on visual-related resources when
443 upstream evidence accumulation regions are impaired.

444 We further explored whether this TMS-induced increase in functional coupling between the left SFS
445 and OCC is related to changes in behaviour and specific neural computations during perceptual
446 decisions. To test this, we related these effects to individual measures of choice behaviour and latent
447 DDM parameters for each participant. This revealed that stimulation-induced increases in SFS-OCC
448 coupling were associated with lower accuracy (OCC \times stimulation \times task interaction, $\beta = -0.225 \pm$

449 0.142, $p = 0.002$; **Fig. 5c**) and shorter RTs (OCC \times stimulation \times task interaction, $\beta = -0.325 \pm$
450 0.238, $p = 0.007$; **Fig. 5c**) for PDM, but not VDM. Taken together, these results show that the causal
451 behavioural and computational changes during perceptual decision-making due to left SFS-TMS may
452 relate not just to local neural changes in SFS, but also to the way this brain structure communicates
453 with visual cortex.

454

455 DISCUSSION

456 Our study shows that the left SFS serves a domain-specific causal role in the accumulation of
457 perceptual evidence, and particularly, the underlying computations affected by non-invasive brain
458 stimulation is the setting of the choice criterion during perceptual, but not value-based choice. Our
459 findings are more in line with that of Rahnev et al. (2016), who also suggested that SFS disruption
460 leads to lower threshold setting. In contrast, previous work has also shown that SFS activity correlates
461 with the evidence accumulation process reflected by the drift rate. These findings are not necessarily
462 incompatible, but rather, they may reflect the interlinked computational mechanisms of the SFS in
463 perceptual evidence accumulation, where the SFS plays a role in setting the decision threshold.
464 Furthermore, our findings, in a way, contribute in closing the double dissociation gap left by previous
465 work (Polanía et al., 2015), where it was shown that frontoparietal connectivity is causally specific to
466 the precision of value-based, not perceptual choice using the same matched perceptual- and value-
467 based choice task. More importantly, our study provided results above and beyond current standards
468 of causal studies in humans (Philiastides et al., 2011; Rahnev et al., 2016; Polanía et al., 2015; Murd
469 et al., 2020), that was only observed in animal studies (Ding and Gold, 2012b; Erlich et al., 2015;
470 Hanks et al., 2015). Here, we simultaneously showed that causal TMS effects affected behaviour,
471 latent computations, and more crucially, neural circuitry, as observed by changes in fMRI-BOLD
472 activation after stimulation.

473 Many human decision neuroscience studies have employed model-based approaches to identify
474 BOLD signals that correspond to computational processes (Forstmann et al., 2011; Palmeri et al.,
475 2017; Wijeakumar et al., 2017). However, the links between neural and latent computational
476 processing established by these studies is largely correlational (Logothetis, 2008; Poldrack, 2006;
477 Ramsey et al., 2010), and there are many model alternatives that could possibly account for BOLD
478 signals. Our study illustrates that causal manipulations induced by targeted functional inhibition of
479 brain areas can provide decisive information and provide more direct support for neurocomputational
480 mechanisms posited by cognitive models. Specifically, our study underlines that the DDM provides a
481 plausible mechanistic account of the decision process (Herz et al., 2016, 2017; Turner et al., 2015),
482 by showing that left SFS inhibition by cTBS affects the evidence representation posited by the model
483 consistently across behavioural, computational, neural, neural-behavioural levels. Importantly, our
484 results directly link changes in behaviour to changes in both latent computations and neural
485 processing, by demonstrating how raw trialwise neural signals from the left SFS can augment the
486 DDM to explain behaviour. This suggests that once brain stimulation studies have established (causal)
487 correspondence between neural activity and latent variables in decision models, such models can be
488 fruitfully extended by neural measures to provide a more complete characterisation and prediction of
489 choice behaviour and potentially its malfunctions. Our fMRI inferences rest on model-based
490 assumptions linking accumulated evidence to BOLD amplitude. Alternative mechanisms—such as
491 time-dependent (collapsing) boundaries—could attenuate the prediction that weaker-evidence trials
492 yield longer accumulation and larger BOLD signals. While our behavioural and neural results converge
493 under the DDM framework, we acknowledge this as a general limitation of model-based fMRI. The
494 within-participant design enhances statistical sensitivity, yet the absence of an a priori power analysis
495 constrains our ability to rule out small effects, particularly for null results in VDM.

496 **Specificity of the SFS during perceptual decisions – only in humans?** To this end, our study
497 reinforces already established findings by showing that the causal role of SFS during perceptual
498 decisions (Heekeren et al., 2004, 2006; Philiastides et al., 2011; Rahnev et al., 2016) is a specialised
499 function of evidence integration. Furthermore, our finding of a selective role of left SFS in perceptual
500 evidence accumulation is particularly intriguing. The area appears to be uniquely developed in the
501 human brain, with no close anatomical homologue in other species. In the animal literature, most
502 prefrontal disruption studies in non-human primates have focused on the frontal eye fields (FEF) (Ding
503 and Gold, 2012a; Hanks and Summerfield, 2017; Shadlen and Newsome, 1996) and in rodents on the
504 frontal orienting fields (FOF) (Erlich et al., 2015; Hanks et al., 2015). While we and others observed
505 disruption of the evidence accumulation process after interfering with SFS function in humans
506 (Philiastides et al., 2011; Rahnev et al., 2016), disruption of the FOF in rodents has not affected
507 behaviour at all or in a qualitatively different manner (Brody and Hanks, 2016; Erlich et al., 2015; Hanks
508 et al., 2015). However, the results of electrical stimulation of the FEF in monkeys (Ding and Gold,
509 2012a; Hanks and Summerfield, 2017) cannot necessarily be directly compared with TMS studies of
510 human SFS, since FEF and SFS in humans are both structurally and functionally distinct (Murd et al.,
511 2020; Rahnev et al., 2016). Thus, while it is tempting to speculate that the SFS perceptual evidence
512 accumulation process identified here may be specific to humans, it is possible that researchers may
513 have to further consider other putative homologues across species that may truly correspond to the
514 SFS area stimulated here (Brunton et al., 2013; Hanks and Summerfield, 2017).

515 **Do value-based decisions also rely on distinct PFC areas?** At the same time, our findings do not
516 rule out the possibility of SFS involvement during value-based choice, where it may perhaps have a
517 secondary function (but one that does not involve evidence accumulation) or even other specialised
518 functions in decision-making. For example, previous work has suggested that during value-based
519 decisions, the dlPFC overall interacts with the vmPFC in modulating the value signal to facilitate self-
520 control (Hare et al., 2009). Moreover, value-based decision-making entails a large array of choice
521 types with varying degrees of complexity. For instance, more complex types of value-based decisions
522 entail decisions under risk (Glickman et al., 2019), intertemporal choice (Peters and D'Esposito, 2020),
523 and strategic and social decisions (Hutcherson et al., 2015), which may plausibly recruit the PFC due
524 to working memory demands (Barbey et al., 2013), adjustment of decision time (Sokol-Hessner et al.,
525 2012), or cost-benefit computations (Basten et al., 2010). In light of these many additional decision
526 types based on preferences in the value-based choice domain, the functional specificity of SFS to
527 perceptual decisions we claim here may have to be viewed with caution. Future studies should
528 consider exploring the comparison between more complex types of value-based decisions with
529 perceptual decisions, while taking great care in matching the degree of complexity between the two
530 choice domains to avoid confounds induced by context or task difficulty.

531 **The role of SFS in choice criterion setting during perceptual decisions.** That being said, the same
532 holds true with the varying degrees of complexity across perceptual decision-making processes. Our
533 findings show that the mechanism of which the left SFS is causally involved is modulating the decision
534 threshold, with clearly consistent results across behavioural, computational, neural, and neural-
535 behavioural levels. Our findings are more in line with that of Rahnev et al. (2016), who also suggested
536 that SFS disruption leads to lower threshold setting. In contrast, previous work has also shown that
537 SFS activity correlates with the evidence strength in the accumulation process, as reflected by the drift
538 rate (Basten et al., 2010; Heekeren et al., 2004, 2006). In support of this notion, cortical activity
539 disruption with repetitive transcranial magnitude stimulation (rTMS) resulted in lower choice accuracy
540 and slower RTs (Philiastides et al., 2011). However, it is important to note that these results are not at
541 all incompatible, but reflect the interlinked computational mechanisms of the SFS in perceptual
542 evidence accumulation. All these studies, including ours, point out that the DDM's drift rate and
543 decision boundary are both decision-relevant latent mechanisms with distinct as well as overlapping
544 implications on choice behaviour: impairments in both boundary and drift lead to lower choice
545 consistency (Cavanagh et al., 2011; Green et al., 2012; Herz et al., 2016; Philiastides et al., 2011;
546 Rahnev et al., 2016). The main difference in fact concerns reaction times: lower drift rate implies slower

547 RTs while a lower boundary implies faster RTs. The differences in RT-TMS effects of our study and
548 that of Philiastides et al. (2011) may reveal the differences in task design and the nature of the stimuli.
549 For instance, the study by Philiastides et al. (2016) used dynamic series of briefly presented sequential
550 face-house stimuli, varying the strength of each stimulus within noise to vary the evidence levels. By
551 contrast, our study and that by Rahnev et al. (2016) presented a static stimulus pair simultaneously
552 during a 2AFC task and varied evidence not with noise but by stimulus difference.

553 We speculate that the goals of these tasks (i.e., discriminability from noisy dynamic stimuli versus
554 stimulus size difference between static stimuli) may sensitively affect different latent processes.
555 Previous studies have shown that different tasks can produce proximally similar behaviour but may
556 involve different goal functions and therefore, computationally distinct processes (Heng et al., 2020).
557 For instance, noisy dynamic stimuli entail the accumulation of sensory evidence until the decision-
558 maker can form representations suitable for choice discrimination (Ratcliff and McKoon, 2008); thus,
559 such stimuli are sensitively modulated by evidence strength, and reflected by a lower drift-rate when
560 SFS is impaired (Philiastides et al., 2011) and where consequently, the circuitry takes more time to
561 form perceptual representations. In contrast, evidence in the form of size difference may depend on
562 the sensitivity to which SFS can detect the difference, and this is modulated by the decision threshold
563 (Herz et al., 2016; Cavanagh et al., 2011; Green et al., 2012, 2013). Here, SFS impairment to
564 accumulate evidence in the context of static, simultaneously presented stimuli may result in the
565 inability of the circuitry to reliably discriminate size differences, resulting in the early termination of the
566 accumulation process, which is behaviourally reflected as lower choice accuracy and faster RTs and
567 computationally as lower thresholds. While a common evidence framework can plausibly reconcile our
568 findings and that of previous studies, future studies should consider addressing this issue directly, by
569 comparing the different goal functions and stimulus displays within perceptual decision-making tasks.

570 **Functional coupling between left SFS and visual cortex.** Furthermore, our study further expands
571 our understanding of SFS function vis-à-vis other brain regions. It is well-established that the prefrontal
572 cortex is structurally connected with many other brain regions (Wycoco et al., 2013) and may flexibly
573 interact functionally with different areas depending on choice demands. Our exploratory connectivity
574 results suggest that the SFS role for domain-specific accumulation of perceptual evidence is not just
575 a local phenomenon but extends to functional communication with visual areas. Inhibition of this area's
576 functional contribution to evidence accumulation led to an increase in its functional coupling with areas
577 in occipital cortex representing the stimuli visually upon which choices were based. The changes in
578 functional coupling strength between the two cortical regions also corresponded to observed
579 behavioural and latent computational changes. This suggests that perceptual choices rely not only on
580 local processing in SFS but on an integrated functional circuit, comprising both SFS and occipital
581 cortex, at least for decisions based on visual stimuli as studied here. Though exploratory, our results
582 are generally consistent with an occipito-frontal information exchange but extend it specifically to the
583 SFS during perceptual evidence accumulation (Bullier et al., 1996).

584 We can speculate why the occipital cortex may have been recruited after inhibition of the left SFS via
585 cTBS stimulation. For example, it is possible that cTBS-related impairments in the accumulation
586 mechanism implemented by the SFS biases the system to rely on second-best suboptimal
587 mechanisms for solving the tasks, such as template matching from working memory. Previous work
588 has provided converging evidence that maintenance of visual information in working memory
589 enhances coupling between sensory processing in visual cortex and information storage in lateral
590 prefrontal cortex (Gazzaley et al., 2007; Serences et al., 2009). In fact, it has been suggested that
591 SFS is canonically organised in "memory receptive fields" (Postle, 2016) that may be more heavily
592 taxed when direct accumulation mechanisms for sensory input are impaired, as in the case of cTBS
593 manipulations. Of course, there are many other candidate mechanisms, such as attention or working
594 memory, that may be more heavily taxed to compensate for the excitability manipulation of the SFS
595 area specialized for processing the sensory evidence, as suggested by previous work on prefrontal-
596 occipital interactions during various attention and working memory tasks (Zanto et al., 2011). Overall,

597 the exploratory nature of our analysis warrants future investigation on the directionality of information
598 flow between occipital cortex and SFS. Additionally, future studies should also test whether perceptual
599 choices based on other sensory modalities (e.g., touch, audition) lead to a flexible coupling of SFS
600 with the specific sensory areas processing these stimuli. In any case, our study shows clearly that in
601 the healthy, undisrupted human brain, left SFS plays a key role in transforming perceptual evidence
602 into choices.

603 **Implications for theories of PFC organisation.** Our study also contributes to our understanding of
604 prefrontal cortex (PFC) functional organisation, given the considerable debates surrounding its
605 organising principles (Owen, 1997). Previous studies have posited that different PFC regions
606 contribute to specific aspects of information processing, in a manner that can be flexibly applied
607 to all types of information, be it from different sensory modalities or in different cognitive formats
608 (Petrides, 2005). Prevailing perspectives have also proposed an anterior-to-posterior hierarchy in PFC
609 for the purpose of general cognitive control and executive function (Nee and D'Esposito, 2016),
610 suggesting that the main role of the PFC is largely in the domain of higher-order cognitive and abstract
611 operations that transcend specific functional domains (Domenech and Koechlin, 2015; Koechlin and
612 Summerfield, 2007). In contrast, our finding of a domain-specific causal role of SFS in evidence
613 accumulation for perceptual decision-making suggests that the PFC is organised as a collection of
614 fractionated sub-regions, such that each region processes different types of information (Goldman-
615 Rakic and Leung, 2002), as opposed to a systematic hierarchy. Moreover, the fact that the SFS is
616 even involved in the integration of low-level perceptual evidence (Heekeren et al., 2004, 2006, 2008;
617 Philiastides et al., 2011; Rahnev et al., 2016) implies that the PFC's role is not limited to higher-order
618 cognitive function. Overall, our findings are in no position of proposing an overarching framework of
619 overall PFC organisation, given the limited area in posterior dlPFC targeted by our study, but rather a
620 call to consider alternative views where the underlying organisational principles are more fractionated
621 and less hierarchical.

622 **Implications for computational psychiatry.** Finally, our finding of SFS causal involvement in
623 decision-threshold-setting during perceptual decision-making may offer clinical implications.
624 Particularly, manifestations of impulsive behaviour (Heyes et al., 2012) are largely apparent in clinical
625 populations with aberrations in decision threshold setting (Herz et al., 2016). However, most studies
626 of these disorders have focused on impulsive behaviour induced by reward or preferences (Glimcher
627 et al., 2007). It is important to note here that reward impulsivity is only one of the many domains of
628 aberrant behaviour in clinical populations. Perceptual impulsivity is also important, since many of the
629 behavioural and cognitive deficits are closely linked to impairments in perceptual function (Fuermaier
630 et al., 2018). For instance, impulsive behaviour can also arise in non-reward-related settings, such as
631 when perceptually discriminating size differences where less accurate and faster responses have
632 been observed in people with addiction disorders (Banca et al., 2016) and borderline personality
633 disorder (Berlin and Rolls, 2004). Perceptual deficiencies are also prevalent in clinical populations with
634 attention-deficit hyperactivity disorder (ADHD) or Parkinson's disease, and thought to be linked to
635 impairments in the dopaminergic system (Fuermaier et al., 2018). Prior causal evidence from deep-
636 brain stimulation (DBS), in particular, has shown that disrupting the STN lowered decision thresholds,
637 thus increasing this perceptual impulsivity among Parkinson's patients (Herz et al., 2016, 2017). Our
638 findings that TMS of the left SFS causally and selectively lowered the decision boundary during
639 perceptual decisions suggest that the lateral prefrontal cortex may be functionally integrated with these
640 cortico-striatal and cortico-subthalamic nuclei (STN) pathways (Bogacz et al., 2010; Green et al., 2012,
641 2013).

642 Overall, impulsive behaviour is not exclusive to the reward domain, and our results suggest that there
643 is something to gain from understanding impulsive behaviour in non-reward settings requiring
644 decisions on perceptual information. Maladaptive behaviour may not only reflect individual wants or
645 likings, often assumed by addiction studies, but could also be a function of low-level sensory or higher-
646 order cognitive processes that have so far not fully been accounted for (Fuermaier et al., 2018). This

647 may have serious implications for how cognitive therapies or interventions are designed, and our
648 findings may provide useful insights in guiding such future work. Particularly, it is worth exploring to
649 what degree the left SFS and its connections are structurally or functionally different in clinical
650 populations, and whether these impulsive tendencies can be captured by sequential sampling models,
651 such as the DDM.

652

653 MATERIALS AND METHODS

654 **Participants.** Twenty healthy right-handed volunteers (ages 20-30; 8 female) with normal or
655 corrected-to-normal vision participated in the study. Participants were fully informed about the features
656 of the experiment. No participant suffered from any neurological or psychological disorder or took
657 medication that interfered with their participation in the study. Participants received monetary
658 compensation for participation and performance of the perceptual choices, as well as one food item
659 to consume after the experiment depending on a random value-based choice trial. The experiments
660 conformed to the Declaration of Helsinki and the experimental protocol was approved by the Ethics
661 Committee of the Canton of Zurich.

662 **Experimental paradigm.** We asked participants to refrain from eating for 3 hours before the start of
663 the experiment. Our experiments took place between 0800 and 1900 hr during the day. The
664 experiment consisted of two steps: (1) a rating task outside the scanner and (2) a decision-making
665 task inside the scanner. During the rating task, we asked participants to provide perceptual- and value-
666 based ratings of the same set of 61 food images using an on-screen slider scale. All of the food items
667 were in stock in our lab and participants were informed about this via visual inspection. For perceptual
668 ratings, participants rated—on a scale from 5 to 100 percent in steps of 5 percent—how much of the
669 black background within the white square perimeter was occupied by the food item. For value-based
670 ratings, participants rated—on a scale from 5 to 100 in steps of 5—how much they wanted to eat the
671 presented food item at the end of the experiment. We instructed participants that the midpoint of the
672 scale in value-based ratings indicated indifference.

673 After rating the food items, an algorithm selected a balanced set of perceptual and value-based trials
674 divided into four evidence levels, E . The evidence levels are based on the absolute difference between
675 the average ratings of the food items paired in each trial. We define perceptual evidence as the
676 absolute size difference between the two food items. On the other hand, we define value-based
677 evidence as the absolute value difference between the two food items. In particular, the evidence
678 levels for perceptual trials, E_p , are:

$$679 \quad E_p = |r_{\text{biggest}} - r_{\text{smallest}}| \in \{5\%, 10\%, 15\%, 20\%\}$$

680 while the evidence levels for value-based trials, E_v , are:

$$681 \quad E_v = |r_{\text{best}} - r_{\text{worst}}| \in \{1, 2, 3, 4\}$$

682 where $r = \frac{r_1 + r_2}{2}$ is the average food item from the two ratings while $r_{\text{biggest}} - r_{\text{smallest}}$ and $r_{\text{best}} - r_{\text{worst}}$
683 represent the ratings' difference for the pairs presented for perceptual and value-based choices,
684 respectively.

685 Inside the scanner, participants performed the decision-making task for which they chose between
686 two food items, based on whether they were accumulating perceptual or value-based evidence. We
687 matched the visual sensory stimuli of the food items as well as their motor outputs across the two

688 choice types. The only difference was the type of evidence participants had to accumulate to make a
689 choice. Each trial started with presentation of a central fixation marker (length ~ 0.8°, height ~ 0.3°).
690 Next, a centrally presented word indicated whether participants would perform a perceptual (word
691 'AREA') or value-based (word 'LIKE') choice. On the subsequent screen, the task cue was replaced
692 by either the letter 'A' or 'L' (~ 0.2°) to remind participants that they were in a perceptual or value-
693 based block, respectively. Two food items were simultaneously displayed, one above and one below
694 the screen (y eccentricity 3.6°; a white square of 6° width surrounded each food item). Blocks
695 alternated between perceptual and value-based choices in a given session (7-9 trials per task block).
696 Participants pressed one of two buttons on a keypad with their right middle finger (upper item) or right
697 index finger (lower item) to indicate their choice. On a given trial, participants had 3 seconds for their
698 choice; otherwise, the trial would be regarded as a 'missed trial' and would not enter the analysis.
699 Analyses were conducted on valid trials only, defined as trials with a registered response within the
700 task's response window and passing pre-specified validity checks; trials without a response were
701 excluded and not analysed. Participants made correct or consistent choices when they chose the food
702 item with the higher rating as indicated in the double ratings task prior to entering the scanner. After
703 the experiment, participants stayed in the room with the experimenter while they ate the food that was
704 selected based on the participants choice in one randomly selected VDM trial. During perceptual
705 decisions-making blocks, participants were rewarded with 0.5 CHF every time they correctly
706 discriminated between the size difference of the two food items presented on the monitor screen.

707 The experiment had a total of 256 trials divided into 8 sessions of 32 trials each. The first 4 sessions
708 were pre-stimulation sessions where participants performed the task without stimulation. The last 4
709 sessions were post-stimulation sessions during which participants performed the choices with
710 decreased neural excitability in the SFS due to the preceding continuous theta-burst stimulation. The
711 256 trials were fully balanced across all factors (trial type: perceptual or value-based; evidence levels:
712 1 to 4; correct response: up or down).

713 **Stimulation protocol.** We applied continuous theta-burst stimulation (cTBS) (Huang et al., 2005; di
714 Lazzaro et al., 2005, 2008) to exogenously induce cortical inhibition of our region of interest (ROI), an
715 area in the left superior frontal sulcus (SFS) (MNI coordinates: $x = -24, y = 24, z = 36$) (Heekeren et
716 al., 2004; Philiastides et al., 2011). Before the main fMRI experiment, we identified the stimulation site
717 over the left SFS (MNI coordinates: $x = -24, y = 24, z = 36$) (Heekeren et al., 2004; Philiastides et al.,
718 2011) based on previous studies and each individual's stimulation intensity. In an initial fMRI session,
719 we acquired high-resolution T1-weighted 3D fast-field echo anatomical scans used for subsequent
720 neuro-navigation (181 sagittal slices, matrix size = 256 × 256, voxel size = 1 mm³, TR/TE/TI =
721 8.3/2.26/181 ms, 3T Philips Achieva). The hand area of the left M1 (motor hotspot) was determined
722 by identifying the first dorsal interosseous (FDI) movement-evoked potentials (MEPs) induced by
723 transcranial magnetic stimulation (TMS) pulses. We delivered single monophasic TMS pulses using a
724 figure-of-eight coil attached to the TMS stimulator. We then marked an equidistant circular grid on
725 each individual's anatomical MRI scan using a neuro-navigation system over the hand motor region,
726 located at the anterior portion of the central sulcus. We localised the optimal motor hotspot as the point
727 in the grid that elicited the strongest FDI MEPs from TMS pulses. Once we selected the motor hotspot,
728 we asked participants to activate their FDI by pressing their thumb and index finger at about 20%
729 maximum force in order to obtain their active motor threshold (AMT). We defined the AMT as the
730 minimal TMS intensity required to produce MEPs of ≥ 200 mV amplitude (measured with Magventure
731 MRI-B91) in ≥ 5–10 consecutive pulses. We retested the AMT by visually inspecting the FDI twitches
732 triggered by TMS pulses over the marked optimal hotspot. The average AMT outside the scanner was
733 52.35 ± 6.27 percent while the AMT inside the scanner was 52.91 ± 6.18 percent. We applied cTBS
734 at an intensity of 80% of the individual's AMT. The cTBS protocol contained bursts of 3 pulses at 50
735 Hz. This protocol has been shown to reduce cortical excitability for at least 30 minutes (Huang et al.,
736 2005). Every burst was repeated at a rate of 5 Hz, resulting in 200 bursts with a total of 600 pulses
737 delivered within 40 seconds.

738 Before moving our participant into the scanner, we marked the motor hotspot as well as the stimulation
 739 site on a swimming cap fixed in position by straps. Participants wore this cap while they were inside
 740 the scanner. Before the start of the fifth session, participants received cTBS over the left SFS. We
 741 used a figure-of-eight MR-compatible TMS coil (MRI-B91) attached to a TMS stimulator. Participants
 742 returned to the scanner after receiving stimulation and proceeded to complete the last four sessions.
 743 On average, the post-TMS fMRI task started 228 ± 41 sec after the end of theta-burst stimulation
 744 following established protocols from previous studies (Knecht et al., 2003; Philiastides et al., 2011;
 745 Thut and Pascual-Leone, 2010). Given the established timeline of cTBS effects (Huang et al., 2005),
 746 we expected the stimulation effects to weaken over time due to neural recovery. In line with established
 747 procedures, we treated the first two post-stimulation sessions as the actual post-cTBS period and the
 748 last two post-stimulation sessions as a recovery period (Philiastides et al., 2011).

749 **Differences-in-differences.** We implemented a differences-in-differences (DID) regression analysis
 750 to identify the causal relationships based on stimulation-induced neural inhibition in SFS. We used the
 751 identical DID for behavioural, computational, neuroimaging and connectivity analyses. Here, we use
 752 the following notation: task conditions *Task* (perceptual, *Task* = 1; value-based, *Task* = 0); stimulation
 753 conditions *TMS* (pre- *TMS* = 0 and post- *TMS* = 1); *V* is our variable of interest, which may be
 754 behavioural or neural; and, the causal treatment effect, $\phi(V|Task, TMS)$, takes the following form:

$$\begin{aligned} 755 \quad \phi(V|Task, TMS) \\ 756 \quad &= [\mathbb{E}(V|TMS = 1, Task = 1) - \mathbb{E}(V|TMS = 0, Task = 1)] \\ 757 \quad &\quad - [\mathbb{E}(V|TMS = 1, Task = 0) - \mathbb{E}(V|TMS = 0, Task = 0)] \end{aligned}$$

758 where $\mathbb{E}(V|Task, TMS)$ is the expected value of the variable of interest, *V*, given task and TMS
 759 condition. The first difference on the right-hand side captures the average stimulation effect for PDM
 760 while the second difference captures the average stimulation effect for VDM. The overall difference
 761 assumes that if behaviour will be the same after stimulation, then there is no effect, $\phi = 0$ (Angrist and
 762 Pischke, 2009; Bertrand et al., 2004). But if there is a stimulation effect and it impairs behaviour or
 763 neural activity, then $\phi < 0$.

764 **Behavioural analyses for choice.** We analysed the influence of continuous theta-burst stimulation
 765 on choice using a logit regression on choices, ρ (correct = 1, incorrect = 0) over various regressors of
 766 interest, such as TMS condition, *TMS* (pre-cTBS = 0, post-cTBS = 1); task, *Task* (perceptual = 1,
 767 value-based = 0); its interaction (*Task* \times *TMS*), which measures the causal stimulation effect, ϕ ; and,
 768 other regressors, X^k that we use as controls. This includes task-relevant evidence (SD for perceptual
 769 and VD for value-based, 1 to 4), response times (RTs), and task-irrelevant evidence (i.e. VD for
 770 perceptual and SD for value-based, 1 to 4). The full model is,

$$771 \quad \Pr(\rho_{t,c,s,i}^{DID}) = \frac{1}{1 + \exp(-[\beta_0 + \beta_1 Task_{(t,c,s,i)} + \beta_2 TMS_{(t,c,s,i)} + \phi Task_{(t,c,s,i)} TMS_{(t,c,s,i)} + \sum_{k=4}^n \beta_k X_{(t,c,s,i)}^k])}$$

772 where *t* indexes task, *c* for TMS, *s* for subject, and *i* for trial. Since our model contains a DID interaction
 773 term, nonlinearity of the logit regression results is a non-zero estimate even if the true causal effect is
 774 zero, $\phi = 0$.

775 To remove nonlinearity bias and isolate the true causal effect, we ran another logit regression
 776 without the interaction term,

$$777 \quad \Pr(\rho_{t,c,s,i}^{NODID}) = \frac{1}{1 + \exp(-[\beta_0 + \beta_1 Task_{(t,c,s,i)} + \beta_2 TMS_{(t,c,s,i)} + \sum_{k=4}^n \beta_k X_{(t,c,s,i)}^k])}$$

778 and we take the difference between the two logits (Ai and Norton, 2003; Karaca-Mandic et al., 2012;
779 Puhani, 2012),

780 $\Pr(\rho_{(t,c,s,i)}^{TRUE DID}) = \Pr(\rho_{(t,c,s,i)}^{DID}) - \Pr(\rho_{(t,c,s,i)}^{NO DID}).$

781 We also ran variations of the model to test for robustness, particularly GLMs with or without control
782 variables, and we also tested robustness using various stimulation runs (see **Supplementary Table**
783 **5**). We used cluster-robust standard errors at the subject level under the assumption that each
784 individual performance is independent across participants. We implemented this analysis using
785 STATA/SE 13.1.

786 **Behavioural analyses for response times.** We similarly used DID regressions to analyse the
787 influence of cTBS on response times (rt). Here, we simply ran a general linear model (GLM) for our
788 regression,

789 $rt_{t,c,s,i} = \beta_0 + \beta_1 Task_{(t,c,s,i)} + \beta_2 TMS_{(t,c,s,i)} + \phi Task_{(t,c,s,i)} TMS_{(t,c,s,i)} + \sum_{k=4}^n \beta_k X_{(t,c,s,i)}^k + \varepsilon_{(t,c,s,i)}$

790 and we also ran variations of the model (see also **Supplementary Table 5**). We similarly used cluster-
791 robust standard errors at the subject level.

792 Hierarchical Bayesian DDM. We analysed the effect of cTBS on PDM and VDM using hierarchical drift
793 diffusion model (HDDM). The model assumes evidence is accumulated through a one-dimensional
794 Wiener process, whereby the state of evidence, x_t at time t evolves through a stochastic differential
795 equation,

796 $\frac{dx_t}{dt} \sim \mathbb{N}(\delta, \sigma^2).$

797 Here, δ is the amount of evidence being accumulated at time t ,

798 $\delta = \kappa_{c,s} E_{c,s,i}$

799 where E represents the evidence level and κ is the drift-rate that linearly scales the evidence and this
800 is typically interpreted as quality of information processing. The model assumes evidence is
801 accumulated at the starting point, β , and the accumulation process continues until a choice, ρ , is
802 made at time t_d at a given threshold, α . Once the accumulation process terminates, the state of
803 evidence is either $x_t > \alpha$ (a correct decision) or $x_t \leq 0$ (an incorrect decision). We also accounted for
804 visual sensory processing and motor response delays with the non-decision time parameter (nDT), τ .

805 The hierarchical Bayesian model is implemented whereby each observed choice, $y_{c,s,i}(\rho, rt)$, follows
806 a Wiener distribution, ω ,

807 $y_{(c,s,i)} \sim \omega(\delta, \alpha, \tau, \beta)$

808 where c indexes task ($c = p$ for perceptual, $c = v$ for value-based), s for participants ($s =$
809 $1, \dots, N_{subjects}$), and i for trials ($i = 1, \dots, N_{trials}$). Furthermore, the hierarchical structure contains three
810 random variations at the trial, subject, and condition levels. We treated all interindividual differences
811 per stimulation condition level as random effects:

812 $\delta_{(c,s,i)} \sim N(\mu_{\delta(s)} E_{(c,s,i)}, \sigma_{\delta(s)}^2)$

813 $\tau_{(c,s,i)} \sim N(\mu_{\tau(s)}, \sigma_{\tau(s)}^2)$

814 $\alpha_{(c,s,i)} \sim N(\mu_{\alpha(s)}, \sigma_{\alpha(s)}^2)$

815 where $N(\mu, \sigma)$ is a normal distribution with mean, μ and standard deviation, σ . Here, E represents the
816 trial-by-trial evidence levels, which we measure in absolute terms; and we fix the starting point, $\beta_{c,s,i} =$
817 0.5. We used Bayesian hypothesis testing to compare posterior probability densities.

818 **Measure of accumulated evidence.** We computed estimates for decision times ($t_{d(c,s)}$) and
819 accumulated evidence ($aE_{c,s}$) to test whether aE is a plausible representation of the accumulation
820 process at the neural level. Following the literature (Bogacz et al., 2006, 2010), we define mean
821 decision time as the ratio between the decision threshold and the drift rate shaped by a hyperbolic
822 tangent function,

823
$$t_{d(c,s)} = \left(\frac{\alpha_{c,s}}{\kappa_{c,s}} \right) \tanh(\kappa_{c,s} \times \alpha_{c,s})$$

824 It is important to note that reaction time, rt , is the sum of both decision and non-decision times, $rt =$
825 $t_d + \tau$.

826 We define accumulated evidence (aE) as the area below the drift process up until the accumulator
827 reaches the decision boundary:

828
$$aE_{c,s} = \frac{\alpha_{c,s} \times t_{d(c,s)}}{2}.$$

829 Here, we derive aE using the area equation of a triangle, where decision time $t_{d(c,s)}$ is the base and
830 the decision boundary, $\alpha_{c,s}$, is the height.

831 **MCMC sampling.** To estimate all parameters, we performed Gibbs sampling via Markov Chain
832 Montecarlo (MCMC) in JAGS (Plummer, 2016) to generate parameter posterior inferences. We drew
833 a total of 100,000 samples from an initial burn-in step and subsequently drew a total of new 100,000
834 samples with three chains each. We derived each chain based on different random number generator
835 engines with different seeds. We applied a thinning of 100 to this final sample, resulting in a final set
836 of 1,000 samples for each parameter. This thinning assured auto-decorrelation for all latent variables
837 of interest. We conducted Gelman-Rubin tests for each parameter to confirm chain convergence. All
838 latent parameters in our Bayesian model had $\hat{R} < 1.05$, suggesting that all three chains converged to
839 a target posterior distribution. We compared the difference in posterior population distributions
840 estimated for each parameter between the stimulation conditions as well as the differences-in-
841 differences (DID), which included differences between tasks. We tested whether the resulting
842 distribution (i.e., the causal stimulation effect) is significantly different from zero (i.e., the null
843 hypothesis) using the cumulative function up to or from 0 depending on the direction of the effect. We
844 refer to this probability as Bayesian “p-values,” p_{mcmc} .

845 **fMRI data analysis.** Participants performed eight choice-task sessions while BOLD images were
846 recorded with a Philips Achieva 3T whole-body scanner. We used statistical parametric mapping
847 (SPM8, Wellcome Trust Center for Neuroimaging) for image pre-processing and analysis. In particular,
848 images were slice-time corrected (to the acquisition time of the middle slice) and realigned to account

849 for subject's head motion. Each participant's T1-weighted structural image was co-registered with the
850 mean functional image and normalised to the standard T1 MNI template using the new-segment
851 procedure in SPM8. The functional images were normalised to the standard MNI template using the
852 same transformation, spatially resampled to 3mm isotropic voxels, and smoothed using a Gaussian
853 kernel (FWHM, 8mm).

854 We estimated two general linear models (GLMs), constructed by convolving a series of appropriately
855 placed indicator functions with the default model of the BOLD response embedded in SPM8. GLM1
856 contained only two indicator functions for the onsets of PDM or VDM trials. On the other hand, GLM2
857 contained four indicator functions for the onsets of task (PDM and VDM trials) and stimulation (pre- or
858 post-TMS) runs, coupled with one regressor each for parametric modulation of the BOLD response by
859 the trialwise accumulated evidence (aE). We earlier demonstrated that the theoretical average
860 accumulated evidence is derived from population-level as well as subject-level latent DDM
861 parameters, by dividing the estimated decision boundary by the estimated drift rate. To construct a
862 trialwise measure of aE , we exploit the fact that the length of the RTs is directly proportional to the
863 size of the decision boundary while the evidence level, E , is directly proportional to the drift rate (Basten
864 et al., 2010; Domenech et al., 2017; Kiani et al., 2014). With this mapping, we can then construct a
865 parametric trialwise measure of accumulated evidence, $aE_{t,c,s,i}$,

866
$$aE_{t,c,s,i} = \sqrt{\frac{RT_{t,c,s,i}}{E_{t,c,s,i}}},$$

867 where the square root function accounts for the concave nonlinearity in accumulated evidence.
868 Previous work (Tajima et al., 2016) has shown theoretically that the shape of the accumulated
869 evidence is indeed concave, where it suggests that the rate of accumulating evidence is decreasing
870 as the decision process continues to accumulate. This concavity in aE is consistent with DDM
871 predictions where evidence accumulation is steeper during earlier responses and begins to plateau at
872 later responses (Ratcliff and McKoon, 2008; Ratcliff and Smith, 2004).

873 We convolved our GLMs with a canonical haemodynamic response function (HRF), modelled MR
874 image autocorrelations with first-order autoregressive model, and included 6 motion parameters
875 (obtained during realignment) as regressors of no interest. After fitting the model to the BOLD data,
876 we tested regressors for statistical significance at the second-level, in random-effects group one-
877 sample t-tests of the corresponding single-subject contrast images. We performed statistical inference
878 at the cluster level, using whole-brain family-wise-error-corrected (FWE-corrected) statistical threshold
879 of $p < 0.05$, based on a cluster-forming voxel cutoff at $p < 0.005$ (or $T(19) = 2.9$). For hypothesis-
880 guided region-of-interest (ROI) analysis (i.e., left SFS stimulation site, MNI coordinates: $x = -24, y =$
881 $24, z = 36$), we corrected for multiple comparisons using small-volume correction (SVC, $p < 0.05$)
882 restricted within a 10 mm sphere around the target coordinates. We extracted neural betas from this
883 spherical SFS ROI for each participant to perform hypothesis testing and correlational analysis.

884 **Functional connectivity.** We ran a psychophysiological interaction (PPI) analysis (Friston et al.,
885 1997) to investigate the changes in functional connectivity between the left SFS and other brain
886 regions due to cTBS. Here, we extracted physiological time series in the SFS seed region, which
887 corresponds to the time-course of the first eigenvariate across all voxels in the region using principal
888 component analysis (Friston et al., 1993). The psychological regressor corresponded to the difference
889 in accumulated evidence, aE (as described in GLM2) between PDM and VDM. We generated PPI
890 estimates from the psychological regressors and the time series from the left SFS, and we then
891 computed the PPI contrasts-of-interest for PDM and VDM. Statistical inference on subject-specific PPI
892 maps was performed using second-level random-effects analysis across participants to allow for
893 group-level inferences. For each participant, we also extracted PPI neural betas, which measures the

894 degree of functional coupling between the left SFS, and we then performed hypothesis testing and
 895 correlational analysis.

896 **Hierarchical Bayesian neural-DDM.** We also analysed whether the inclusion of raw trial-by-trial
 897 BOLD response extracted from left SFS and attach it to any of the DDM parameters can improve
 898 model evidence. Such a result would suggest that neural activity in the left SFS directly related to the
 899 model's latent decision-relevant parameters. We used z-scored single-trial neural beta estimates
 900 extracted from the left SFS target site. We implemented four a-priori models regarding the role of the
 901 left SFS on the decision parameters: **Model 1** assumes that the left SFS modulated the decision
 902 threshold (**Supplementary Fig. 8a**), while **Model 2** assumes that left SFS modulated the drift rate
 903 (**Supplementary Fig. 8b**):

$$904 \quad \alpha_{c,s,i}^{NEURAL} = \alpha_{c,s,i} + \gamma \theta_{c,s,i}$$

$$905 \quad \delta_{c,s,i}^{NEURAL} = \kappa E_{c,s,i} + \gamma \theta_{c,s,i}$$

906 where γ is the scale parameter for trial-by-trial left SFS activity, θ . On the other hand, Models 3 and 4
 907 assume that the left SFS modulates both boundary and drift: **Model 3** assumes separate scale
 908 parameters for each latent process (see **Supplementary Fig. 8c**) while **Model 4** assumes a common
 909 scale parameter for both boundary and drift (see **Supplementary Fig. 8d**). Model comparison used
 910 the Deviance Information Criterion ($DIC = \bar{D} + pD$), where pD is the effective number of parameters;
 911 thus DIC penalizes model complexity, and lower DIC denotes better predictive accuracy after
 912 accounting for complexity. We then used the best model to re-estimate our latent parameters and to
 913 perform Bayesian post-hoc inferences.

914 **Correlating causal changes between neural, latent, and behavioural variables.** We tested
 915 whether there were any correlational changes between neural, v , and behavioural, π , measures after
 916 stimulation. The marginal effect, r , measures the correlational change in neural measure, v , given
 917 behavioural measure, π ,

$$918 \quad r(v_{c,s}|\pi_{c,s}) = \frac{\partial}{\partial \pi_{c,s}} \mathbb{E}(v_{c,s}|\pi_{c,s}).$$

919 We test the marginal effect, r , of the correlational change between our neural and behavioural
 920 measures using our DID regression at trial and subject levels. With trialwise data, we used logit
 921 regression to test whether the marginal effect of trialwise changes in left SFS, $Neur$, will affect choices,
 922 ρ . Similar to previous models, we included various regressors of interest, especially the triple
 923 interaction ($Neur \times Task \times TMS$), which accounts for the causal TMS effect, ϕ , as well as other
 924 regressors, X^k . The full model is,

$$925 \quad \Pr(\rho_{(t,c,s,i)}^{DID}) = \left(1 \right. \\ 926 \quad \left. + \exp \left[- \left(\beta_0 + \beta_1 Task_{(t,c,s,i)} + \beta_2 TMS_{(t,c,s,i)} + \beta_3 Neur_{(t,c,s,i)} + \beta_4 [Task_{(t,c,s,i)} TMS_{(t,c,s,i)}] \right. \right. \right. \\ 927 \quad \left. \left. + \beta_5 [Neur_{(t,c,s,i)} Task_{(t,c,s,i)}] + \beta_6 [Neur_{(t,c,s,i)} TMS_{(t,c,s,i)}] \right) \right. \\ 928 \quad \left. \left. + \phi [Neur_{(t,c,s,i)} Task_{(t,c,s,i)} TMS_{(t,c,s,i)}] + \sum_{k=4}^n \beta_k X_{(t,c,s,i)}^k \right) \right] \right)^{-1}.$$

929 To remove nonlinearity bias and isolate the true causal effect, we ran another logit regression without
 930 ϕ ,

$$\Pr(\rho_{(t,c,s,i)}^{NODID}) = \left(1 + \exp \left[- \left(\beta_0 + \beta_1 Task_{(t,c,s,i)} + \beta_2 TMS_{(t,c,s,i)} + \beta_3 Neur_{(t,c,s,i)} + \beta_4 [Task_{(t,c,s,i)} TMS_{(t,c,s,i)}] \right. \right. \right. \\ \left. \left. \left. + \beta_5 [Neur_{(t,c,s,i)} Task_{(t,c,s,i)}] + \beta_6 [Neur_{(t,c,s,i)} TMS_{(t,c,s,i)}] + \sum_{k=4}^n \beta_k X_{(t,c,s,i)}^k \right) \right] \right)^{-1},$$

934 and then we took the difference between the two logit models,

$$\Pr(\rho_{(t,c,s,i)}^{TRUE DID}) = \Pr(\rho_{(t,c,s,i)}^{DID}) - \Pr(\rho_{(t,c,s,i)}^{NODID}).$$

936 We similarly ran a DID-GLM to test whether the marginal effect of trialwise left SFS neural betas will
 937 causally affect RTs,

$$rt_{(t,c,s,i)} = \beta_0 + \beta_1 Task_{(t,c,s,i)} + \beta_2 TMS_{(t,c,s,i)} + \beta_3 Neur_{(t,c,s,i)} + \beta_4 [Task_{(t,c,s,i)} TMS_{(t,c,s,i)}] \\ + \beta_5 [Neur_{(t,c,s,i)} Task_{(t,c,s,i)}] + \beta_6 [Neur_{(t,c,s,i)} TMS_{(t,c,s,i)}] \\ + \phi [Neur_{(t,c,s,i)} Task_{(t,c,s,i)} TMS_{(t,c,s,i)}] + \varepsilon_{(t,c,s,i)}.$$

941 We also used cluster-robust standard errors at the subject level in all of our analysis.

942 With subject-level data, we similarly used linear mixed-effects regression models to test whether the
 943 marginal effect of subject-level neural betas (left SFS or PPI) ν , will affect behavioural outcomes or
 944 DDM-latent parameters, π . Similarly, we estimated the marginal effect, ϕ , with a three-way interaction,
 945 $(\nu \times Task \times TMS)$,

$$\pi_{(c,s)} = \beta_0 + \beta_1 Task_{(c,s)} + \beta_2 TMS_{(c,s)} + \beta_3 \nu_{(c,s)} + \beta_4 [Task_{(c,s)} \times TMS] + \beta_5 [\nu_{(c,s)} \times Task_{(c,s)}] \\ + \beta_6 [\nu_{(c,s)} \times TMS_{(c,s)}] + \phi [\nu_{(c,s)} \times Task_{(c,s)} \times TMS_{(c,s)}] + \varepsilon_{(c,s)}.$$

948 This three-way interaction measures whether the correlations between neural activity (left SFS, PPI
 949 betas) and behaviour (choice, DDM parameters) are causally affected by stimulation, TMS , and
 950 whether the effect is specific only during the perceptual task.

951 DATA AND CODE AVAILABILITY

952 Behavioural and neuroimaging data and the code for data analysis are available at 10.17605/OSF.IO/
 953 3DMH9.

954 ACKNOWLEDGEMENTS

955 This work was supported by grants of the SNSF (105314_152891, CRSII3_141965 and 51NF40_
 956 144609) and the SNSF NCCR Affective Sciences to CCR.

957 CONTRIBUTIONS

958 MBG, MG, MM, RP and CCR conceived the experiment. MBG, MG, and MM collected andanalysed
959 the data with inputs from RP and CCR. MBG, MG, and CCR wrote the manuscript with inputs from RP
960 and MM.

961 REFERENCES

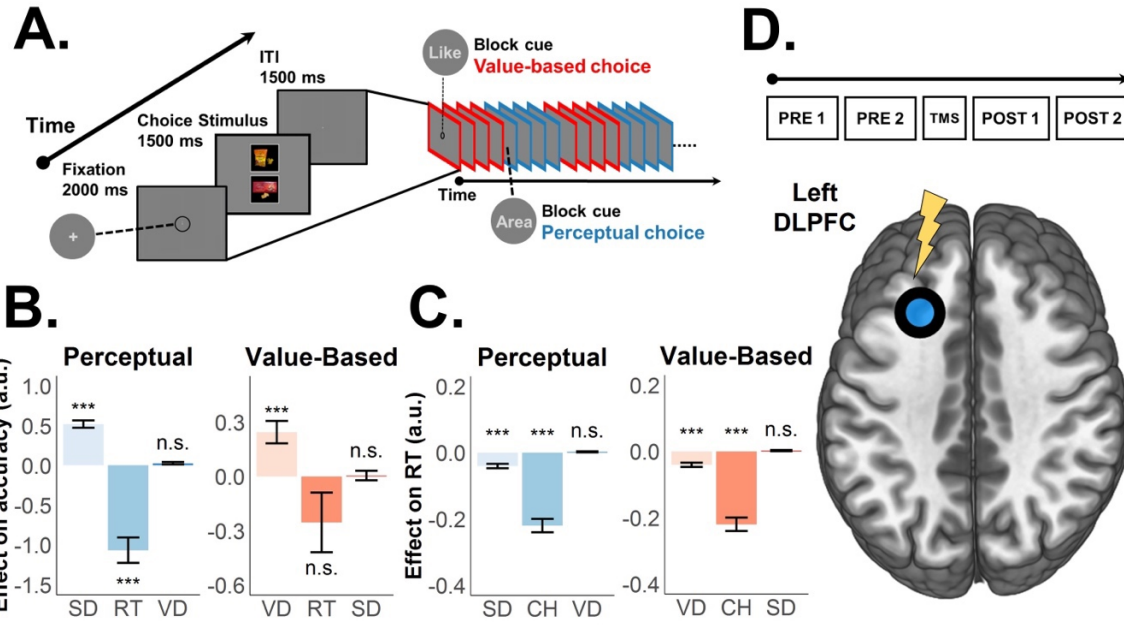
- 962 1 Ai, C., and Norton, E.C. (2003). Interaction terms in logit and probit models. *Economics Letters* 80, 123–129.
963
964 2 Angrist, J.D., and Pischke, J.-S. (2009). *Mostly Harmless Econometrics: An Empiricist's Companion* (Princeton, NJ: Princeton University Press).
965
966 3 Badre, D., and D'Esposito, M. (2007). Functional Magnetic Resonance Imaging Evidence for a Hierarchical Organization of the Prefrontal Cortex. *Journal of Cognitive Neuroscience* 19, 2082–2099.
967
968 4 Banca, P., Lange, I., Worbe, Y., Howell, N.A., Irvine, M., Harrison, N.A., Moutoussis, M., and Voon, V. (2016). Reflection impulsivity in binge drinking: Behavioural and volumetric correlates. *Addiction Biology* 21, 504–515.
969
970 5 Barbey, A.K., Koenigs, M., and Grafman, J. (2013). Dorsolateral prefrontal contributions to human working memory. *Cortex* 49, 1195–1205.
971
972 6 Basten, U., Biele, G., Heekeren, H.R., and Fiebach, C.J. (2010). How the brain integrates costs and benefits during decision making. *Proceedings of the National Academy of Sciences* 107, 21767–21772.
973
974 7 Berlin, H.A., and Rolls, E.T. (2004). Time Perception, Impulsivity, Emotionality, and Personality in Self-Harming Borderline Personality Disorder Patients. *Journal of Personality Disorders* 18, 358–378.
975
976 8 Bertrand, M., Duflo, E., and Mullainathan, S. (2004). How Much Should We Trust Differences-In-Differences Estimates? *The Quarterly Journal of Economics* 119, 249–275.
977
978 9 Bogacz, R., Brown, E., Moehlis, J., Holmes, P., and Cohen, J.D. (2006). The physics of optimal decision making: A formal analysis of models of performance in two-alternative forced-choice tasks. *Psychological Review* 113, 700–765.
979
980 10 Bogacz, R., Wagenmakers, E.J., Forstmann, B.U., and Nieuwenhuis, S. (2010). The neural basis of the speed-accuracy tradeoff. *Trends in Neurosciences* 33, 10–16.
981
982 11 Brody, C.D., and Hanks, T.D. (2016). Neural underpinnings of the evidence accumulator. *Current Opinion in Neurobiology* 37, 149–157.
983
984 12 Brunton, B.W., Botvinick, M.M., and Brody, C.D. (2013). Rats and Humans Can Optimally Accumulate Evidence for Decision-Making. *Science* 340, 95–98.
985
986 13 Bullier, J., Schall, J.D., and Morel, A. (1996). Functional streams in occipito-frontal connections in the monkey. *Behavioural Brain Research* 76, 89–97.
987
988 14 Busemeyer JR, Townsend JT. (1993). Decision Field-Theory - a Dynamic Cognitive Approach to Decision-Making in an Uncertain Environment. *Psychological Review* 100: 432-59
989
990 15 Cavanagh, J.F., Wiecki, T. v., Cohen, M.X., Figueiroa, C.M., Samanta, J., Sherman, S.J., and Frank, M.J. (2011). Subthalamic nucleus stimulation reverses mediofrontal influence over decision threshold. *Nature Neuroscience* 14, 1462–1467.
991
992 16 de Martino, B., Fleming, S.M., Garrett, N., and Dolan, R.J. (2013). Confidence in value-based choice. *Nature Neuroscience* 16, 105–110.
993
994 17 di Lazzaro, V., Pilato, F., Saturno, E., Oliviero, A., Dileone, M., Mazzone, P., Insola, A., Tonali, P.A., Ranieri, F., Huang, Y.Z., et al. (2005). Theta-burst repetitive transcranial magnetic stimulation suppresses specific excitatory circuits in the human motor cortex. *The Journal of Physiology* 565, 945–950.
995
996 18 di Lazzaro, V., Ziemann, U., and Lemon, R.N. (2008). State of the art: Physiology of transcranial motor cortex stimulation. *Brain Stimulation* 1, 345–362.
997
998 19 Ding, L., and Gold, J.I. (2012a). Neural Correlates of Perceptual Decision Making before, during, and after Decision Commitment in Monkey Frontal Eye Field. *Cerebral Cortex* 22, 1052–1067.
999
1000 20 Ding, L., and Gold, J.I. (2012b). Separate, Causal Roles of the Caudate in Saccadic Choice and Execution in a Perceptual Decision Task. *Neuron* 75, 865–874.
1001
1002 21 Domenech, P., and Dreher, J.-C. (2010). Decision Threshold Modulation in the Human Brain. *Journal of Neuroscience* 30, 14305–14317.
1003
1004
1005
1006
1007
1008
1009
1010
1011
1012

- 1013 22 Domenech, P., and Koechlin, E. (2015). Executive control and decision-making in the
1014 prefrontal cortex. *Current Opinion in Behavioral Sciences* 1, 101–106.
1015 23 Domenech, P., Redouté, J., Koechlin, E., and Dreher, J.-C. (2017). The Neuro-Computational
1016 Architecture of Value-based Selection in the Human Brain. *Cerebral Cortex* 1–17.
1017 24 Dutilh G, Rieskamp J. (2016). Comparing perceptual and preferential decision making.
1018 *Psychon Bull Rev* 23: 723-37
1019 25 Erlich, J.C., Brunton, B.W., Duan, C.A., Hanks, T.D., and Brody, C.D. (2015). Distinct effects
1020 of prefrontal and parietal cortex inactivations on an accumulation of evidence task in the rat.
1021 *ELife* 4.
1022 26 Feltgen, Q., and Daunizeau, J. (2020). Fitting drift-diffusion decision models to trial-by-trial
1023 data. *BioRxiv*.
1024 27 Filimon, F., Philiastides, M.G., Nelson, J.D., Kloosterman, N.A., and Heekeren, H.R. (2013).
1025 How Embodied Is Perceptual Decision Making? Evidence for Separate Processing of
1026 Perceptual and Motor Decisions. *Journal of Neuroscience* 33, 2121–2136.
1027 28 Forstmann, B.U., Wagenmakers, E.-J., Eichele, T., Brown, S., and Serences, J.T. (2011).
1028 Reciprocal relations between cognitive neuroscience and formal cognitive models: opposites
1029 attract? *Trends in Cognitive Sciences* 15, 272–279.
1030 29 Friston, K.J., Frith, C.D., Liddle, P.F., and Frackowiak, R.S.J. (1993). Functional Connectivity:
1031 The Principal-Component Analysis of Large (PET) Data Sets. *Journal of Cerebral Blood Flow
& Metabolism* 13, 5–14.
1032 30 Friston, K.J., Buechel, C., Fink, G.R., Morris, J., Rolls, E., and Dolan, R.J. (1997).
1033 Psychophysiological and Modulatory Interactions in Neuroimaging. *NeuroImage* 6, 218–229.
1034 31 Fuurmaier, A.B.M., Hüpen, P., de Vries, S.M., Müller, M., Kok, F.M., Koerts, J., Heutink, J.,
1035 Tucha, L., Gerlach, M., and Tucha, O. (2018). Perception in attention deficit hyperactivity
1036 disorder. *ADHD Attention Deficit and Hyperactivity Disorders* 10, 21–47
1037 32 Gazzaley, A., Rissman, J., Cooney, J., Rutman, A., Seibert, T., Clapp, W., and D'Esposito, M.
1038 (2007). Functional Interactions between Prefrontal and Visual Association Cortex Contribute
1039 to Top-Down Modulation of Visual Processing. *Cerebral Cortex* 17, i125–i135.
1040 33 Glickman, M., Sharoni, O., Levy, D.J., Niebur, E., Stuphorn, V., and Usher, M. (2019). The
1041 formation of preference in risky choice. *PLoS Computational Biology* 15, e1007201.
1042 34 Glimcher, P.W., Kable, J., and Louie, K. (2007). Neuroeconomic Studies of Impulsivity: Now
1043 or Just as Soon as Possible? *American Economic Review* 97, 142–147.
1044 35 Gold JI, Shadlen MN. (2007). The neural basis of decision making. *Annual Review of
1045 Neuroscience* 30: 535-74
1046 36 Goldman-Rakic, P.S., and Leung, H.-C. (2002). Functional Architecture of the Dorsolateral
1047 Prefrontal Cortex in Monkeys and Humans (Oxford University Press).
1048 37 Green, N., Biele, G.P., and Heekeren, H.R. (2012). Changes in Neural Connectivity Underlie
1049 Decision Threshold Modulation for Reward Maximization. *Journal of Neuroscience* 32, 14942–
1050 14950.
1051 38 Green, N., Bogacz, R., Huebl, J., Beyer, A.K., Kühn, A.A., and Heekeren, H.R. (2013).
1052 Reduction of influence of task difficulty on perceptual decision making by stn deep brain
1053 stimulation. *Current Biology* 23, 1681–1684.
1054 39 Grueschow, M., Polania, R., Hare, T.A., and Ruff, C.C. (2015). Automatic versus Choice-
1055 Dependent Value Representations in the Human Brain. *Neuron* 85, 874–885.
1056 40 Grueschow, M., Polania, R., Hare, T.A., and Ruff, C.C. (2018). Arousal Optimizes Neural
1057 Evidence Representation for Human Decision-Making. *SSRN Electronic Journal*.
1058 41 Hanks, T.D., and Summerfield, C. (2017). Perceptual Decision Making in Rodents, Monkeys,
1059 and Humans. *Neuron* 93, 15–31.
1060 42 Hanks, T.D., Kopec, C.D., Brunton, B.W., Duan, C.A., Erlich, J.C., and Brody, C.D. (2015).
1061 Distinct relationships of parietal and prefrontal cortices to evidence accumulation. *Nature* 520,
1062 220–223.
1063 43 Hare, T.A., Camerer, C.F., and Rangel, A. (2009). Self-Control in Decision-Making Involves
1064 Modulation of the vmPFC Valuation System. *Science* 324, 646–648.
1065

- 1066 44 Heekeren, H.R., Marrett, S., Bandettini, P.A., and Ungerleider, L.G. (2004). A general
1067 mechanism for perceptual decision-making in the human brain. *Nature* 431, 859–862.
1068 45 Heekeren, H.R., Marrett, S., Ruff, D.A., Bandettini, P.A., and Ungerleider, L.G. (2006).
1069 Involvement of human left dorsolateral prefrontal cortex in perceptual decision making is
1070 independent of response modality. *Proceedings of the National Academy of Sciences* 103,
1071 10023–10028.
1072 46 Heekeren, H.R., Marrett, S., and Ungerleider, L.G. (2008). The neural systems that mediate
1073 human perceptual decision making. *Nature Reviews Neuroscience* 9, 467–479.
1074 47 Heng, J.A., Woodford, M., and Polania, R. (2020). Efficient sampling and noisy decisions. *ELife*
1075 9.
1076 48 Herz, D.M., Zavala, B.A., Bogacz, R., and Brown, P. (2016). Neural Correlates of Decision
1077 Thresholds in the Human Subthalamic Nucleus. *Current Biology* 26, 916–920.
1078 49 Herz, D.M., Tan, H., Brittain, J.S., Fischer, P., Cheeran, B., Green, A.L., Fitzgerald, J., Aziz,
1079 T.Z., Ashkan, K., Little, S., et al. (2017). Distinct mechanisms mediate speed-accuracy
1080 adjustments in cortico-subthalamic networks. *ELife* 6, 1–25.
1081 50 Heyes, S.B., Adam, R.J., Urner, M., van der Leer, L., Bahrami, B., Bays, P.M., and Husain, M.
1082 (2012). Impulsivity and rapid decision-making for reward. *Frontiers in Psychology* 3, 1–11.
1083 51 Huang, Y.Z., Edwards, M.J., Rounis, E., Bhatia, K.P., and Rothwell, J.C. (2005). Theta burst
1084 stimulation of the human motor cortex. *Neuron* 45, 201–206.
1085 52 Hutcherson, C.A., Bushong, B., and Rangel, A. (2015). A Neurocomputational Model of
1086 Altruistic Choice and Its Implications. *Neuron* 87, 451–462.
1087 53 Karaca-Mandic, P., Norton, E.C., and Dowd, B. (2012). Interaction terms in nonlinear models.
1088 *Health Services Research* 47, 255–274.
1089 54 Kiani, R., Corthell, L., and Shadlen, M.N. (2014). Choice certainty is informed by both evidence
1090 and decision time. *Neuron* 84, 1329–1342.
1091 55 Kim JN, Shadlen MN. (1999). Neural correlates of a decision in the dorsolateral prefrontal
1092 cortex of the macaque. *Nature Neuroscience* 2: 176-85.
1093 56 Knecht, S., Ellger, T., Breitenstein, C., Ringelstein, E.B., and Henningsen, H. (2003). Changing
1094 cortical excitability with low-frequency transcranial magnetic stimulation can induce sustained
1095 disruption of tactile perception. *Biological Psychiatry* 53, 175–179.
1096 57 Koechlin, E., and Summerfield, C. (2007). An information theoretical approach to prefrontal
1097 executive function. *Trends in Cognitive Sciences* 11, 229–235.
1098 58 Krajbich I. (2019). Accounting for attention in sequential sampling models of decision making.
1099 *Curr Opin Psychol* 29: 6-11
1100 59 Liu, T., and Pleskac, T.J. (2011). Neural correlates of evidence accumulation in a perceptual
1101 decision task. 48824, 2383–2398.
1102 60 Logothetis, N.K. (2008). What we can do and what we cannot do with fMRI. *Nature* 453, 869–
1103 878.
1104 61 Mawase, F., Lopez, D., Celnik, P.A., and Haith, A.M. (2018). Movement repetition facilitates
1105 response preparation. *Cell Reports* 24, 801–808.
1106 62 Mulder MJ, van Maanen L, Forstmann BU. (2014). Perceptual decision neurosciences - a
1107 model-based review. *Neuroscience* 277: 872-84
1108 63 Murd, C., Moisa, M., Grueschow, M., Polania, R., and Ruff, C.C. (2020). Causal contributions
1109 of human frontal eye fields to distinct aspects of decision formation. *Scientific Reports* 10,
1110 7317.
1111 64 Nee, D.E., and D'Esposito, M. (2016). The hierarchical organization of the lateral prefrontal
1112 cortex. *ELife* 5.
1113 65 Owen, A.M. (1997). The Functional Organization of Working Memory Processes Within
1114 Human Lateral Frontal Cortex: The Contribution of Functional Neuroimaging. *European
1115 Journal of Neuroscience* 9, 1329–1339.
1116 66 Palmeri, T.J., Love, B.C., and Turner, B.M. (2017). Model-based cognitive neuroscience.
1117 *Journal of Mathematical Psychology* 76.

- 1118 67 Peters, J., and D'Esposito, M. (2020). The drift diffusion model as the choice rule in inter-
1119 temporal and risky choice: a case study in medial orbitofrontal cortex lesion patients and
1120 controls. PLoS Computational Biology 16, e1007615.
- 1121 68 Petrides, M. (2005). Lateral prefrontal cortex: architectonic and functional organization.
1122 Philosophical Transactions of the Royal Society B: Biological Sciences 360, 781–795.
- 1123 69 Philiastides, M.G., Auksztulewicz, R., Heekeren, H.R., and Blankenburg, F. (2011). Causal
1124 role of dorsolateral prefrontal cortex in human perceptual decision making. Current Biology 21,
1125 980–983.
- 1126 70 Piet AT, Erlich JC, Kopec CD, Brody CD. (2017). Rat Prefrontal Cortex Inactivations during
1127 Decision Making Are Explained by Bistable Attractor Dynamics. Neural Comput 29: 2861-86
- 1128 71 Plummer, M. (2016) rjags: Bayesian graphical models using MCMC. R package version, 4(6).
- 1129 72 Polanía, R., Krajbich, I., Grueschow, M., and Ruff, C.C. (2014). Neural Oscillations and
1130 Synchronization Differentially Support Evidence Accumulation in Perceptual and Value-based
1131 Decision Making. Neuron 82, 709–720.
- 1132 73 Polanía R, Moisa M, Opitz A, Grueschow M, Ruff CC. (2015). The precision of value-based
1133 choices depends causally on fronto-parietal phase coupling. Nat Commun 6
- 1134 74 Poldrack, R. (2006). Can cognitive processes be inferred from neuroimaging data? Trends in
1135 Cognitive Sciences 10, 59–63.
- 1136 75 Postle, B.R. (2016). How Does the Brain Keep Information “in Mind”? Current Directions in
1137 Psychological Science 25, 151–156.
- 1138 76 Puhani, P.A. (2012). The treatment effect, the cross difference, and the interaction term in
1139 nonlinear “difference-in-differences” models. Economics Letters 115, 85–87.
- 1140 77 Rahnev, D., Nee, D.E., Riddle, J., Larson, A.S., and D'Esposito, M. (2016). Causal evidence
1141 for frontal cortex organization for perceptual decision making. Proceedings of the National
1142 Academy of Sciences 113, 6059–6064.
- 1143 78 Ramsey, J.D., Hanson, S.J., Hanson, C., Halchenko, Y.O., Poldrack, R.A., and Glymour, C.
1144 (2010). Six problems for causal inference from fMRI. NeuroImage 49, 1545–1558.
- 1145 79 Ratcliff R, Rouder JN. (1998). Modeling response times for two-choice decisions. Psychol Sci
1146 9: 347-56
- 1147 80 Ratcliff, R. and Smith, P. (2004) A comparison of sequential sampling models for two-choice
1148 reaction time. Psychological Review 111(2): 333-367.
- 1149 81 Ratcliff, R. and McKoon, G. (2004) The diffusion decision model: theory and data for two
1150 choice-decision tasks. Neural Computation 20(4): 873-922.
- 1151 82 Ratcliff, R., and McKoon, G. (2008). The Diffusion Decision Model: Theory and Data for Two-
1152 Choice Decision Tasks. Neural Computation 20, 873–922.
- 1153 83 Serences, J.T., Ester, E.F., Vogel, E.K., and Awh, E. (2009). Stimulus-Specific Delay Activity
1154 in Human Primary Visual Cortex. Psychological Science 20, 207–214.
- 1155 84 Shadlen, M.N., and Newsome, W.T. (1996). Motion perception: seeing and deciding.
1156 Proceedings of the National Academy of Sciences 93, 628–633.
- 1157 85 Sokol-Hessner, P., Hutcherson, C., Hare, T., and Rangel, A. (2012). Decision value
1158 computation in DLPFC and VMPFC adjusts to the available decision time. European Journal
1159 of Neuroscience 35, 1065–1074.
- 1160 86 Smith PL, Ratcliff R. (2004). Psychology and neurobiology of simple decisions. Trends
1161 Neurosci 27: 161-68
- 1162 87 Starns, J.J., and Ma, Q. (2018). Response biases in simple decision making: Faster decision
1163 making, faster response execution, or both? Psychonomic Bulletin & Review 25, 1535–1541.
- 1164 88 Summerfield C, Tsetsos K. (2012). Building bridges between perceptual and economic
1165 decision-making: neural and computational mechanism. Front Neurosci-Switz 6
- 1166 89 Tajima S, Drugowitsch J, Pouget A. (2016). Optimal policy for value-based decision-making.
1167 Nat Commun 7: 12400.
- 1168 90 Thut, G., and Pascual-Leone, A. (2010). A review of combined TMS-EEG studies to
1169 characterize lasting effects of repetitive TMS and assess their usefulness in cognitive and
1170 clinical neuroscience. Brain Topography 22, 219–232.

- 1171 91 Tosoni, A., Galati, G., Romani, G.L., and Corbetta, M. (2008). Sensory-motor mechanisms in
1172 human parietal cortex underlie arbitrary visual decisions. *Nature Neuroscience* 11, 1446–
1173 1453.
1174 92 Turner, B.M., van Maanen, L., and Forstmann, B.U. (2015). Informing cognitive abstractions
1175 through neuroimaging: the neural drift diffusion model. *Psychological Review* 122, 312–336.
1176 93 Usher M, McClelland JL. (2001). The time course of perceptual choice: The leaky, competing
1177 accumulator model. *Psychological Review* 108: 550-92
1178 94 Vandekerckhove, J., Tuerlinckx, F., and Lee, M.D. (2011). Hierarchical diffusion models for
1179 two-choice response times. *Psychological Methods* 16, 44–62.
1180 95 White, C.N., Servant, M., and Logan, G.D. (2018). Testing the validity of conflict drift-diffusion
1181 models for use in estimating cognitive processes: A parameter-recovery study. *Psychonomic
1182 Bulletin & Review* 25, 286–301.
1183 96 Wycoco, V., Shroff, M., Sudhakar, S., and Lee, W. (2013). White Matter Anatomy.
1184 *Neuroimaging Clinics of North America* 23.
1185 97 Wijekumar, S., Ambrose, J.P., Spencer, J.P., and Curtu, R. (2017). Model-based functional
1186 neuroimaging using dynamic neural fields: An integrative cognitive neuroscience approach.
1187 *Journal of Mathematical Psychology* 76, 212–235.
1188 98 Zanto, T.P., Rubens, M.T., Thangavel, A., and Gazzaley, A. (2011). Causal role of the
1189 prefrontal cortex in top-down modulation of visual processing and working memory. *Nature
1190 Neuroscience* 14, 656–661.



1191

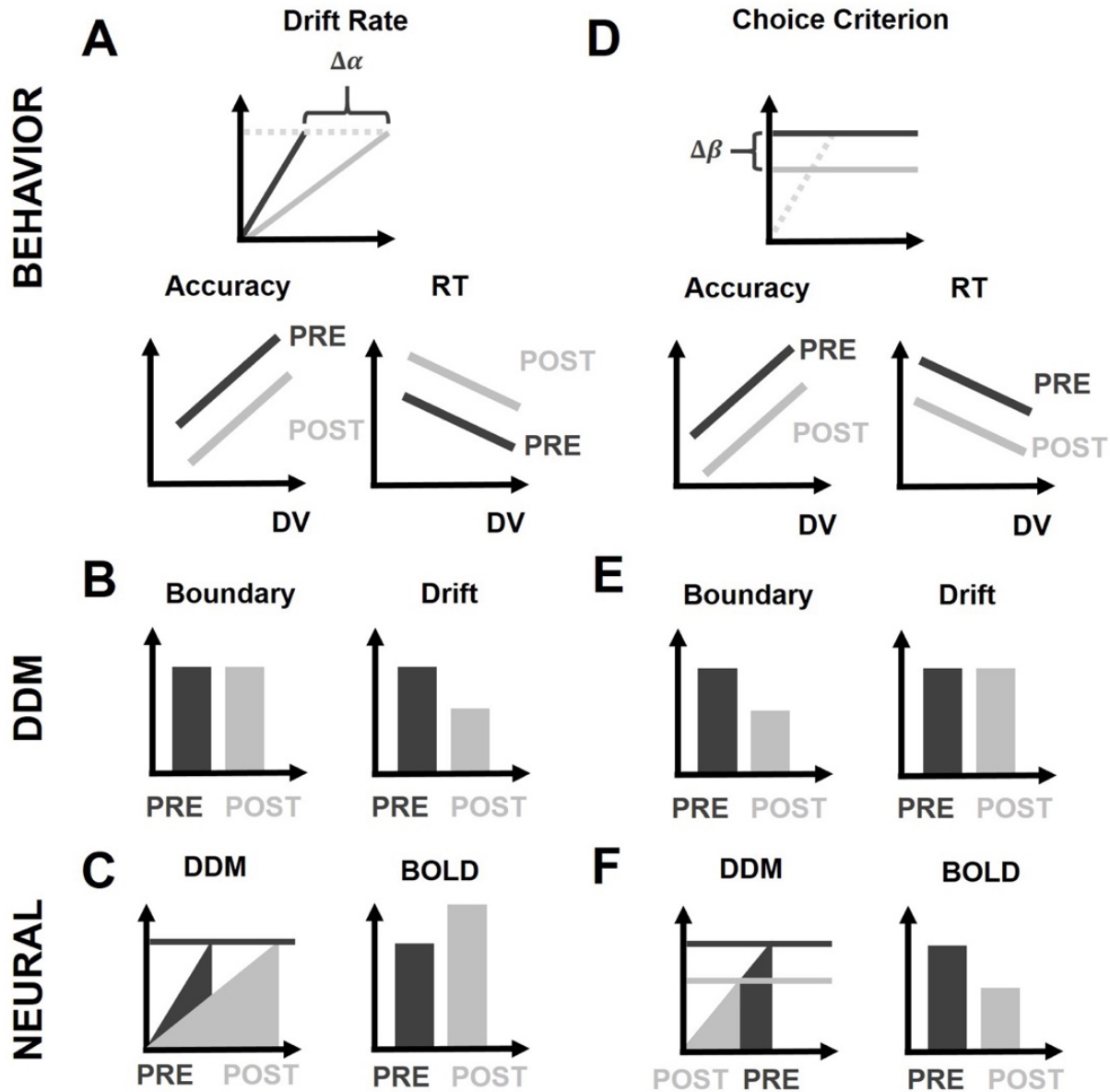
1192

Figure 1. Behavioural food choice paradigm, theta-burst stimulation protocol, and behavioural regressions. (a) Example of decision stage. Participants were cued in advance about the type of decision required. Perceptual decisions required participants to choose the food item with the largest size while value-based decisions required participants to choose the food item they preferred to consume at the end of the experiment. Participants alternated between blocks of perceptual (blue) or value-based (red) choice trials (7-9 trials per task-block). (b) Logistic regression results show that the larger the evidence strength, the more likely decision makers will respond accurately. Choice accuracy is only related to the evidence that is currently task-relevant (size difference SD for perceptual or value difference VD for value-based choice), not to the task-irrelevant evidence (RT is reaction time of current choice). (c) Similarly, our linear regressions show that RTs are negatively associated only with the task-relevant evidence (and lower for perceptual choices overall, captured by regressor CH (1 = perceptual, 0 = value-based)). Consistent with previous findings, the results in (b) and (c) confirm that our paradigm can distinguish and compare evidence processing for matched perceptual- and value-based decisions. Error bars in (b) and (c) represent the 95% confidence interval range of the estimated effect sizes. * $p < 0.05$, ** $p < 0.01$, and *** $p < 0.001$. (d) Theta-burst stimulation protocol. After the fourth pre-TMS run, participants received continuous theta-burst stimulation (cTBS) over the left SFS region of interest (ROI) (area encircled and colored blue). cTBS consisted of 200 trains of 600 pulses of 5 Hz frequency for 50 s.

1210

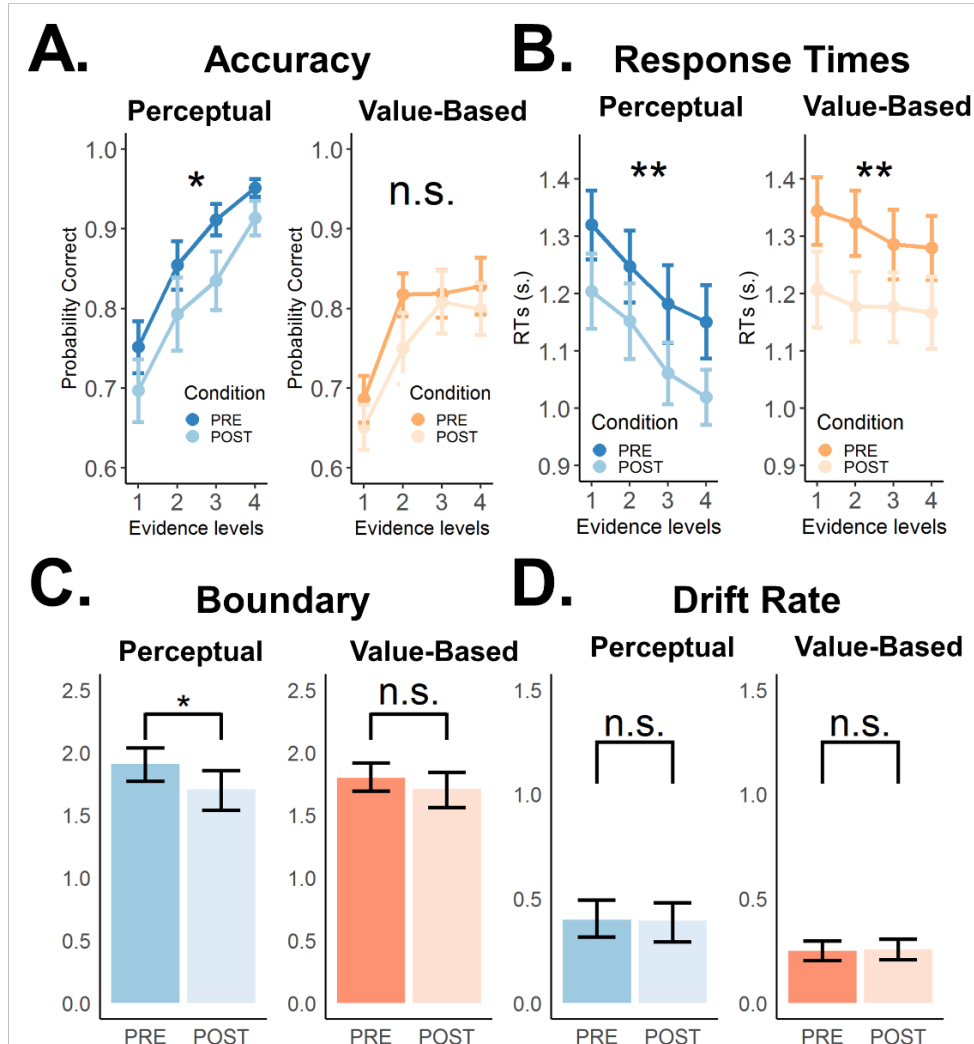
1211

1212



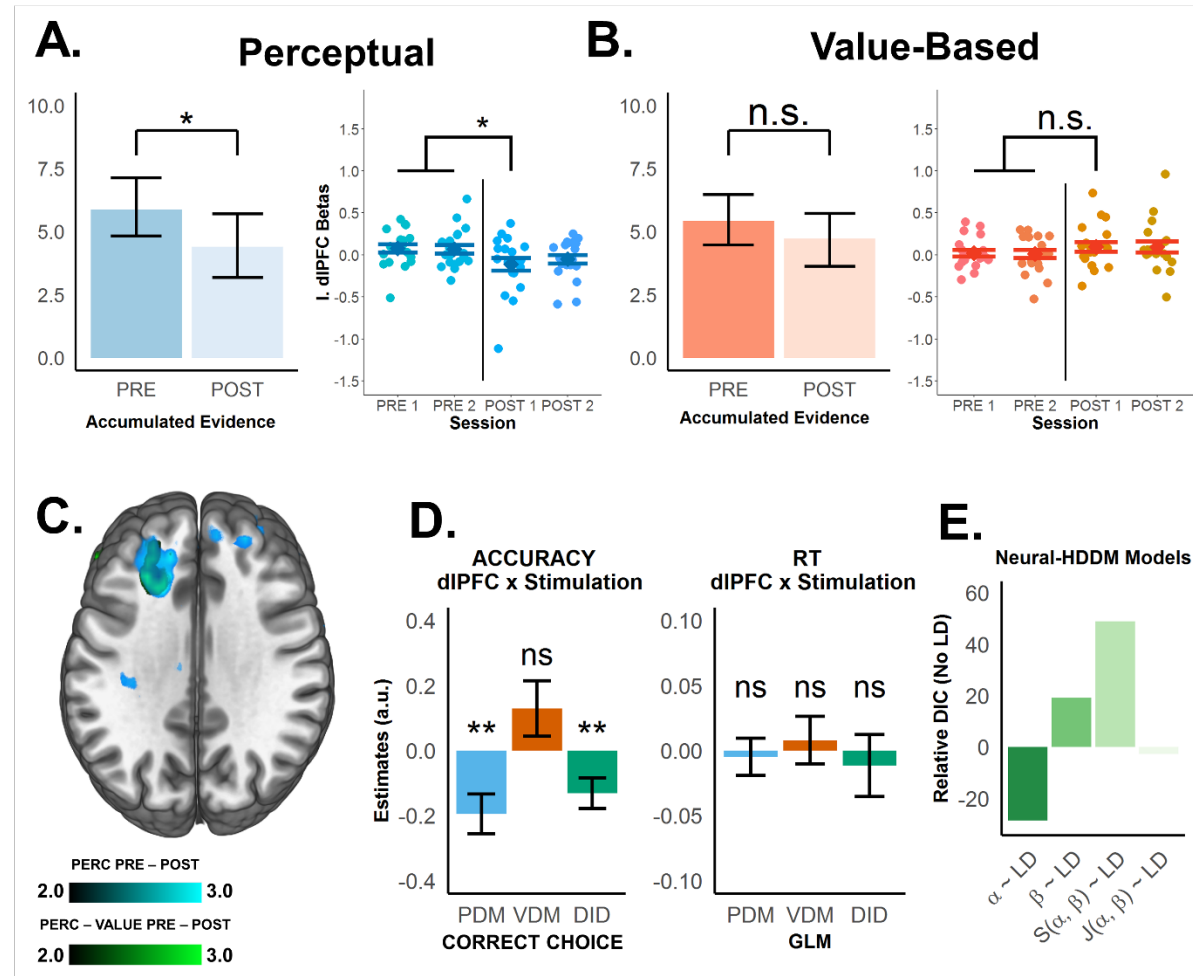
1213

1214 **Figure 2. Study hypotheses.** Scenario 1: left SFS is causally involved in evidence accumulation.
 1215 Theta-burst induced inhibition of left SFS should lead to reduced evidence accumulation (a),
 1216 expressed as lower accuracy (a, 2nd row, left), slowing of RTs (a, 2nd row, right), and a reduction of
 1217 DDM drift rate (b, right) without any effect on the boundary parameter (b, left). Since the neural activity
 1218 devoted to evidence accumulation (area under the curve) should increase (c, left), we would expect
 1219 higher BOLD signal in this case (c, right). Scenario 2: left SFS is causally involved in setting the choice
 1220 criterion. Theta-burst induced inhibition of left SFS should lead to a lower choice criterion (d),
 1221 expressed as lower choice accuracy (d, 2nd row, left), faster RTs (d, 2nd row, right), and a reduced
 1222 DDM decision boundary parameter (e, left) without any effect on the DDM drift-rate (e, right). At the
 1223 neural level, we should observe reduced BOLD activity due to the lower amount of evidence processed
 1224 by the neurons (f, right), and reflected by the smaller area under the evidence-accumulation curve
 1225 when it reaches the lower boundary (f, left).



1226

Figure 3. Theta-burst stimulation over the left SFS affects choice behavior and selectively lowers the decision boundary for perceptual but not value-based choices. (a) Choice accuracies/consistencies and (b) response times (RTs) for perceptual (blue) and value-based (orange) decisions for different evidence levels during pre-cTBS (dark) and post-cTBS (light) stimulation periods. Error bars in (a) and (b) represent s.e.m. Consistent with previous findings, stronger evidence leads to more accurate choices and faster RTs in both types of decisions. Importantly, theta-burst stimulation significantly lowered choice accuracy selectively for perceptual, not value-based decisions (negative main stimulation effect for perceptual decisions and negative stimulation \times task interaction; **Supplementary Fig. 2c** and see also **Supplementary Fig. 2a** for changes in choice accuracy across runs). Additionally, theta-burst stimulation also significantly lowered RTs in both choice types (negative main stimulation effect; **Supplementary Fig. 2c** and see also **Supplementary Fig. 2b** for changes in RTs across runs). (c) Theta-burst stimulation selectively decreased the decision boundary in perceptual decisions only (difference between estimated posterior population distributions; see **Methods** and **Supplementary Fig. 5a** for a detailed post-hoc analysis). All the other parameters, particularly (d) the drift rate (see also **Supplementary Fig. 5b** for post-hoc analysis) remain unaffected by stimulation. Error bars in (c) and (d) represent the 95% confidence interval range of the posterior estimates of the DDM parameters. * $p < 0.05$, ** $p < 0.01$, and *** $p < 0.001$.

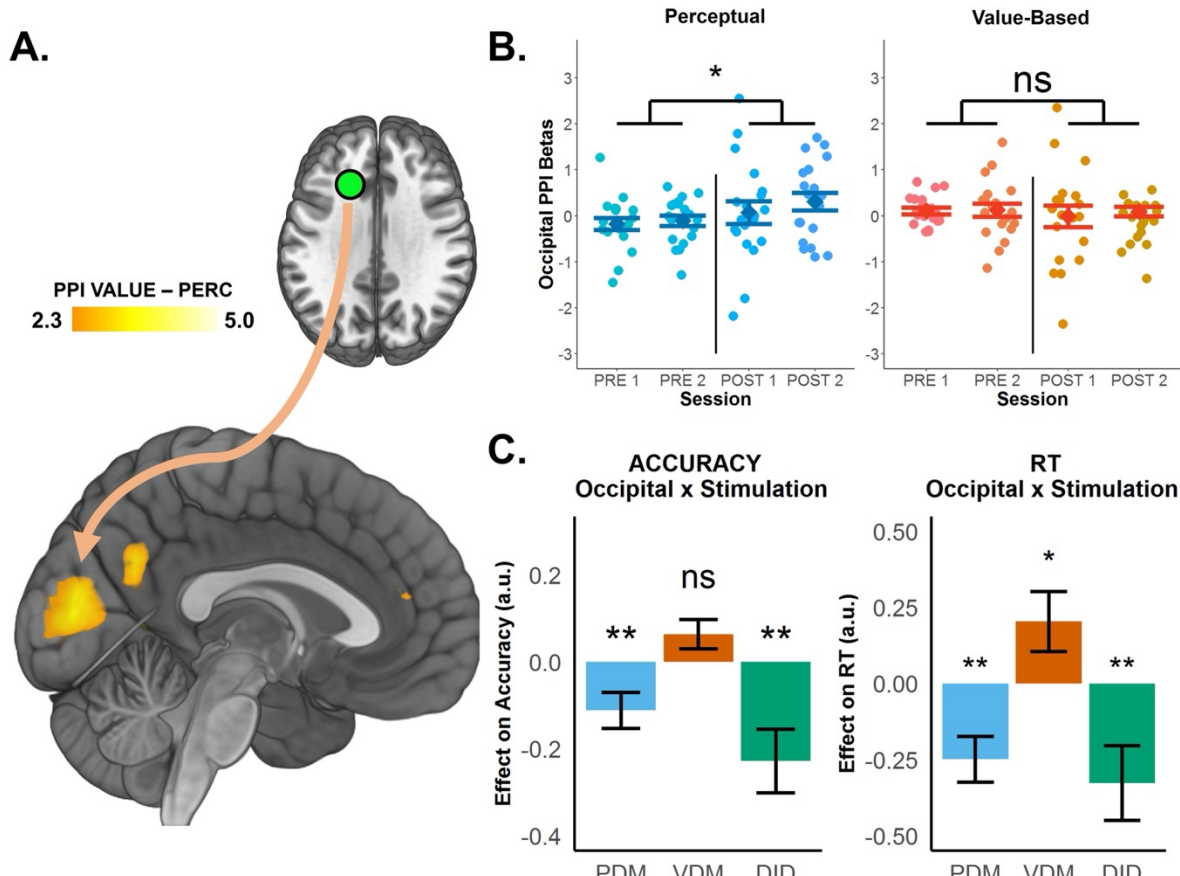


1244

1245 **Figure 4. Neural representation of accumulated evidence in the left SFS is disrupted after theta-**
 1246 **burst stimulation, and is linked with behavior and neural computation. (a)** Left panel:
 1247 Accumulated evidence (AE) simulation derived from the fitted DDM (left panel). Previous studies have
 1248 illustrated how the accumulation-to-bound process convolved with the hemodynamic response
 1249 function (HRF) results in BOLD signals; hence, the simulated AE provides a suitable prediction of
 1250 BOLD responses in brain regions involved in evidence accumulation. Theta-burst stimulation
 1251 selectively decreased AE for (a) perceptual (blue), not (b) value-based (orange) decisions (see
 1252 **Supplementary Fig. 6b** for post-hoc analysis). We constructed a trialwise measure of accumulated
 1253 evidence using RTs and evidence strength for our parametric modulator (see **Methods**). Individual
 1254 ROIs extracted from the left SFS representing accumulated evidence across runs (right panels; see
 1255 **Methods**) show that consistent with the DDM prediction, theta-burst stimulation selectively decreased
 1256 BOLD response representing AE in left SFS during perceptual, not value-based decisions. Error bars
 1257 in the left panels of (a) and (b) represent the 95% confidence interval range of the posterior estimates
 1258 of the DDM parameters, while error bars in their respective right panels represent s.e.m. (c) Post-pre
 1259 contrasts for the trialwise accumulated-evidence regressor show reduced left-SFS BOLD during
 1260 perceptual decisions (green overlay), with a significantly stronger reduction for perceptual vs value-
 1261 based decisions (blue overlay). No reduction is observed for value-based decisions. (d) To test the
 1262 link between neural and behavioural effects of TMS, regression results show that after stimulation,
 1263 BOLD changes in left SFS are associated with lower choice accuracy (left panel) for perceptual (PDM,
 1264 blue) (negative left SFS \times stimulation interaction) but not value-based choices (VDM, red), with
 1265 significant differences between the effects on both choice types (difference-in-difference, DID, green,

1266 negative left SFS × stimulation × task interaction). On the other hand, cTBA-induced changes in left
1267 SFS activity are unrelated to changes in RT (right panel). Error bars in (d) represent the 95%
1268 confidence interval range of the estimated effect sizes. * $p < 0.05$, ** $p < 0.01$, and *** $p < 0.001$. (e)
1269 To test the link between neural activity and DDM computations, we included trialwise beta estimates
1270 of left-SFS BOLD signals as inputs to the DDM. Alternative models tested whether trialwise left-SFS
1271 (LD) activity modulates the decision boundary (α) (**Model 1**), the drift rate (β), or a combination of both
1272 (**Models 3 and 4**, see **Methods** and **Supplementary Fig. 8** for more details). Model comparisons
1273 using the deviance information criterion (**DIC**, smaller values mean better fits) showed that Model 1
1274 fits the data best, confirming that the left SFS is involved in selectively changing the decision boundary
1275 for perceptual decisions.

1276



1277

1278 **Figure 5. SFS-TMS-related changes in behaviour and neural computations are accompanied by**
1279 **increased functional coupling between the left SFS and occipital cortex. (a)** Psychophysiological
1280 interaction (PPI) analysis reveals an area in occipital cortex showing increased functional coupling
1281 with the left SFS during perceptual choices. **(b)** ROI analysis of individual PPI betas shows that aE-
1282 related functional coupling between the left SFS and OCC is selectively increased post stimulation
1283 during perceptual (left panel) but not value-based decisions (right panel). Error bars in (b) represent
1284 s.e.m. **(c)** Regression results testing the link between cTBS effects on left SFS-OCC functional
1285 coupling and behaviour. Increased SFS-OCC coupling is associated with lower choice accuracy (left
1286 panel) specifically for perceptual (PDM, blue, negative OCC × stimulation interaction) but not value-
1287 based choices (VDM, red). In addition, increased functional coupling is also associated with faster RTs
1288 (right panel) for perceptual (blue, negative OCC × stimulation interaction) and slower RTs for value-
1289 based choice (red, positive OCC × stimulation interaction). Error bars in (c) represent the 95%
1290 confidence interval range of the estimated effect sizes. * $p < 0.05$, ** $p < 0.01$, and *** $p < 0.001$.

1291

1292

1293

1294

1295

1296

1297

1298

1299

1300

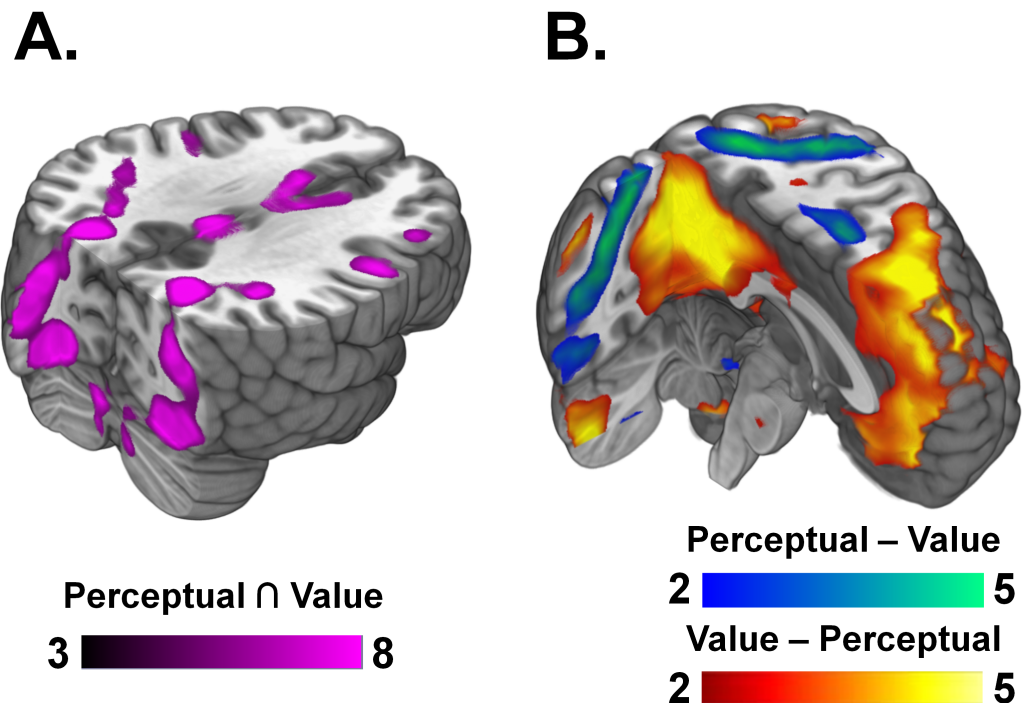
1301

1302

1303

SUPPLEMENTARY MATERIAL

1304



1305

1306 **Supplementary Figure 1. Domain-general and domain-specific regions involved in perceptual**
1307 **and value-based decisions. (a)** Domain-general regions. We found domain-general regions shared
1308 by both perceptual decision making (PDM) and value-based decision making (VDM), such as areas
1309 in the visual stream along the fusiform gyrus, cerebellar areas including the brainstem and motor areas
1310 such as premotor cortex and SMA (conjunction $p < 0.05$, cluster-corrected, see **Supplementary**
1311 **Table 1** for the complete list of regions). **(b)** Domain-specific regions. Comparing average decision-
1312 related activity between perceptual and value-based decisions revealed distinct brain activations.
1313 Blue-green represents significant neural activity for PDM > VDM decisions while red-yellow represents
1314 significant activity for VDM > PDM (see **Supplementary Table 2**). Among the active regions in the
1315 VDM > PDM contrast include the orbitofrontal cortex, the posterior cingulate cortex, and the media
1316 prefrontal cortex while the regions active in the PDM > VDM contrast include the frontal eye fields, the
1317 intraparietal sulcus and premotor cortex.

1318

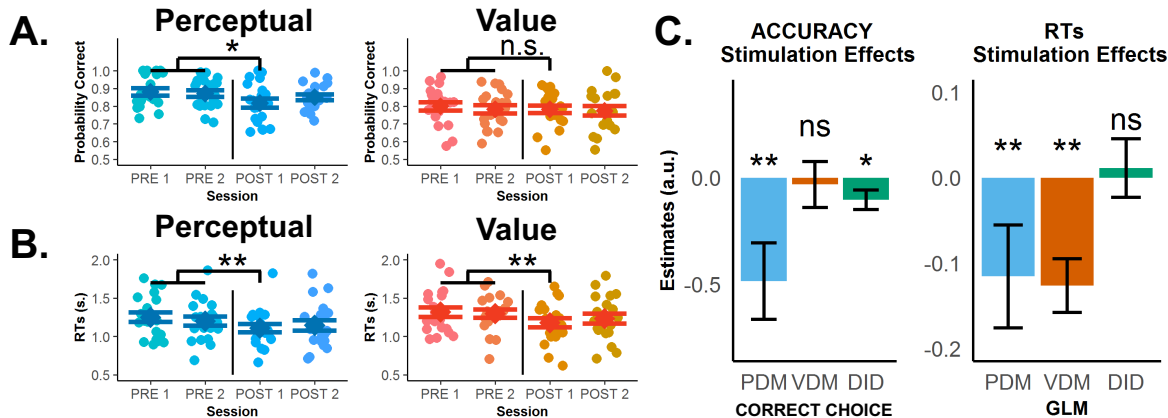
1319

1320

1321

1322

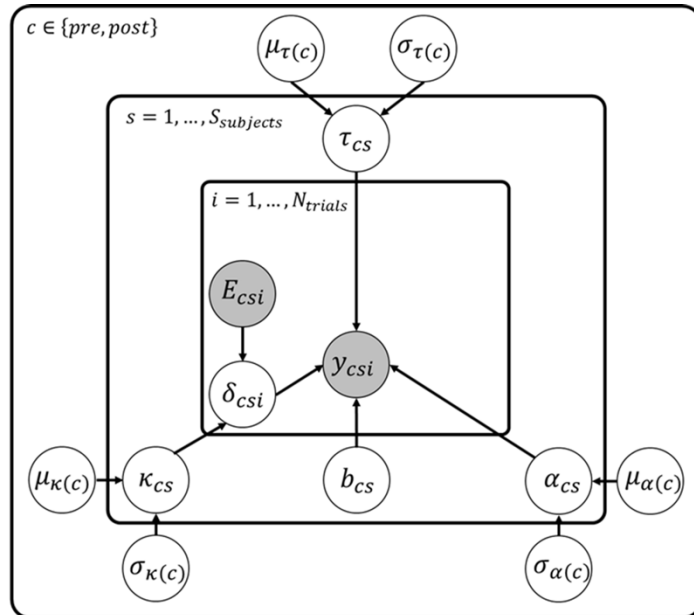
1323



1324

1325 **Supplementary Figure 2. Theta-burst stimulation in left SFS selectively lowers choice accuracy**
1326 **for perceptual decisions, but RTs become faster after stimulation in both choice types. (a)**
1327 Observed accuracies and (b) mean RTs of individual participants for perceptual decision making, PDM
1328 (blue) and value-based decision making, VDM (orange-yellow) across pre-stimulation and post-
1329 stimulation runs. Error bars in (a) and (b) represent s.e.m. Theta-burst stimulation significantly lowered
1330 choice accuracy for PDM, not VDM, especially during the first post-stimulation run. On the other hand,
1331 RTs sped up in both perceptual and value-based decisions. Unsurprisingly, both accuracy levels and
1332 RTs began to recover during the second post-stimulation run for PDM. (c) In our regression analysis,
1333 comparing the pre-post PDM difference in accuracy with the pre-post VDM difference confirm the
1334 significant effect of theta-burst stimulation in selectively lowering choice accuracy (left panel) for
1335 perceptual decisions (green, negative stimulation \times task interaction). In contrast, the effect is
1336 nonspecific for RTs (right panel). Error bars in (c) represent the 95% confidence interval range of the
1337 estimated effect sizes. * $p < 0.05$, ** $p < 0.01$, and *** $p < 0.001$.

1338



1339

1340 **Supplementary Figure 3. Hierarchical Bayesian DDM.** Graphical representation of the hierarchical
 1341 Bayesian DDM fitted to choice data. Clear circles represent latent variables while filled circles
 1342 represent observed variables, i.e. choice data, y , and evidence, E , for each trial i . Choice data contain
 1343 both accuracy and response times. The following equations show the distributions assumed for each
 1344 of the latent variables in the model:

1345

$$\text{Trial-by-trial, } i \quad y_{c,s,i} \sim \text{Wiener}(\alpha_{cs}, \beta, \tau_{c,s}, \delta_{c,s,i})$$

$$\delta_{c,s,i} = \kappa_{c,s} \times E_{c,s,i}$$

$$\text{Subject, } c \quad \alpha_{c,s} \sim \mathcal{N}(\mu_\alpha(c), \sigma_{\alpha(c)}^2)$$

$$\tau_{c,s} \sim \mathcal{N}(\mu_\tau(c), \sigma_{\tau(c)}^2)$$

$$\kappa_{c,s} \sim \mathcal{N}(\mu_\kappa(c), \sigma_{\kappa(c)}^2)$$

$$b_{c,s} = 0.5$$

Observable variables

$$y_{c,s,i} = \begin{cases} rt_{c,s,i}, & \text{correct} = 1 \\ -rt_{c,s,i}, & \text{correct} = 0 \end{cases}$$

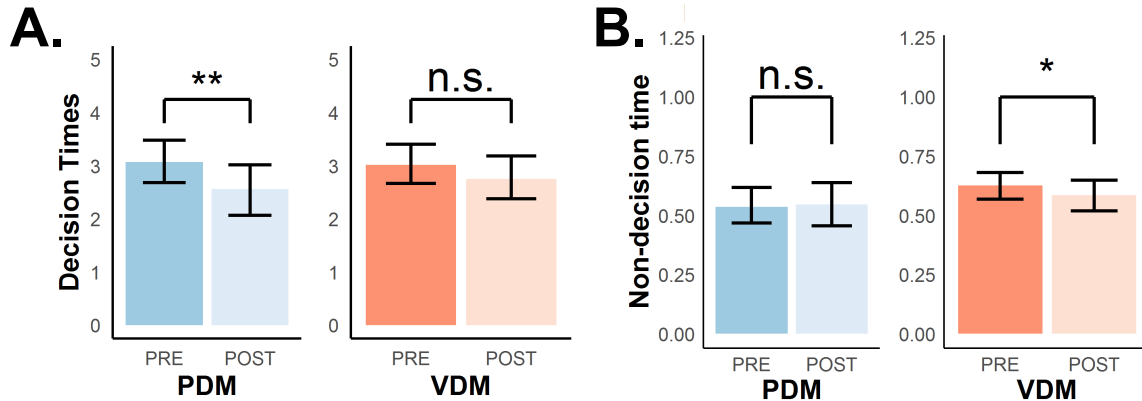
$$E = \{V_{best} - V_{worst}\} \text{ or } \{S_{biggest} - S_{smallest}\}$$

1346

1347 For the hyper-group or latent parameters at the highest level of the hierarchy (represented by μ_x and
1348 σ_x), we assumed flat uniform priors. The distributions for the following are:

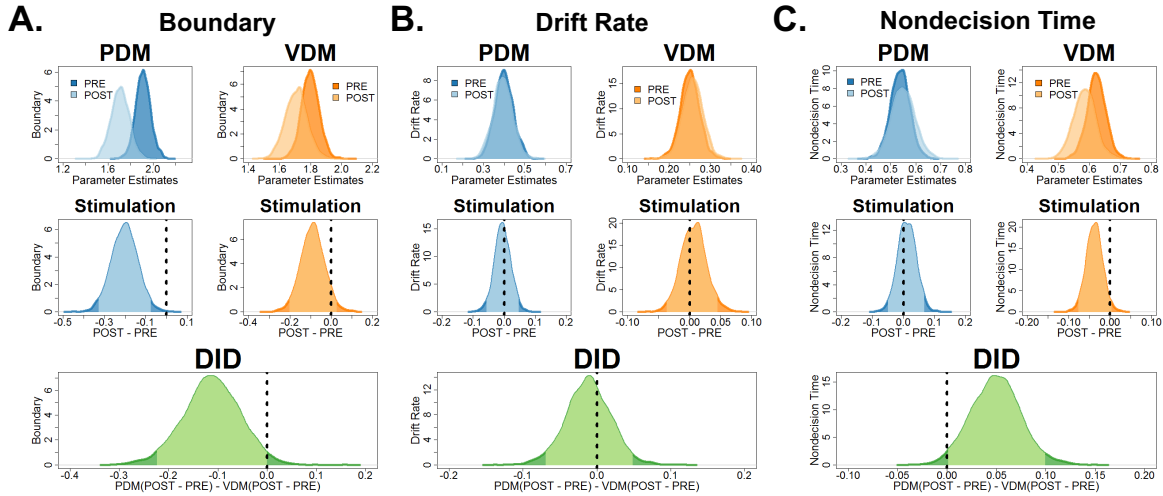
1349 $\kappa \sim U(-8,8)$, $\alpha \sim U(0.001,5)$, $\kappa \sim U(0.01,2)$

1350 The following model parameters are: α (decision threshold), κ (drift rate parameter scaling the
1351 evidence, E), and τ (nondecision times).



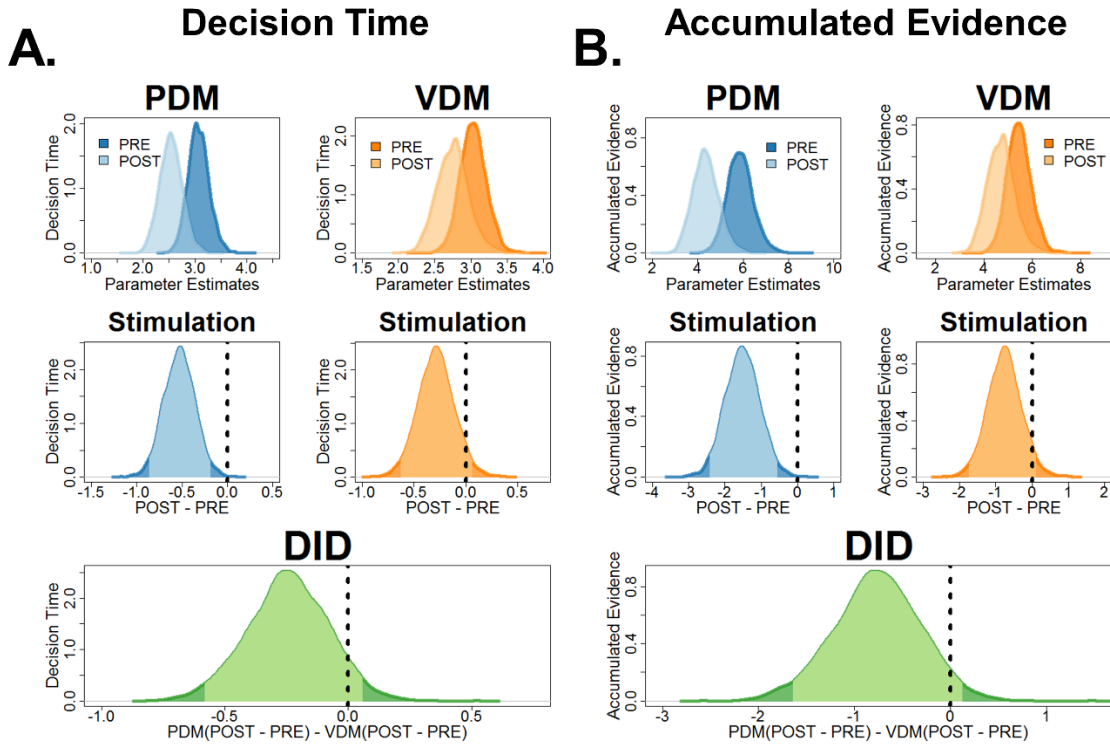
1352

1353 **Supplementary Figure 4. The DDM disentangles the latent decision-relevant and decision-**
1354 **irrelevant processes observed with faster RTs. (a)** We derived a measure of decision times (DT,
1355 upper row) and **(b)** estimated non-decision times (nDT, lower row) from the DDM. We derived and
1356 estimated these parameters to test whether faster RTs in both perceptual decision making (PDM) and
1357 value-based decision making (VDM) after stimulation is due to the same or different latent processes
1358 in the DDM, and whether these processes are decision-relevant or not. These results show that
1359 different latent processes are driving faster RTs for PDM and VDM. Theta-burst stimulation
1360 significantly lowered decision times in perceptual (blue), not value-based (orange) decisions. In
1361 contrast, stimulation marginally but selectively decreased nondecision times for VDM, not PDM. A
1362 Post-hoc analysis confirms domain-specificity of lower nDT for VDM (**Supplementary Fig. 5c**). Taken
1363 together, these results explain what processes underlie observed faster RTs in both decisions. Error
1364 bars represent the 95% confidence interval range of the posterior estimates of the DDM parameters.
1365 * $p < 0.05$, ** $p < 0.01$, and *** $p < 0.001$.



1366

1367 **Supplementary Figure 5. Theta-burst stimulation in the left SFS reduced decision boundary for**
 1368 **perceptual decisions. (a)** Bayesian poster probability distributions of DDM parameters (top row of
 1369 panel) before (dark color) and after stimulation (light color) for perceptual (blue) and value-based
 1370 (yellow-orange) decisions. Theta-burst stimulation has lowered the decision boundary for perceptual
 1371 decision (PDM) not value-based decisions (VDM). **(b)** Drift-rate was unaffected after theta-burst
 1372 stimulation, while **(c)** nondecision times decreased in VDM, not PDM. To test for a stimulation effect,
 1373 post-hoc tests (middle row of panel) compare pre- and post-stimulation DDM parameters for each type
 1374 of decision. The highest density interval (HDI) spans within the 95% interval (light color) and represents
 1375 a null effect. We can statistically confirm the effect of theta-burst stimulation if the decision criterion
 1376 (dashed vertical line) is outside the 95% HDI (dark color). In our post-hoc analysis, only the decision
 1377 boundary during PDM had its criterion outside the 95% HDI and marginally for nondecision times.
 1378 However, the criterion for the drift rate was well within the 95% HDI. Hence, these results show that
 1379 theta-burst stimulation significantly decreased the decision boundary for PDM and nondecision times
 1380 for VDM. To test whether stimulation is selective for only one decision domain, our post-hoc test
 1381 (green, bottom row) compared the pre-post PDM differences with the pre-post VDM differences. In
 1382 this analysis, both the criterion for the decision boundary and nondecision times were outside the 95%
 1383 HDI.



1384

1385 **Supplementary Figure 6. Simulations of fitted model: Theta-burst stimulation in the left SFS**
1386 **reduced decision times and accumulated evidence.** (a) Bayesian posterior probability distributions
1387 (top row) of decision times and (b) accumulated evidence before (dark color) and after (light color) for
1388 perceptual (blue) and value-based (yellow-orange) decisions. Post-hoc tests (middle row) comparing
1389 pre- and post-stimulation revealed that theta-burst stimulation significantly decreased both decision
1390 times and accumulated evidence for perceptual, not value-based decisions. However, post-hoc tests
1391 comparing the pre-post PDM differences with the pre-post VDM differences showed that the criterion
1392 is marginally inside the 95% HDI.

1393

1394

1395

1396

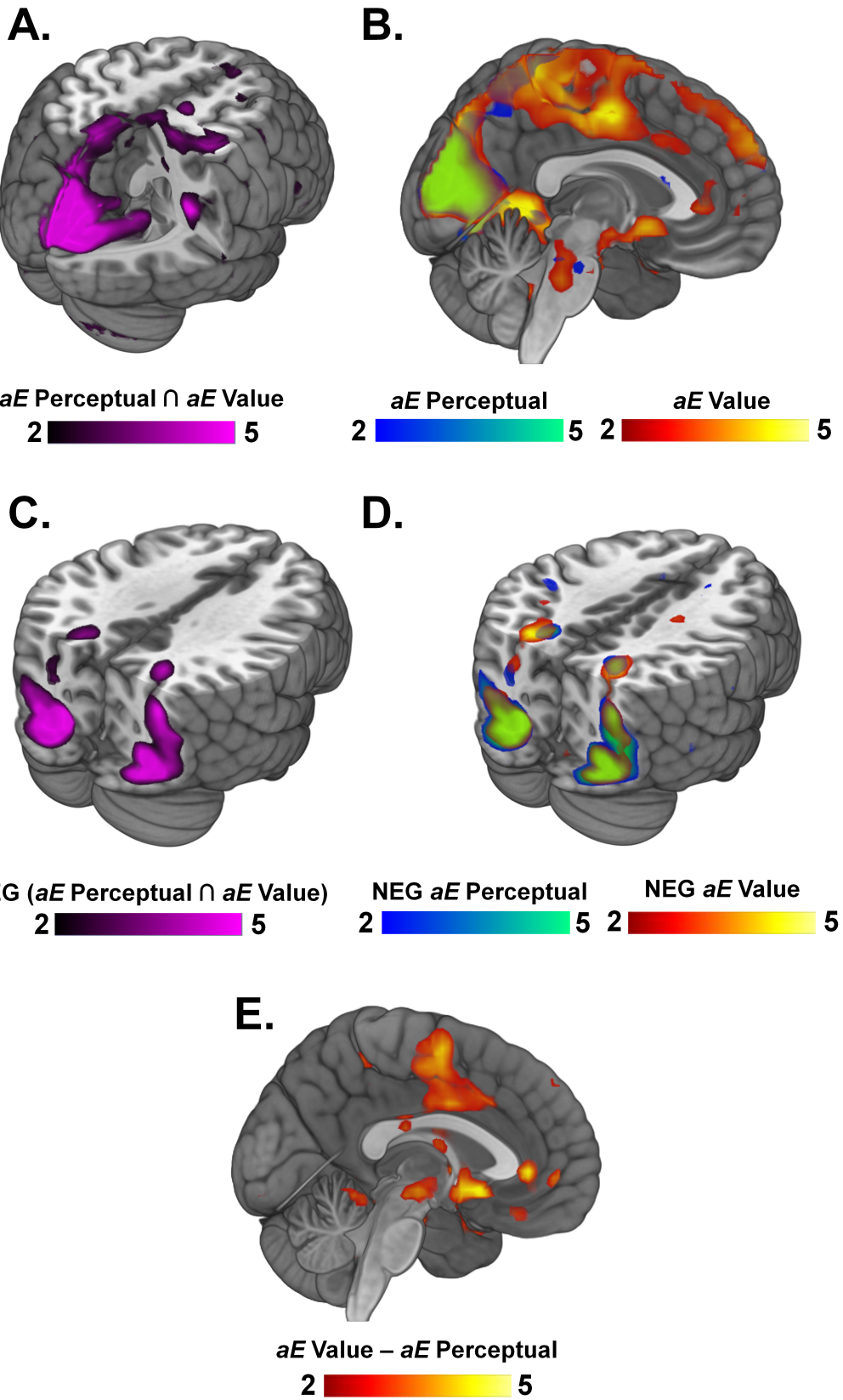
1397

1398

1399

1400

1401



1403

1404 **Supplementary Figure 7. Neural representations of accumulated evidence across the whole**
1405 **brain for PDM and VDM.** (a) Conjunction between areas representing accumulated evidence (*aE*)
1406 during perceptual (PDM) and value-based decisions (VDM) reveals activations in visual and parietal
1407 areas, such as the cuneus, postcentral gyrus, and lingual gyrus (see **Supplementary Table 3**). (b)
1408 Representations of accumulated evidence for PDM and VDM. Particularly, BOLD responses
1409 associated with AE in perceptual decisions are seen in the left SFS (see **Supplementary Table 3**).
1410 (c) Negative conjunction contrasts shared by both PDM and VDM represent the efficiency of evidence
1411 accumulation (i.e., the inverse of accumulated evidence). These contrasts reveal activations in
1412 occipital and parietal areas (see **Supplementary Table 3**). Particularly, parietal areas have been
1413 previously implicated in the efficiency of accumulating evidence. (d) Negative contrasts for each choice
1414 domain reveal activations in parietal and occipital areas (see **Supplementary Table 4**). (e) Contrasts
1415 comparing the neural representation of accumulated evidence between value-based and perceptual
1416 decisions revealed activations in areas such as the ventromedial prefrontal cortex (vmPFC) and the
1417 nucleus accumbens (see **Supplementary Table 4**).

1418

1419

1420

1421

1422

1423

1424

1425

1426

1427

1428

1429

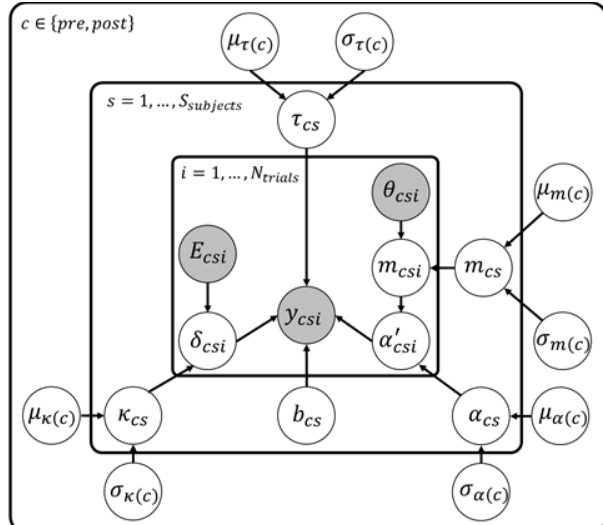
1430

1431

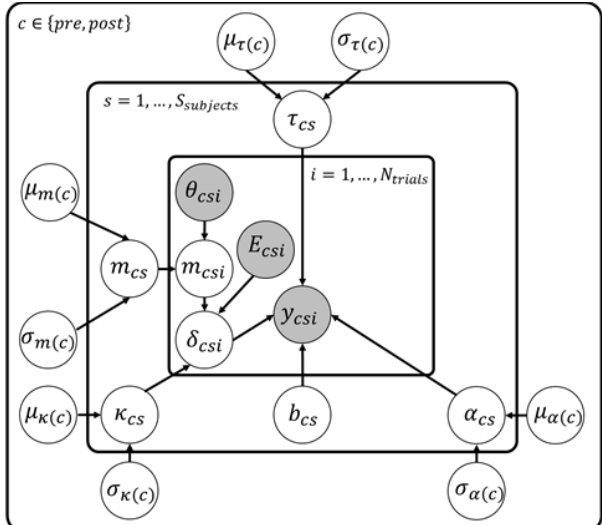
1432

1433

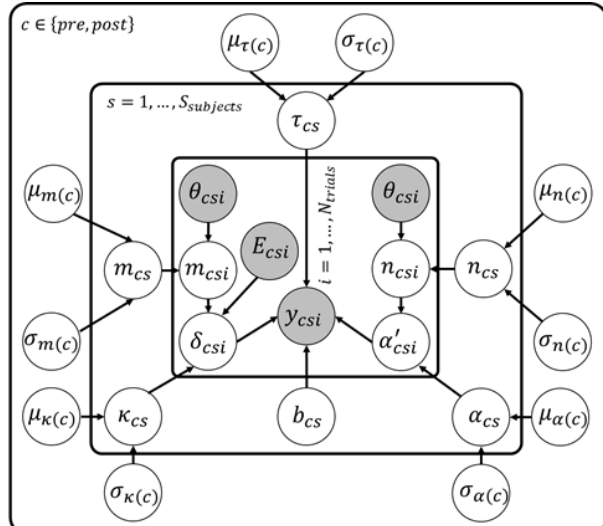
1434



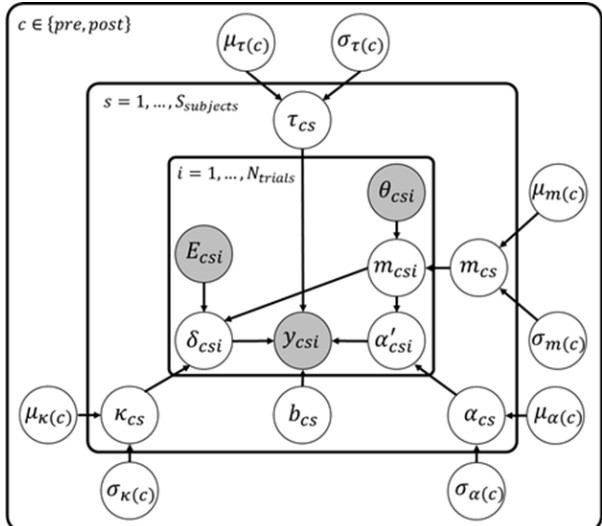
Model 1. SFS modulation of boundary



Model 2. SFS modulation of drift rate



Model 3. Separate SFS Modulation of boundary and drift rate



Model 4. Joint SFS modulation of both boundary and drift rate

1435 **Supplementary Figure 8. Neural-HDDM Alternatives.** To test whether the left SFS is mechanistically
 1436 involved in the latent decision-relevant processes, we included trial-by-trial left SFS neural betas as
 1437 an input to our hierarchical drift diffusion model. We compared our neural HDDM with the HDDM
 1438 without neural inputs. We additively incorporated trialwise left SFS and used a scale parameter, $m_{c,s}$,
 1439 to account for its modulatory effects. The following equations show the distributions assumed for each
 1440 of the latent variables in the model:

Trial-by-trial, i

$$y_{c,s,i} \sim Wiener(\alpha_{c,s}, \beta, \tau_{c,s}, \delta_{c,s,i})$$

Model 1: $\delta_{c,s,i} = \kappa_{c,s} \times E_{c,s,i}$
 $\alpha_{c,s,i} = \alpha_{c,s} + (m_{c,s} \times \theta_{c,s,i})$

Model 2: $\delta_{c,s,i} = \kappa_{c,s} \times E_{c,s,i} + (m_{c,s} \times \theta_{c,s,i})$

Model 3: $\delta_{c,s,i} = \kappa_{c,s} \times E_{c,s,i} + (m_{c,s} \times \theta_{c,s,i})$
 $\alpha_{c,s,i} = \alpha_{c,s} + (n_{c,s} \times \theta_{c,s,i})$

Model 4: $\delta_{c,s,i} = \kappa_{c,s} \times E_{c,s,i} + (m_{c,s} \times \theta_{c,s,i})$
 $\alpha_{c,s,i} = \alpha_{c,s} + (m_{c,s} \times \theta_{c,s,i})$

Subject, c : $\alpha_{c,s} \sim \mathbb{N}(\mu_{\alpha(c)}, \sigma_{\alpha(c)}^2)$

$\tau_{c,s} \sim \mathbb{N}(\mu_{\tau(c)}, \sigma_{\tau(c)}^2)$

$\kappa_{c,s} \sim \mathbb{N}(\mu_{\kappa(c)}, \sigma_{\kappa(c)}^2)$
 $b_{c,s} = 0.5$
 $m_{c,s} \sim \mathbb{N}(\mu_{m(c)}, \sigma_{m(c)}^2)$ (All Models)

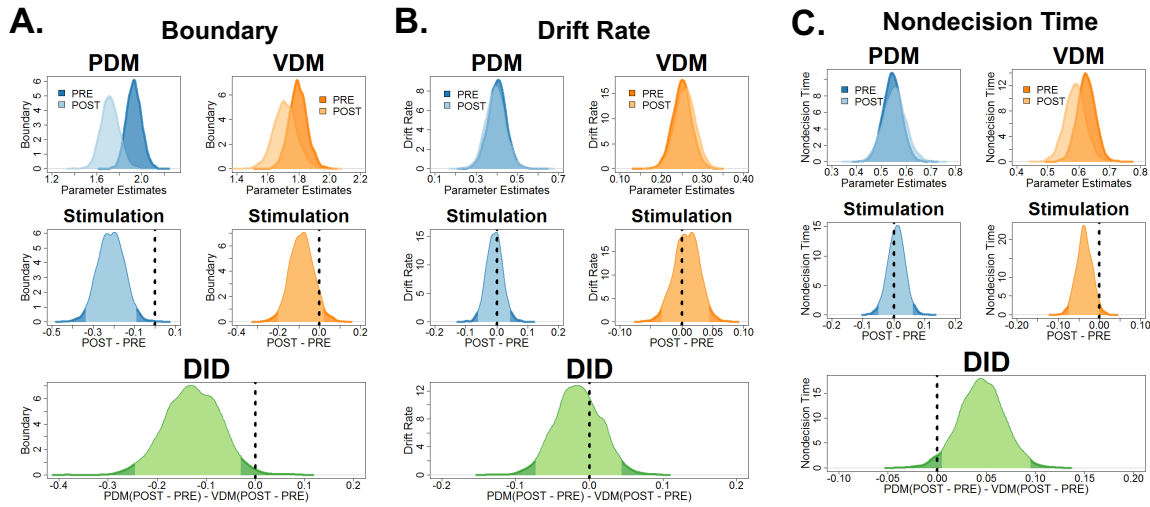
$n_{c,s} \sim \mathbb{N}(\mu_{n(c)}, \sigma_{n(c)}^2)$ (Model 3 only)

Observable variables: $y = \begin{cases} rt, & \text{correct} = 1 \\ -rt, & \text{correct} = 0 \end{cases}$

$E = \{V_{best} - V_{worst}\}$ or $\{S_{biggest} - S_{smallest}\}$

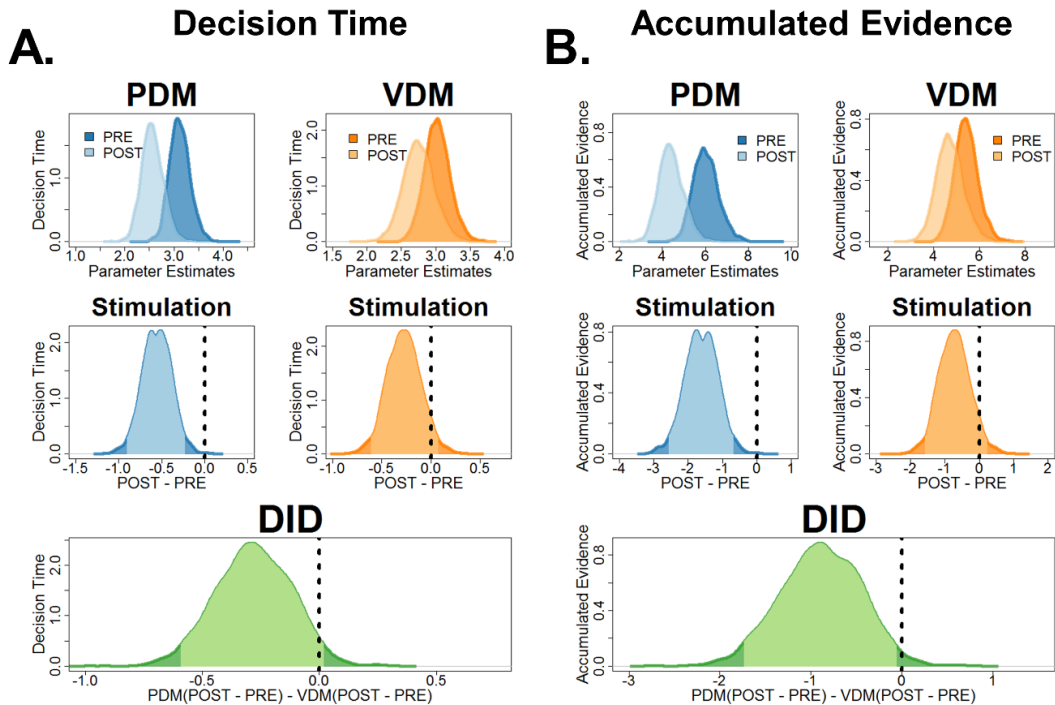
θ , z-scored

1441 Particularly, **(a) Model 1** incorporates trialwise left SFS betas into the decision boundary. **(b) Model 2**
1442 incorporates trialwise left SFS betas into the drift rate. **(c) Model 3** includes trial-by-trial betas in both
1443 decision thresholds and the drift rate, but with separate scale parameters. **(d) Model 4** includes trial-
1444 by-trial betas in both latent parameters but with one common scale parameter.



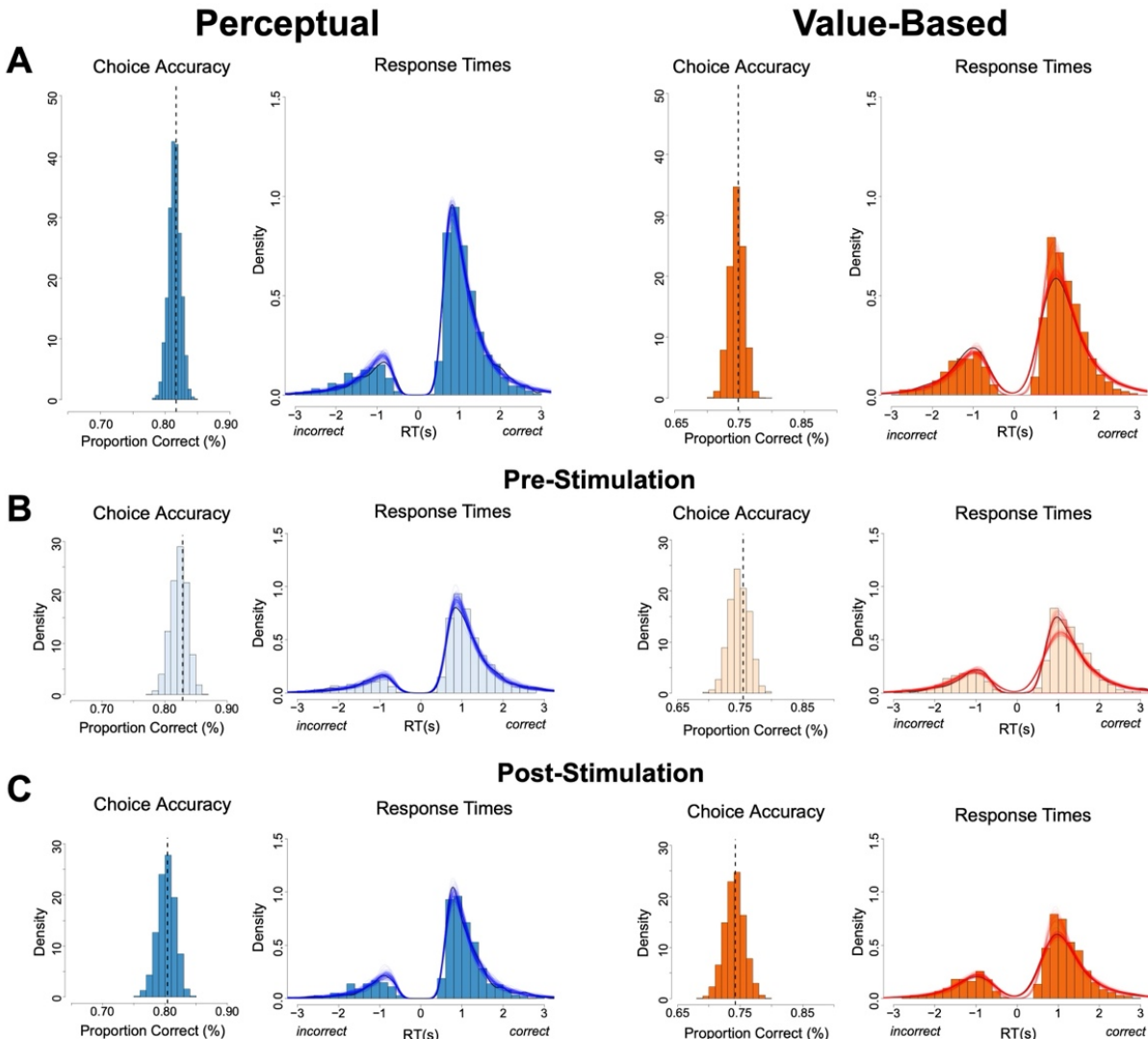
1445

1446 **Supplementary Figure 9. Reanalysis of latent DDM parameters using the neural-HDDM**
1447 **confirmed the results of lower decision boundary in PDM and lower nondecision times in VDM.**
1448 We used the winning neural-HDDM model where the left SFS is modulating the decision threshold
1449 (**Supplementary Fig. 8a**). **(a)** Bayesian posterior probability distributions (top row) of all DDM
1450 parameters show similar effects with the DDM without neural inputs. Post-hoc tests (middle and bottom
1451 rows) comparing pre-post perceptual decision making (PDM) differences with pre-post value-based
1452 decisions show that theta-burst stimulation selectively reduced the decision
1453 boundary for perceptual, not value-based decisions. In particular, the criterion is well outside the 95%
1454 HDI. **(b)** The mean drift rate remained unaffected even with our neural-HDDM model (the criterion is
1455 within the 95% HDI). **(c)** Post-hoc tests also revealed lower nondecision times specifically for VDM,
1456 not PDM after stimulation (the criterion is outside the 95% HDI).



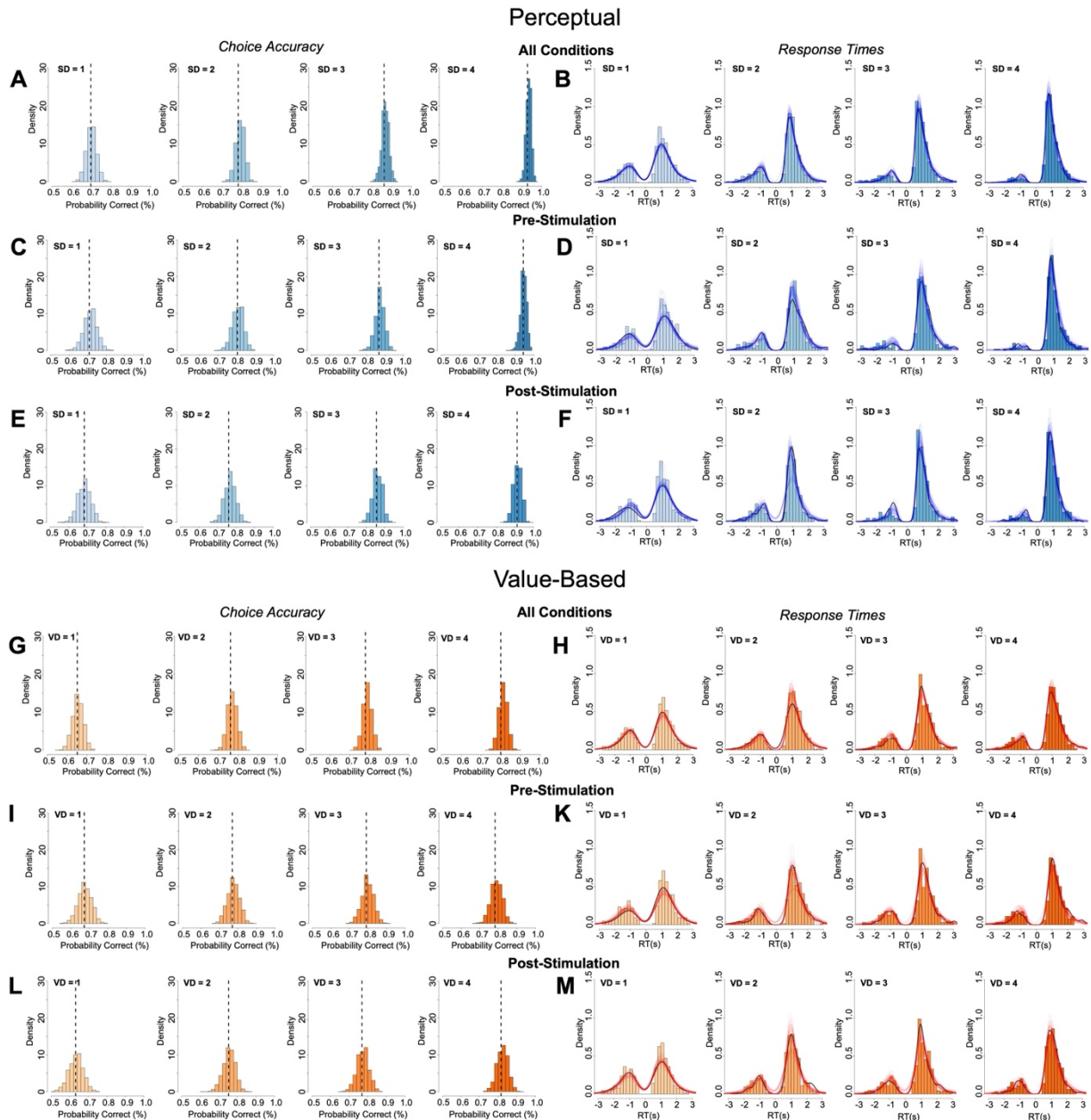
1458 **Supplementary Figure 10. Reanalysis of decision times and accumulated evidence using the**
1459 **neural-HDDM provide improvements in model evidence and clearer statistical inference.** Using
1460 the winning neural-HDDM model (**Supplementary Fig. 8a**), we derived measures for **(a)** decision
1461 times and **(b)** accumulated evidence and tested whether improvements in model evidence reflect
1462 improvements in statistical inference. Post-hoc tests comparing pre-post PDM difference revealed a
1463 main stimulation effect in both DT and AE for PDM (middle row, criteria outside the 95% HDI). Further
1464 post-hoc analysis (bottom row) comparing the pre-post PDM difference with the pre-post VDM
1465 difference show that decision times are now marginally close to the border of the 95% HDI while
1466 accumulated evidence is now outside the 95% HDI.

1467



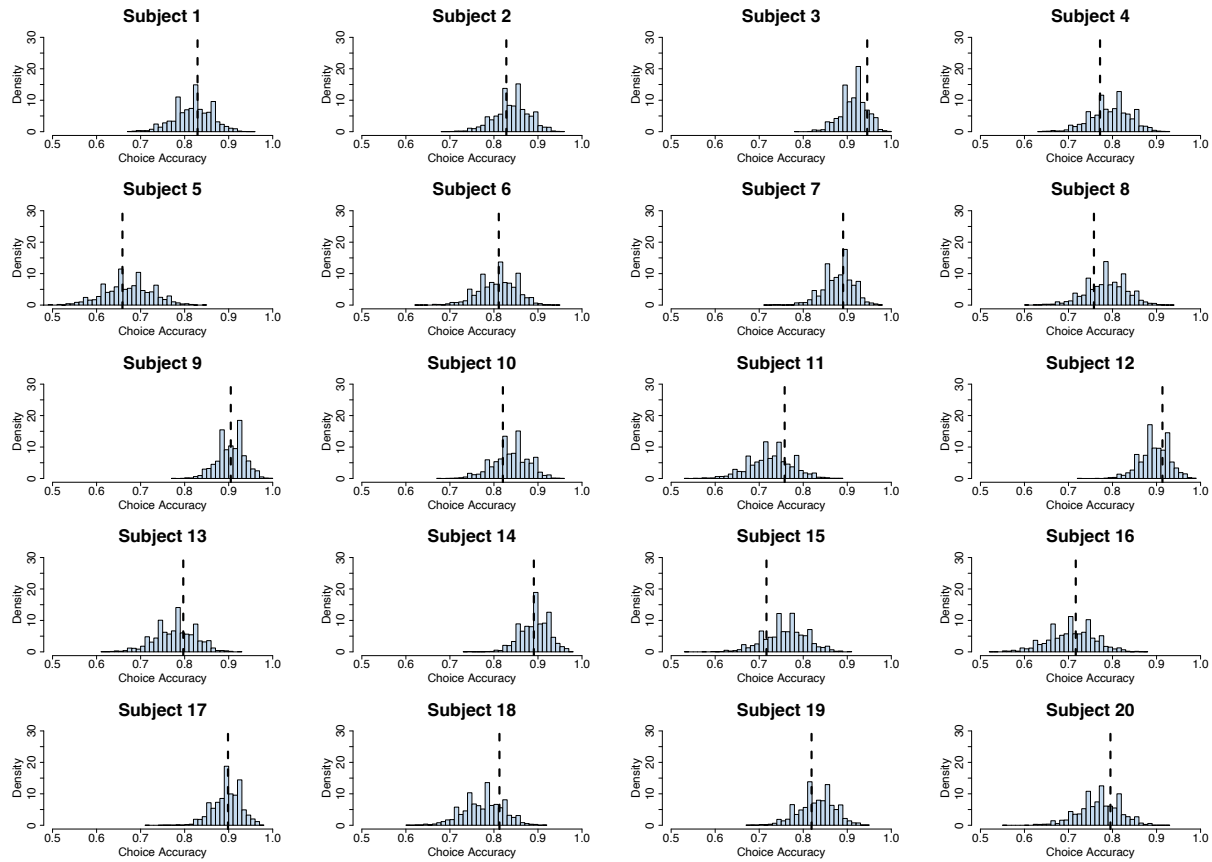
1468

1469 **Supplementary Figure 11. Posterior predictive checks: overall accuracy and RT distributions.**
1470 Posterior predictive simulations from the fitted HDDM compared to observed data. **Left column:**
1471 histograms show the simulated distribution of mean accuracy across 3,000 posterior draws; the
1472 vertical dashed line marks the observed mean accuracy. **Right column:** observed RT histograms
1473 (positive = correct; negative = error) with posterior predictive density curves overlaid. Panels show (a)
1474 PDM vs VDM (pooled over TMS), (b) pre-TMS, and (c) post-TMS. The model reproduces both
1475 accuracy and RT patterns in each condition.



1476

1477 **Supplementary Figure 12. Posterior predictive checks by evidence level.** As in Response Figure
 1478 5, but split by evidence level 1–4 (left-to-right within each row). Rows display: (top) **PDM** pooled over
 1479 TMS, (middle) **pre-TMS**, and (bottom) **post-TMS**; the corresponding three rows for **VDM** are arranged
 1480 analogously. Simulations closely match accuracy and RT distributions at each evidence level in both
 1481 tasks.



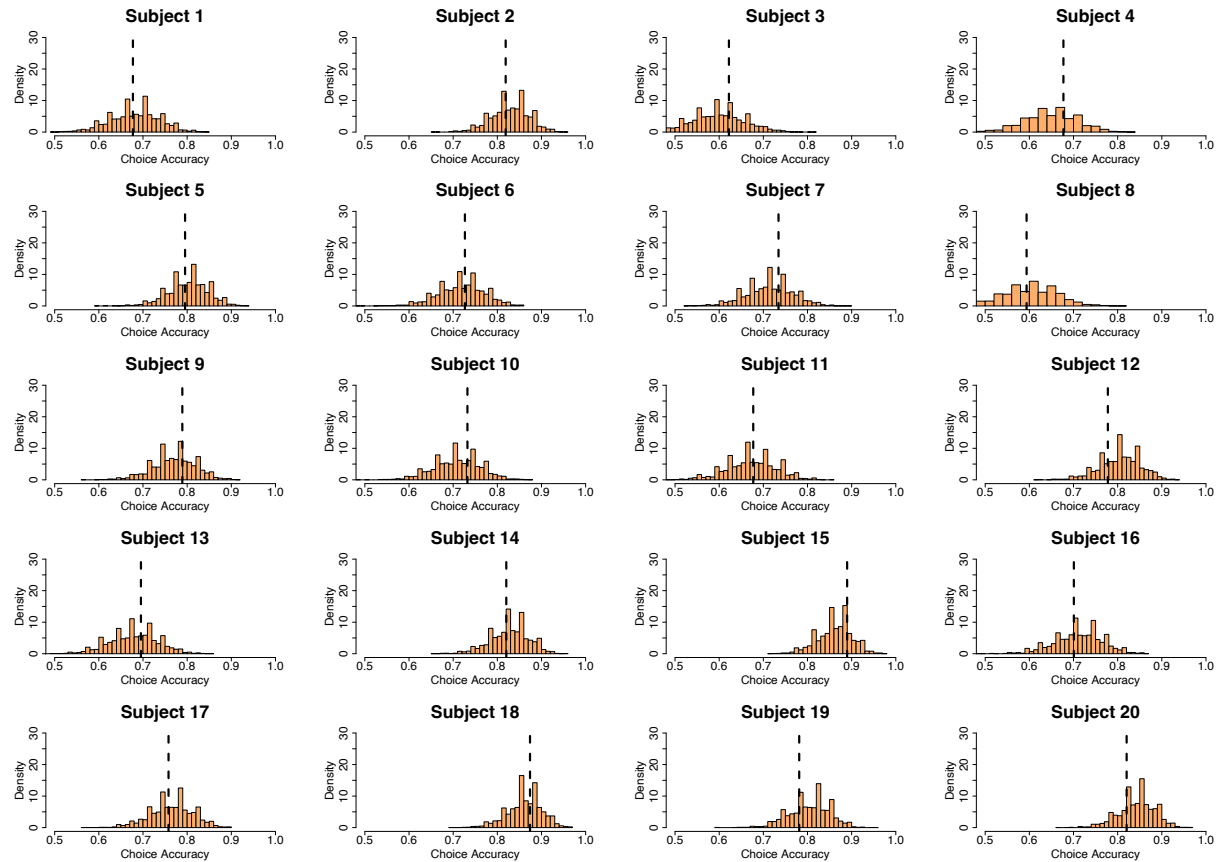
1482

1483 **Supplementary Figure 13. Subject-level accuracy fits for PDM.** For each participant, histogram
1484 shows the posterior predictive distribution of that participant's mean accuracy from 3,000 simulations;
1485 the **vertical dashed line** marks the observed mean accuracy for that participant. The HDDM captures
1486 the dispersion of accuracies across individuals in PDM.

1487

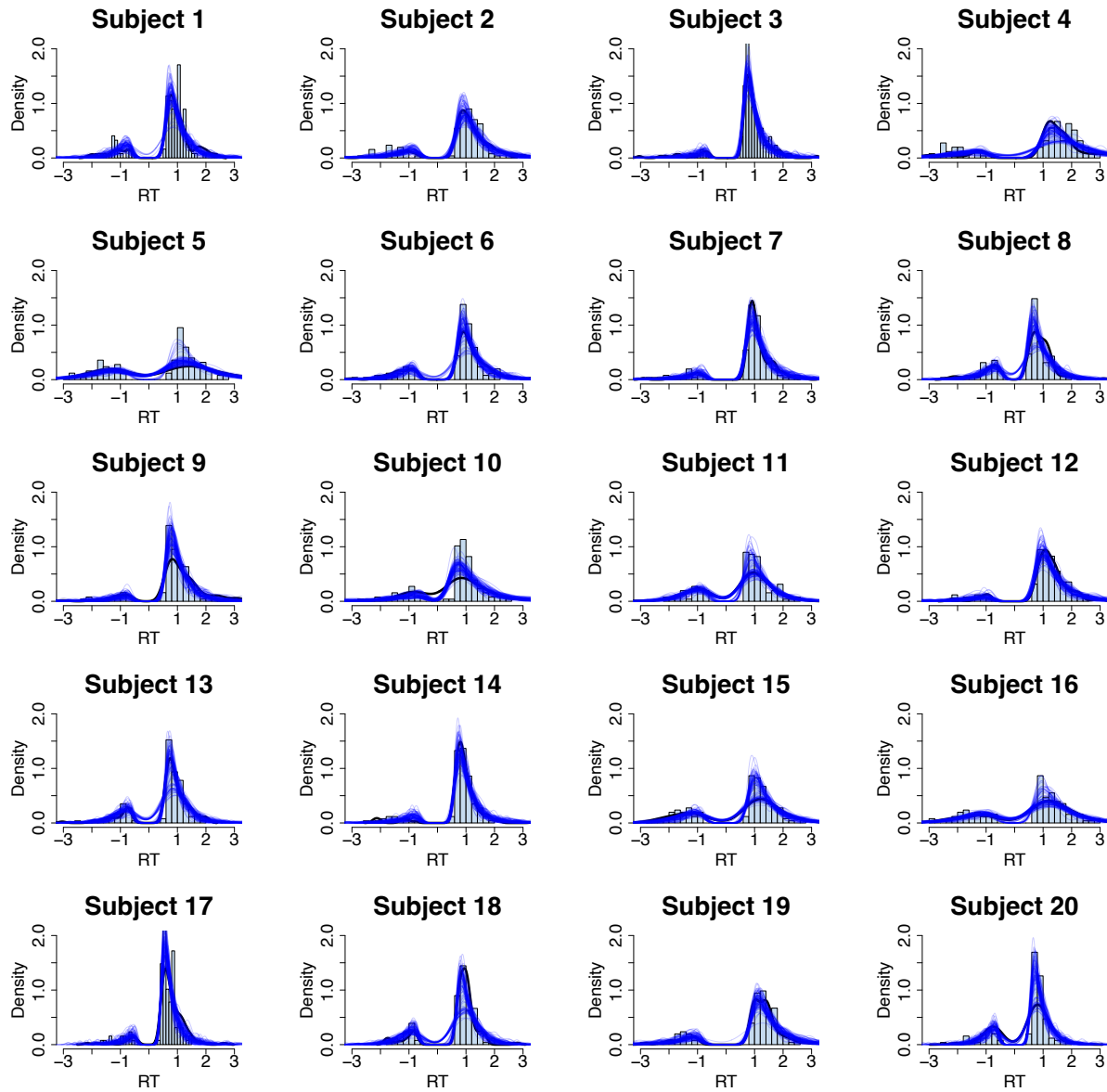
1488

1489



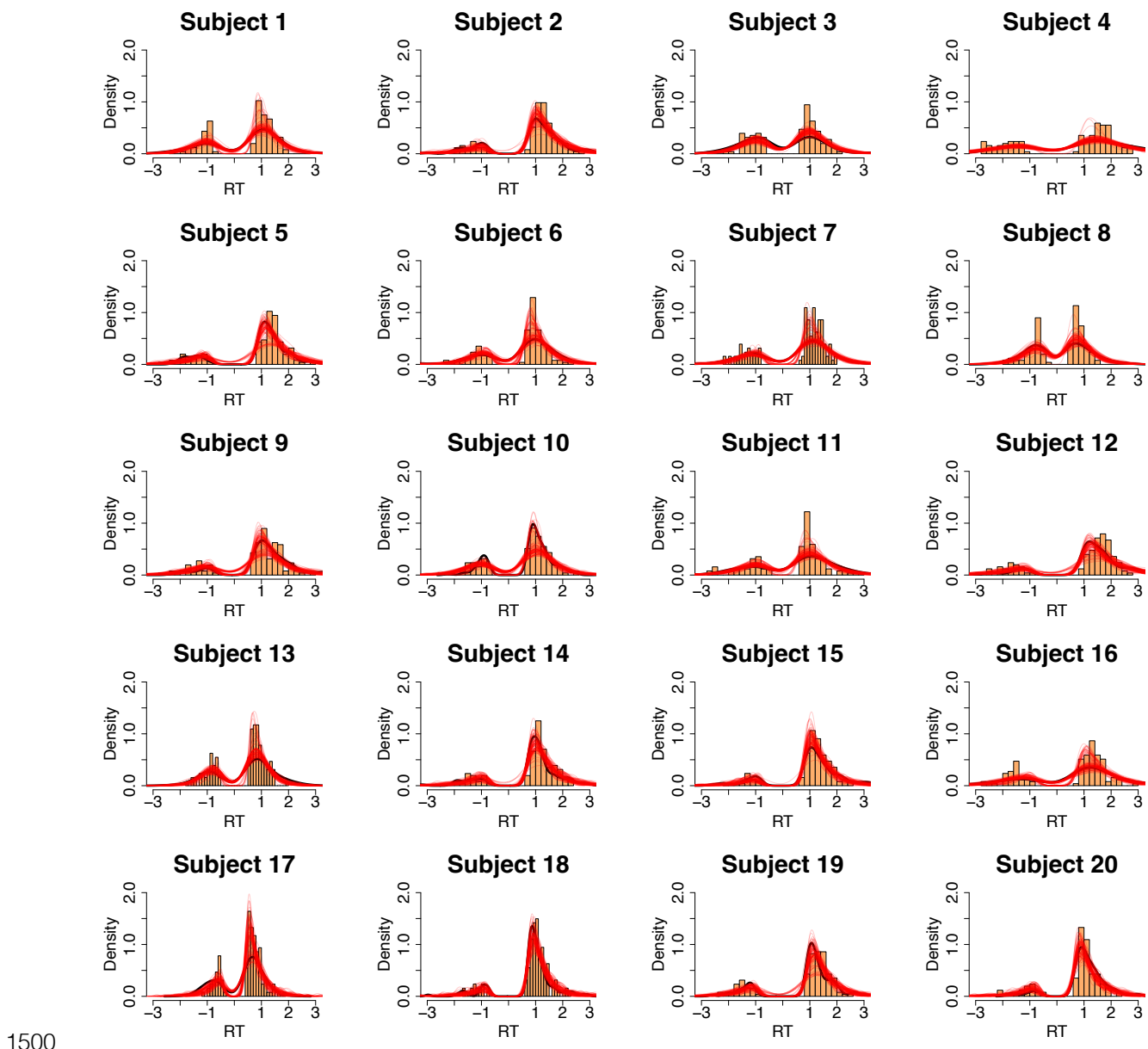
1490

1491 **Supplementary Figure 14. Subject-level accuracy fits for VDM.** Same format as Response Figure
1492 7, for **VDM**. Posterior predictive distributions align with observed subject-level accuracies, indicating
1493 good recovery of between-subject variability in the value-based task.



1494

1495 **Supplementary Figure 15. Subject-level RT distribution fits for PDM.** For each participant,
1496 observed PDM RT histograms (positive = correct; negative = error) are overlaid with posterior
1497 predictive density curves from the HDDM. The model reproduces the full shape of individual RT
1498 distributions, including correct/error asymmetries.
1499



1501 **Supplementary Figure 16. Subject-level RT distribution fits for VDM.** Same format as Response
1502 Figure 9, for VDM. Posterior predictive densities closely track the observed RT distributions across
1503 participants.

1504

1505

1506

1507

1508

1509

1510 **Supplementary Table 1.**

1511 Average brain activity that is common for both types of choice (conjunction between PDM and VDM
1512 trials)

1513

Region	Peak-Side	Cluster Size	x	y	z	Z score	T score	p-value
Fusiform gyrus	L	1072	-33	-52	-17	Inf.	22.61	< 0.001
Fusiform gyrus	R	1523	33	-52	-11	7.23	17.24	< 0.001
Anterior intraparietal sulcus	L	845	-48	-34	46	7.13	16.53	< 0.001
Caudal supplementary motor	L	525	-3	14	49	7.05	15.98	< 0.001
Middle cingulate cortex	L	99	-6	-31	28	6.92	15.17	< 0.001
Anterior insula	L	219	-33	23	1	6.62	13.49	< 0.001
Hippocampus/Thalamus	R	42	21	-28	4	6.40	12.36	< 0.001
Hippocampus/Thalamus	L	483	-21	-31	1	6.35	12.11	< 0.001
Anterior insula	R	187	30	26	-2	6.18	11.36	< 0.001
Somatosensory	L	55	-36	-4	10	5.89	10.18	< 0.001
Cerebellum	R	32	0	-52	-35	5.69	9.45	< 0.001
Cerebellum	L	18	-9	-76	-26	5.33	8.29	< 0.001
Premotor cortex / Inferior frontal sulcus	R	25	51	8	28	5.32	8.25	< 0.001
Premotor cortex / Inferior frontal sulcus	L	33	-54	8	34	5.25	8.06	< 0.001
Cerebellum	R	3	9	-76	-38	5.16	7.80	0.004
Frontal eye field	R	19	24	-1	49	5.14	7.73	< 0.001
Cerebellum	L	4	-6	-79	-41	5.12	7.69	0.002
Medial temporal lobe	L	3	-27	-4	-32	5.12	7.68	0.004
Dorsolateral prefrontal	R	6	42	32	25	5.09	7.59	0.001
Cerebellum	R	5	15	-55	-47	5.03	7.44	0.001
Cerebellum	R	3	18	-67	-47	4.94	7.18	0.004
Cerebellum	R	1	9	-73	-23	4.86	6.99	0.015
Basal ganglia	L	4	-15	5	4	4.86	6.98	0.002
Frontal eye field	L	1	-30	-4	49	4.83	6.92	0.015
Supplementary motor cortex	L	2	-6	-4	61	4.83	6.92	0.007
Somatosensory cortex	L	1	-54	-19	19	4.82	6.88	0.015
Brainstem	R	1	9	-34	-32	4.80	6.85	0.015
Brainstem	R	1	0	-31	-38	4.80	6.85	0.015
Parietal cortex	L	1	-24	2	55	4.79	6.81	0.015

1514

1515 All p-values are FWE-corrected for the whole brain.

1516

1517

1518

1519 **Supplementary Table 2.**

1520 Average brain activity that is distinct for both types of choice.

Region	Peak-Side	Cluster Size	x	y	Z	Z score	T score	p-value
Value-based choice trials > Perceptual choice trials								
Angular gyrus	L	344	-45	-70	43	5.74	9.62	< 0.001
Superior frontal	L	1560	-18	32	46	5.36	8.40	< 0.001
Temporal parietal junction	R	204	51	-61	37	4.71	6.62	< 0.001
Posterior cingulate cortex	L	1368	-3	-55	22	4.66	6.51	< 0.001
Cerebellum	R	171	39	-61	-47	4.62	6.41	< 0.001
Orbitofrontal cortex	L	130	-39	38	-11	5.31	8.24	< 0.001
Middle temporal gyrus	L	118	-63	-22	-20	4.40	5.90	0.002
Superior frontal	R	75	18	35	46	3.95	5.02	0.042
Medial prefrontal cortex	L	24	-9	50	1	4.02	5.14	0.027
Basal forebrain	L	11	-15	20	-14	3.57	4.33	0.011 ^{SVC}
Superior temporal gyrus	L	1	-63	-22	-5	3.19	3.73	0.033 ^{SVC}
Perceptual choice trials > Value-based choice trials								
Frontal eye fields	R	79	24	-1	55	5.01	7.39	0.035
Premotor cortex	R	176	51	8	19	4.59	6.34	0.001
Intraparietal sulcus	R	646	39	-40	46	4.59	6.34	< 0.001
Inferior temporal sulcus	R	124	45	-55	1	4.36	6.82	0.005
Anterior parietal sulcus	L	319	-51	-31	40	4.29	5.67	< 0.001

1521

1522 All *p*-values are FWE-corrected for the whole brain. SVC = small-volume-correction.

1523

1524 **Supplementary Table 3.**

1525 Regions encoding trialwise accumulated evidence (parametric modulation) during perceptual and
 1526 value-based decisions, including SFS SVC results for both tasks.

Region	Peak-Side	Cluster Size	x	y	z	Z score	T score	p-value
Total Accumulation Value-based Decisions								
Lingual gyrus	L	1338	-9	-88	-2	5.83	9.98	< 0.001
Supplementary Motor Area	L	887	-6	-4	43	4.58	6.32	< 0.001
Primary Auditory Cortex	R	145	36	-31	16	4.53	6.19	< 0.001
Total Accumulation Perceptual Decisions								
Cuneus, V3	R	1215	0	-91	13	5.00	7.36	< 0.001
Lingual gyrus	R	1006	12	-76	-5	4.87	7.01	< 0.001
Superior frontal sulcus*	L	1	-21	26	37	3.13	3.64	0.039 ^{SVC}
Total Accumulation Value-based \cap Perceptual Decisions								
Cuneus, V3	R	1528	6	-88	10	6.99	15.60	< 0.001
Postcentral gyrus	R	316	6	-49	73	4.31	7.73	< 0.001
Lingual gyrus*	L	518	-9	-91	1	4.38	5.98	< 0.001
Total Accumulation Value-based > Perceptual Decisions								
Nucleus Accumbens	R	395	9	11	-11	3.92	4.94	< 0.001
Supramarginal gyrus	L	166	-63	-28	37	3.42	4.09	0.023
Ventromedial prefrontal cortex*	L	2	0	38	-14	3.16	3.68	0.032 ^{SVC}

1527

1528 Note: Trialwise AE during both types of choices correlated negatively with BOLD activity in intraparietal
 1529 sulcus (IPS) (peak at $x = -33, y = -49, z = 58$; SVC < 0.05; Supplementary Fig. 7c) and bilateral
 1530 fusiform gyrus (right peak at $x = 33, y = -49, z = -14$; left peak at $x = -30, y = -52, z = -11$; FWE-
 1531 corrected with cluster-forming thresholds at $T(19) > 2.9$; Supplementary Fig. 7c). Note that the inverse
 1532 of total evidence is directly proportional to the efficiency of evidence accumulation (see **Methods** for
 1533 more details). SVC = small-volume-correction.

1534

1535 **Supplementary Table 4.**

1536 Average brain activity that represents efficiency of evidence accumulation for both types of choice

1537

Region	Peak-Side	Cluster Size	x	y	z	Z score	T score	p-value
Accumulation Rate for Value-based Decisions								
Fusiform gyrus	R	564	33	-55	-11	4.92	7.15	< 0.001
Fusiform gyrus	L	718	-27	-70	-11	4.92	7.14	< 0.001
Occipital	R	349	30	-85	10	3.75	4.65	< 0.001
Intraparietal sulcus	L	58	-28	-66	38	4.35	5.80	0.002 ^{SVC}
Intraparietal sulcus	R	19	27	-61	43	3.52	4.25	0.032 ^{SVC}
Accumulation Rate for Perceptual Decisions								
Fusiform gyrus	L	1095	-24	-82	-8	5.72	9.56	< 0.001
Fusiform gyrus	R	1250	33	-55	-11	5.06	7.51	< 0.001
Intraparietal sulcus	R	58	27	-61	43	3.54	4.29	0.009 ^{SVC}
Accumulation Rate for Value-based ∩ Perceptual Decisions								
Fusiform gyrus	L	1151	-24	-82	-8	5.75	9.69	< 0.001
Fusiform gyrus	R	1369	33	-55	-11	5.47	8.73	< 0.001
Intraparietal sulcus	R	81	27	-61	43	3.66	4.49	0.003 ^{SVC}

1538 SVC = small-volume-correction.

1539

1540 **Supplementary Table 5.**

1541 Differences-in-differences results for choice accuracy/consistency and response times

	Perceptual (a)	(b)	Value-Based (c)	(d)
Accuracy				
(1) active DV	0.5596*** (0.053)	0.5178*** (0.047)	0.249*** (0.061)	0.245*** (0.062)
(2) passive DV	0.0232 (0.178)	0.0258 (0.015)	0.006 (0.026)	0.005 (0.027)
(3) active overall value (OV)	−0.2023*** (0.041)	−0.210*** (0.046)	0.088 (0.151)	0.073 (0.057)
(4) passive OV	−0.060 (0.060)	−0.048 (0.060)	−0.027 (0.063)	−0.027 (0.063)
(5) RTs		−1.0679*** (0.160)		−0.254 (0.165)
(6) Constant	0.720*** (0.221)	2.131*** (0.301)	0.200 (0.239)	0.569 (0.293)
RTs				
(1) active DV	−0.058*** (0.007)	−0.041*** (0.007)	−0.016* (0.033)	−0.013* (0.006)
(2) passive DV	0.002 (0.002)	0.002 (0.002)	−0.003 (0.004)	−0.003 (0.003)
(3) active OV	−0.002 (0.007)	−0.008 (0.007)	−0.057*** (0.004)	−0.056*** (0.007)
(4) passive OV	0.011 (0.007)	0.009 (0.007)	0.006 (0.007)	0.006 (0.006)
(5) Choice response		−0.220*** (0.020)		−0.080*** (0.017)
(7) Constant	1.289 (0.0623)	1.442 (0.062)	1.431 (0.060)	0.010 (0.035)
Total Observations	2,544	2,548	2,544	2,548
Sessions	8	8	8	8
Subjects	20	20	20	20

1542 Significance: * $p < 0.05$, ** $p < 0.01$

1543

1544 **Supplementary Table 6.**

1545 Differences-in-differences results for choice accuracy/consistency and response times

1546

	(a) Pre-Post cTBS	(b) + Training	(c) + Control Variables	(d) + Training & Control Variables
Accuracy				
(1) Perceptual	-0.433* (0.188)	-0.465** (0.174)	-0.459* (0.192)	-0.484** (0.180)
(2) Value-based	0.00298 (0.124)	-0.0415 (0.104)	0.0042 (0.123)	-0.040 (0.104)
(3) DD Estimate	-0.293* (0.114)	-0.273* (0.135)	-0.319** (0.115)	-0.288* (0.136)
(4) Corrected	-0.075** (0.027)	-0.094* (0.045)	-0.087** (0.030)	-0.103* (0.047)
RTs				
(1) Perceptual	-0.090* (0.0331)	-0.116** (0.0343)	-0.089* (0.033)	-0.125** (0.033)
(2) Value-based	-0.117** (0.0298)	-0.125** (0.0328)	-0.117** (0.030)	-0.125** (0.033)
(3) DD Estimate	0.0265 (0.0357)	0.00929 (0.0353)	0.0273 (0.035)	0.010 (0.035)
Perceptual Obs.	1,272	1,907	1,272	1,907
Value-based Obs.	1,276	1,908	1,276	1,908
Total Obs.	2,548	3,815	2,548	3,815
Sessions	4	6	4	6
Subjects	20	20	20	20

1547 Significance: * $p < 0.05$, ** $p < 0.01$

1548 **Note:**

- 1549 (a) **Pre-Post cTBS:** Stimulation effect comparing the last two runs during pre-cTBS and the first
1550 two runs during post-cTBS.
- 1551 (b) **Pre-Post cTBS + Training:** Stimulation effect comparing all runs during pre-cTBS with the
1552 first two runs during post-cTBS.
- 1553 (c) **Pre-Post cTBS + Control Variables:** The same as in (a) but we added control variables to
1554 test for robustness of the stimulation effect.
- 1555 (d) **Pre-Post cTBS + Training + Control Variables:** The same as in (b) but we added control
1556 variables to test for robustness of the stimulation effect.

1558 **Supplementary Table 7.**

1559 Differences-in-differences results for choice accuracy/consistency and response times

1560

	(a) Pre-Post cTBS	(b) + Training	(c) + Control Variables	(d) + Training & Control Variables
Accuracy				
(1) PDM SFS x Stimulation	-0.145** (0.047)	-0.133** (0.043)	-0.195** (0.057)	-0.318** (0.106)
(2) VDM SFS x Stimulation	0.148 (0.084)	0.104 (0.080)	0.167 (0.090)	-0.065 (0.053)
(3) SFS x Stimulation x Task	-0.293** (0.101)	-0.237** (0.088)	-0.356** (0.121)	-0.318** (0.103)
(4) Corrected Triple Interaction	-0.086* (0.034)	-0.093* (0.038)	-0.102* (0.040)	-0.131** (0.047)
RTs				
(1) PDM SFS x Stimulation	-0.003 (0.0140)	-0.005 (0.0148)	-0.009 (0.0137)	-0.005 (0.0142)
(2) VDM SFS x Stimulation	-0.003 (0.0227)	0.011 (0.0182)	-0.003 (0.0232)	0.008 (0.0182)
(3) SFS x Stimulation x Task	-0.0002 (0.0273)	-0.016 (0.0241)	-0.018 (0.0240)	-0.012 (0.0238)
Perceptual Obs.	1,272	1,907	1,272	1,907
Value-based Obs.	1,276	1,908	1,276	1,908
Total Obs.	2,548	3,815	2,548	3,815
Sessions	4	6	4	6
Subjects	20	20	20	20

1561

1562 Significance: * $p < 0.05$, ** $p < 0.01$

1563 **Note:**

- 1564 (a) **Pre-Post cTBS:** Stimulation effect comparing the last two runs during pre-cTBS and the first
1565 two runs during post-cTBS.
- 1566 (b) **Pre-Post cTBS + Training:** Stimulation effect comparing all runs during pre-cTBS with the
1567 first two runs during post-cTBS.
- 1568 (c) **Pre-Post cTBS + Control Variables:** The same as in (a) but we added control variables to
1569 test for robustness of the stimulation effect.
- 1570 (d) **Pre-Post cTBS + Training + Control Variables:** The same as in (b) but we added control
1571 variables to test for robustness of the stimulation effect.

1573 **Supplementary Table 8.** HDDM group-level parameter estimates for perceptual decisions (**PDM**)
1574 across TMS conditions and evidence levels (δ drift, α boundary, τ non-decision time; DIC reported).

Perceptual	δ		α		τ		DIC
	mean	SD	mean	SD	mean	SD	
All	0.388	0.035	1.848	0.065	0.522	0.029	4048.675
Pre-stimulation	0.401	0.041	1.915	0.078	0.537	0.035	2103.361
Post-stimulation	0.394	0.039	1.708	0.070	0.545	0.023	1811.714
Evidence Level (all)							
1	0.502	0.075	1.755	0.071	0.565	0.038	1443.749
2	0.847	0.108	1.734	0.062	0.576	0.029	1111.493
3	1.176	0.126	1.824	0.076	0.530	0.030	898.764
4	1.570	0.143	1.945	0.089	0.523	0.027	599.467
Evidence Level (pre-stimulation)							
1	0.521	0.083	1.815	0.088	0.571	0.043	785.636
2	0.907	0.122	1.738	0.080	0.633	0.044	576.199
3	1.211	0.159	1.908	0.096	0.533	0.036	494.364
4	1.673	0.183	2.070	0.116	0.542	0.036	324.876
Evidence Level (post-stimulation)							
1	0.516	0.110	1.634	0.086	0.596	0.036	675.095
2	0.865	0.164	1.651	0.089	0.573	0.027	520.592
3	1.207	0.150	1.720	0.097	0.547	0.031	429.265
4	1.512	0.144	1.764	0.110	0.537	0.031	295.764

1575

1576

1577

1578

1579

1580

1581

1582

1583

1584

1585

1586

1587 **Supplementary Table 9.** HDDM group-level parameter estimates for value-based decisions (**VDM**)
 1588 across TMS conditions and evidence levels (δ , α , τ ; DIC reported).

Value-Based	δ		α		τ		DIC
	mean	SD	mean	SD	mean	SD	
All	0.217	0.020	1.799	0.057	0.579	0.029	4960.166
Pre-stimulation	0.219	0.021	1.798	0.062	0.627	0.033	2523.472
Post-stimulation	0.222	0.022	1.707	0.066	0.585	0.031	2305.875
Evidence Level (all)							
1	0.386	0.054	1.680	0.064	0.616	0.033	1415.309
2	0.717	0.076	1.882	0.062	0.604	0.035	1274.095
3	0.806	0.088	1.748	0.076	0.618	0.038	1153.058
4	0.888	0.111	1.849	0.079	0.579	0.031	1135.478
Evidence Level (pre-stimulation)							
1	0.453	0.086	1.682	0.060	0.690	0.052	724.036
2	0.726	0.084	1.756	0.080	0.660	0.033	655.603
3	0.838	0.096	1.707	0.083	0.675	0.044	585.722
4	0.848	0.134	1.798	0.083	0.639	0.037	604.951
Evidence Level (post-stimulation)							
1	0.350	0.078	1.585	0.077	0.620	0.038	675.120
2	0.737	0.111	1.631	0.072	0.627	0.043	590.912
3	0.818	0.128	1.619	0.094	0.650	0.048	544.877
4	0.960	0.109	1.721	0.085	0.609	0.044	538.493

1589

1590

1591

1592

1593

1594

1595

1596

1597

1598

1599

1600 **Supplementary Table 10.** HDDM participant-level parameter estimates for **PDM (δ , α , τ)** with model
1601 fit (DIC) per subject.

Subject	δ		α		τ		DIC
	mean	SD	mean	SD	mean	SD	
1	0.416	0.050	1.654	0.086	0.498	0.014	155.658
2	0.378	0.042	2.034	0.104	0.510	0.020	246.230
3	0.668	0.057	1.846	0.120	0.487	0.017	75.702
4	0.257	0.034	2.336	0.112	0.742	0.026	355.873
5	0.147	0.034	2.026	0.086	0.587	0.018	346.635
6	0.358	0.044	1.796	0.086	0.567	0.015	207.893
7	0.504	0.050	1.932	0.109	0.565	0.018	164.511
8	0.338	0.047	1.678	0.075	0.357	0.012	194.419
9	0.571	0.052	2.026	0.120	0.446	0.018	152.084
10	0.330	0.038	2.296	0.116	0.222	0.017	283.846
11	0.252	0.042	1.649	0.075	0.547	0.017	242.651
12	0.482	0.045	2.248	0.135	0.555	0.021	201.924
13	0.361	0.049	1.532	0.071	0.484	0.011	151.426
14	0.578	0.055	1.823	0.106	0.494	0.016	121.826
15	0.271	0.041	1.835	0.083	0.656	0.017	263.821
16	0.189	0.035	1.969	0.086	0.551	0.021	333.834
17	0.676	0.065	1.597	0.088	0.345	0.010	36.774
18	0.359	0.048	1.516	0.072	0.592	0.012	146.552
19	0.360	0.041	2.016	0.101	0.728	0.017	247.041
20	0.375	0.055	1.406	0.067	0.490	0.012	129.653

1602

1603

1604

1605

1606

1607

1608

1609

1610

1611

1612

1613

1614 **Supplementary Table 11.** HDDM participant-level parameter estimates for VDM (δ , α , τ) with model
1615 fit (DIC) per subject.

Subject	δ		α		τ		DIC
	mean	SD	mean	SD	mean	SD	
1	0.165	0.037	1.582	0.067	0.612	0.012	224.450
2	0.280	0.034	2.076	0.103	0.606	0.017	256.215
3	0.085	0.035	1.610	0.068	0.526	0.015	271.958
4	0.097	0.028	2.158	0.091	0.684	0.023	394.165
5	0.257	0.034	1.961	0.096	0.721	0.020	270.684
6	0.198	0.035	1.646	0.074	0.518	0.015	239.416
7	0.187	0.036	1.680	0.074	0.642	0.013	242.186
8	0.090	0.038	1.559	0.064	0.330	0.011	235.979
9	0.220	0.033	1.950	0.093	0.560	0.021	298.440
10	0.184	0.036	1.667	0.075	0.584	0.016	254.361
11	0.137	0.032	1.794	0.078	0.479	0.016	297.167
12	0.226	0.030	2.236	0.109	0.735	0.021	317.836
13	0.185	0.042	1.389	0.060	0.483	0.011	173.978
14	0.291	0.036	1.963	0.094	0.580	0.016	243.953
15	0.342	0.037	1.997	0.106	0.663	0.018	206.759
16	0.160	0.032	1.964	0.084	0.643	0.017	315.890
17	0.288	0.048	1.431	0.062	0.338	0.008	125.692
18	0.379	0.041	1.805	0.097	0.592	0.016	155.570
19	0.273	0.035	1.853	0.088	0.759	0.015	235.053
20	0.331	0.038	1.871	0.093	0.516	0.015	201.545

1616

1617

1618

1619